Chemical Geology 515 (2019) 61–76

Contents lists available at ScienceDirect

Chemical Geology

journal homepage: www.elsevier.com/locate/chemgeo

Tracing the metal dynamics in semi-arid soils near mine tailings using stable Cu and Pb isotopes

Martin Mihaljevič[a,*], Rafael Baieta[a], Vojtěch Ettler[a], Aleš Vaněk[b], Bohdan Kříbek[c], Vít Penížek[b], Petr Drahota[a], Jakub Trubač[a], Ondra Sracek[d], Vladislav Chrastný[e], Benjamin Siyowi Mapani[f]

[a] Institute of Geochemistry, Mineralogy and Mineral Resources, Faculty of Science, Charles University, Albertov 6, CZ-128 43 Prague 2, Czech Republic
[b] Department of Soil Science and Soil Protection, Faculty of Agrobiology, Food and Natural Resources, Czech University of Life Sciences Prague, Kamýcká 129, 165 21 Prague 6, Czech Republic
[c] Czech Geological Survey, Geologická 6, 152 00 Prague 5, Czech Republic
[d] Department of Geology, Faculty of Science, Palacky University in Olomouc, 17. listopadu 12, 771 46 Olomouc, Czech Republic
[e] Department of Environmental Geosciences, Faculty of Environmental Sciences, Czech University of Life Sciences Prague, Kamýcká 129, 165 21 Prague 6, Czech Republic
[f] Department of Geology, Faculty of Science, University of Namibia, Private Bag, 13301, Windhoek, Namibia

ARTICLE INFO

Editor: Donald Porcelli

Keywords:
Lead
Copper
Mine tailings
Soil
Luvisol
Chernozem
Cu isotopes
Pb isotopes
Namibia

ABSTRACT

The dynamics of Cu and Pb were studied in eight soil profiles (Luvisols, Chernozems), located at various distances from the tailing dams near a closed Cu-Pb-(Zn)-Ag mine at Kombat (Namibia) by a combination of isotope and elemental studies, leaching techniques and speciation modelling. Tailings, soils and bedrocks were analyzed for the bulk Cu and Pb concentrations, for their chemical forms using the sequential extraction procedure and for the isotope compositions of Cu (δ^{65}Cu) and Pb (^{206}Pb/^{207}Pb, ^{208}Pb/^{206}Pb).

In spite of the differences in the contamination of the studied profiles by tailing dust, both soil types exhibit characteristic trends in the behaviour of metals and distribution of their isotopes. While most Luvisols exhibit an increase in the metal content towards depth in the profile, Chernozems exhibit the opposite trend (decrease in metal content with depth) or similar contents in the whole profile. Luvisols were mostly characterized by changing δ^{65}Cu values as a function of depth. The value of δ^{65}Cu decreases with depth to the Bt horizon and then the δ^{65}Cu value increases with increasing depth. Chernozems mostly yielded uniform Cu concentrations and isotope compositions in all the soil horizons, clearly contrasting with the isotopically lighter compositions of the carbonate bedrocks. Positive δ^{65}Cu values in the tailing material affect the surface of the soil, especially soil sampled in its vicinity. In most Luvisols and Chernozems, the isotope composition of Pb exhibits similar patterns with a low ^{206}Pb/^{207}Pb ratio on the surface of the profile and with a slight increase to depth. The low ^{206}Pb/^{207}Pb values at the surface of the profiles are caused by dust from the tailings.

The elemental and isotopic patterns of both contaminated and uncontaminated soil types reflect not only the distance from the tailing dam but also pedogenetic processes in the profiles and geochemical behaviour of both contaminants. The copper elemental and isotope patterns reflect the formation of more mobile species in the surface environment and movement of solutions and colloids and precipitation onto secondary minerals in Luvisols. Plant uptake of lighter isotopes in Chernozems can influence the Cu isotope patterns in these soil types. The limited movement of colloids and higher sorption capacity of Chernozems is manifested in the isotope compositions of Cu and Pb in their profiles.

1. Introduction

Mine tailings constitute important point sources of potentially toxic metals and metalloids for the surrounding environment (e.g. Romero et al., 2007; Sracek et al., 2010; Hayes et al., 2012; Grösslová et al., 2018). These contaminants are transported from active and/or remediated mine tailings into the surrounding soils, especially by the movement of atmospheric dust and aerosols (Csavina et al., 2012; Castillo et al., 2013). In soils, the mobility, redistribution and bioavailability of contaminants is highly dependent on their form as well as on the soil properties (soil organic matter; abundance and character of clays and oxides; pH), but also on the character of the plant cover, land

* Corresponding author.
E-mail address: mihal@natur.cuni.cz (M. Mihaljevič).

https://doi.org/10.1016/j.chemgeo.2019.03.026
Received 18 July 2018; Received in revised form 14 March 2019; Accepted 26 March 2019
Available online 31 March 2019

use, including agricultural practices (e.g. Sterckeman et al., 2000) and climate (precipitation/temperature). The stable isotopes of lead (Pb) and copper (Cu) constitute an important tool for identifying the sources of these metals and/or the biogeochemical processes affecting their distribution and cycling in soils (e.g. Erel, 1998; Maréchal et al., 1999; Zhu et al., 2000; Teutsch et al., 2001; Emmanuel and Erel, 2002; Maréchal and Albarède, 2002; Ehrlich et al., 2004; Ettler et al., 2004; Bigalke et al., 2010a; Bigalke et al., 2010b; Bigalke et al., 2011; Wiederhold, 2015; Fekiacova et al., 2015; Kusonwiriyawong et al., 2017). The contents of Pb isotopes reflect especially radiogenic processes. Lead is formed by the radiogenic isotopes ^{206}Pb (24%), ^{207}Pb (23%) and ^{208}Pb (52%), which are formed by the decomposition of ^{238}U, ^{235}U and ^{232}Th. The single nonradiogenic isotope ^{204}Pb is present in the lowest concentration (1%). It is possible that Pb isotopes are also fractionated during environmental cycling, but these smaller effects cannot be resolved within the larger radiogenic variations. These variations are greater (i.e. are on an average at the level of the second decimal point) than the small mass-dependent fractionation effects investigated for Cu (vary in units of ‰). The isotope ratios of Pb, routinely used for this purpose during the past two decades, indicate the source of the Pb minerals, according to their mode of formation, as well as the age of the original Pb deposits or Pb-containing geomaterials/anthropogenic materials and rock-forming minerals (Komárek et al., 2008 and references therein). The isotope signature of Pb in soils in the vicinity of local pollution sources is generally the result of the mixing of lithogenic Pb and Pb-containing contaminants (Ettler et al., 2004).

In contrast to the Pb isotopes, Cu isotopes (^{63}Cu and ^{65}Cu with abundances of 69% and 31%) have only recently started to be adopted into biogeochemical studies, due to advances in instrumentation for their measurement (Balistrieri et al., 2008; Borrok et al., 2008; Bigalke et al., 2010a; Bigalke et al., 2010b; Bigalke et al., 2010c; Bigalke et al., 2011; Weinstein et al., 2011; Jouvin et al., 2012; Mihaljevič et al., 2018). No significant fractionation of Cu isotopes has been observed during Cu metallurgy (Gale et al., 1999). The authors studied the isotope composition of Cu in the source malachite, produced copper, slag containing Cu and refined Cu and established a ratio of ^{63}Cu/^{65}Cu varying in the range from 2.24426 to 2.24519. This data did not exhibit statistically significant differences for the individual analyzed materials (Gale et al., 1999). In contrast to this, it has been demonstrated that the isotope composition of Cu in minerals varies in dependence on the redox conditions in which these minerals were formed (Markl et al., 2006). While primary sulphides generally exhibit lower δ^{65}Cu values (−1 to +1‰), their alteration in low-temperature processes leads to the formation of secondary minerals with δ^{65}Cu values in the range from −17 to +10‰ (Mathur et al., 2012). In an exogenic environment, Cu is readily mobilized from primary mineral (e.g. chalcopyrite $CuFeS_2$) where, if abiotic oxidation of Cu(I) to Cu(II) occurs during dissolution, the resultant solution is enriched in ^{65}Cu (Kimball et al., 2009). On the other hand incorporation of Cu into secondary soil minerals leads to the preferential uptake of the heavier isotope into their structure and isotopical lightening of Cu in the solution (Pokrovsky et al., 2008; Bigalke et al., 2011). Fractionation takes place when Cu enters plants, leading to lighter Cu through the effect of reduction of Cu II and the effect of preferential uptake and faster diffusion of lighter isotope through the plant (Weinstein et al., 2011; Jouvin et al., 2012; Ryan et al., 2013). If the Cu is bonded to the cell walls of the roots, the heavier Cu isotope participates preferentially in this process (Jouvin et al., 2012).

In this study we investigated soils located in the vicinity of the mine tailings dam at Kombat (north of Namibia, Fig. 1), where metals (mainly Cu, Pb) enter the soil systems via long-term wind dispersion of fine-grained materials from the tailings. This site provides a unique opportunity to study Cu and Pb dynamics in semi-arid soils. To decipher the processes of metal distribution and mobility in contaminated vs. uncontaminated areas, the extent of tailings-related contamination in the area, and the effects of long-term irrigation, we used a multi-method approach (bulk geochemistry, chemical forms, leaching tests, and metal speciation calculations) coupled to analysis of Cu and Pb isotope ratios for source tracing.

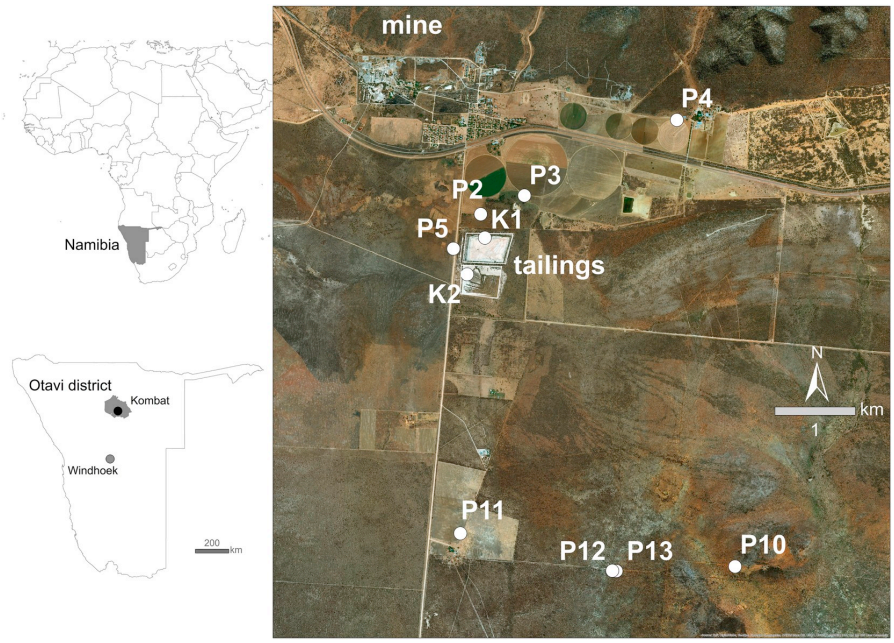

Fig. 1. Schematic map of the Kombat surroundings and location of the studied soil profiles and tailing material samples.

2. Materials and methods

2.1. Study site

The Kombat Cu-Pb-(Zn)-Ag deposit is located in the Otavi Mountain Land (Fig. 1), which is a part of the Northern Carbonate Platform of the Neoproterozoic Damara Orogen (Miller, 1983) in northern Namibia. Similar to the nearby Tsumeb deposit, the primary sulphide mineralization is found in the rocks of the Huttenberg formation, mainly composed of dolostone, chert, shale, stromatolite and breccia (Kamona and Günzel, 2007). Innes and Chaplin (1986) mention the following types of mineralization: bornite (Cu_5FeS_4), chalcopyrite ($CuFeS_2$), galena (PbS), sphalerite (ZnS), tennantite ($Cu_{12}As_4S_{13}$), pyrite (FeS_2); plus the supergene assemblage: chalcocite (Cu_2S), digenite ($Cu_{2-x}S$), malachite [$Cu_2(OH)_2CO_3$], covellite (CuS), cuprite (Cu_2O), and native Cu and Ag. The Kombat mine was closed in 2008 because of flooding-related problems (Mileusnic et al., 2014). Tailings from the ore processing were deposited in the tailings dam without any pre-treatment. Deposition of the tailings began about 100 years ago. After the mine was closed in 2008, attempts were made to reclaim the tips by planting vegetation. The old tailings dam covers an area of approximately 213,000 m^2. Taking into account the average height (20 m) of the dam, the volume of the tailings can be estimated at 4,260,000 m^3 (Kříbek and Kamona, 2006). The tailings comprise the waste from the flotation of both the primary (sulphide) and secondary (oxide and carbonate) ores. High contents of Cu and Pb are mostly present in soluble carbonate minerals (Sracek et al., 2014). The silt fraction (77%) predominates in the tailing material, followed by sand (14%) and clay (9%) (Vaněk et al., 2014). The flow fields for Kombat are dominated by winds from the southeasterly quadrant. During windy periods, dust containing As, Cr, Cu, Pb, and Zn from the old mine tailings dam is transported and deposited in the surrounding area, including adjacent agricultural fields (Mapaure et al., 2011; Mileusnic et al., 2014). Ploughing, resulting in regular mixing of the soil material to a depth of 20–40 cm, eliminates potential strong enrichment of the topsoil at other locations.

The tailings dam has eroded to various degrees and, in some cases during rainy periods, the fine-grained portion of the deposited mine tailings becomes washed out and is deposited in local intermittent drainage rivulets (Kříbek and Kamona, 2006). The area has an average precipitation of 500–550 mm p.a. with seasonal distribution (maximum from December to February), with maximum temperatures in the warmest part of the year (December) reaching values of 32–34 °C, while minimum temperatures in the coldest month (July) are 4–6 °C (Mendelsohn et al., 2002). Maize (*Zea mays L.*) and wheat (*Triticum aestivum L.*) are the principal crops on the adjacent farmlands. *Acacia mellifera, Acacia reficiens, Tarchonanthus camporatus,* and *Dichrostachys cinerea* predominate in areas without agriculture (Mapaure et al., 2011).

2.2. Mine tailings

The tailings materials were sampled at both dry (probe K1) and wet (probe K2) locations (Fig. 1) using an auger drill (Eijkelkamp, the Netherlands). Profile K1 was on the top plateau of the north mine tailings and was completely dry during sampling. The K2 profile was sampled in the southern part of the sludge bed close to the aquatic lagoon; the material was damp, affected by the capillary fringe.

The samples were sieved to < 2 mm, and then dried to constant weight at ambient temperatures. A portion of the sample intended for determining the total elemental concentrations and mineral compositions was ground to analytical fineness in an agate mortar (Fritsch, Germany).

All of the chemicals employed for the digestion and subsequent analyses were of analytical purity; HCl and HNO_3 (p.a. Lach-Ner, Czech Republic) were purified by sub-boiling distillation; deionized water was obtained from a Millipore Academic purifying system (Millipore, USA).

The total concentrations of Pb and Cu in the soils were determined following digestion with HF and $HClO_4$. A weighed amount (0.2 g) of ground sample was dissolved in 10 ml of HF (49% v/v) and 0.5 ml of $HClO_4$ (70% v/v), and then evaporated with evolution of the vapors to dryness on a heating plate. The procedure was repeated with 5 ml HF (49% v/v) and 0.5 ml $HClO_4$ (70% v/v). Following evaporation, the sample was dissolved in 2 ml HNO_3 and transferred to a 100 ml volumetric flask. The concentrations of total inorganic carbon (TIC), total organic carbon (TOC) and total sulphur (TS) were determined by catalytic oxidation (1250 °C) using ELTRA CS 530 and ELTRA CS 500 TIC elemental analysers (ELTRA, Germany).

The Cu and Pb chemical forms in the tailing materials were determined using the optimized BCR sequential extraction procedure (SEP) (Rauret et al., 1999; Sutherland and Tack, 2002): (i) fraction 1 – a weighed amount (1 g) of sample was extracted with 40 ml 0.11 M acetic acid for 16 h at a temperature of 22 ± 5 °C. Samples containing > 3.5 wt% TIC (P5O, P11AC) were extracted in this step with 120 ml 0.11 M acetic acid. The extract was separated from the solid sample by centrifugation; (ii) fraction 2–40 ml 0.5 M $NH_2OH{\cdot}HCl$ acidified with 2 M HNO_3 to pH 1.5 were gradually added to aliquots of the residue from step 1 and the suspension was shaken for 16 h at a temperature of 22 ± 5 °C. The solution from step 2 was separated from the residue by centrifugation; (iii) fraction 3 – a volume of 10 ml of H_2O_2 (pH 2–3) was added to the residue from step 2; the sample was left at laboratory temperature for 1 h and was then heated to a temperature of 85 ± 2 °C for 1 h. Following repeated additions of 10 ml H_2O_2 (pH 2–3) and heating for 1 h at a temperature of 85 ± 2 °C, the mobilized substances were extracted with 1 M NH_4OAc (pH 2) by shaking for 16 h at 22 ± 5 °C. The extract was separated by centrifugation; (iv) fraction 4–3 ml of DI water, 7.5 ml 6 M HCl and 2.5 ml 14 M HNO_3 were added to the residue from step 3; the sample was left to stand overnight and boiled the next day for 2 h under a reflux condenser. Following cooling, the sample from the last step (fraction 4) was filtered and transferred to a 50 ml volumetric flask. Procedural blanks repeatedly were prepared, checked and subtracted from the measured concentrations for each extraction step for each series of 8 samples. These extraction solutions should mobilize the operationally defined fractions: fraction 1 – exchangeable/acid extractable, 2 – reducible (targeting Fe and Mn oxides), 3 – oxidizable (targeting organic matter and sulphides), and 4 – residual.

Extracts of the mine tailings materials were prepared in deionized water to simulate the composition of solutions resulting from tailing/water interactions (Lin, 1997); the obtained leachates were subsequently used for the thermodynamic calculations of metal speciation. A weighed amount (20 g) of sample was leached with 40 ml of deionized (DI) water (MilliQ Academic, Millipore®, USA) and shaken for 8 days on a table shaker at a temperature of 22 ± 5 °C. The solid phase was separated from the solution by centrifuging at 9000 rpm for 20 min. Subsequently, the solutions were filtered through a 0.1-μm membrane filter (Millipore®, USA). The pH, Eh, and electrical conductivity were immediately determined using Schott Handylab multimeters (Schott, Germany). The major cations/anions and trace elements were determined in the extracts (see Section 2.4).

In order to separate the Cu- and Pb-bearing phases, the heavy mineral fraction was separated from the tailing materials using 1,1,2,2-tetrabromethane (density 2.95 g cm^{-3}) (Chisholm et al., 2014). The X-ray diffraction patterns of the bulk samples and the heavy mineral fractions were recorded on a PANalytical X'Pert Pro diffractometer (conditions: CuKα radiation, 40 kV and 30 mA, 2θ range 3–80°, step 0.02°, counting time 150 s). Qualitative analysis of the XRD patterns was performed using PANalytical X'Pert HighScore software, version 1.0d (PANalytical, the Netherlands).

2.3. Soils and rock samples

The soils were sampled at various distances from the tailings dam

using manually dug probes (Fig. 1; GPS positions of individual soil profiles are given in Table A1 in Electronic Annex). The samples were taken on the basis of the value of the Enrichment Index (Kříbek et al., 2010) at sites with low to high contamination (samples P2, P3, P4 and P5) and in an uncontaminated area (samples P10, P11, P12 and P13) (Kříbek and Kamona, 2006).

According to the FAO classification scheme (FAO, 2006), two major soil types occurred in the area, Cutanic Luvisol and Petrocalcic Chernozem (Table A1 in the Electronic Annex) profile P13 was described as Kastanozem, corresponding to a transition between these two types of soil). The samples were taken according to the natural development of diagnostic horizons, air-dried to a constant weight, and sieved to < 2 mm. Whenever possible, bedrock samples were also collected at the bottom of the profiles (only for P3 and P11). The bedrock samples were cleaned in DI water and were then ground and processed in the same manner as the tailing materials and soils. Additional rock samples were taken from the cores drilled at the Kombat deposit. An aliquot portion of each sample was ground to analytical fineness in an agate mortar (Fritsch, Germany). Unfortunately, it was not possible to sample the Quaternary sedimentary rocks below the Luvisol profiles or from the boreholes drilled in the area.

The particle size distributions in the soil samples (fractions of clay, silt, and sand) were obtained using the hydrometer method (Gee and Or, 2002). The soil pH (H_2O and 1 M KCl) was determined in the < 2-mm fraction, using 1:2 (v:v) soil:solution suspensions after 1 h of agitation and subsequent measurement using a Schott Handylab pH meter equipped with a BlueLine 28 pH electrode (Schott, Germany). The cation exchange capacity (CEC) was determined as the sum of the basic cations and Al extracted with 0.1 M $BaCl_2$ solution. Acid oxalate extraction was performed according to Jackson et al. (1986) (0.2 M ammonium oxalate/oxalic acid at pH 3; 1 g soil in 200 ml of solution, 2 h in the dark) in order to evaluate the amount of amorphous/less-crystalline Fe-, Al- and Mn-(hydr)oxides. As with the tailings materials, the heavy mineral fraction was separated from the soils using 1,1,2,2-tetrabromethane, and XRD was performed on both the bulk soils and heavy mineral fractions. The concentrations of TIC, TOC, and TS were determined in the soil and rock samples, which had been ground to analytical fineness. Digestions in mineral acids were performed for the soils and rocks using identical methodology as for the tailing materials.

The analytical precision of the digestion/measurement procedure was given as one relative standard deviation (RSD) from measured standard reference materials (NIST 2711a Montana soil – moderately elevated trace element concentrations) and ranged from 1 to 7% for most of the elements in total digest (the exception was Cr precision of 9.5%). The accuracy was checked using parallel digestions (n = 10) of a similar reference material, NIST 2711a and yielded values better than 15% relative standard deviation (RSD) (Table A2 in the Electronic Annex).

In a similar manner as with the mine tailings materials, the soils were chemically fractionated using BCR SEP (Rauret et al., 1999; Sutherland and Tack, 2002). The accuracy of the SEP was controlled by parallel extraction of BCR-483 certified reference material; the certified reference material (Sewage Sludge Amended Soil) was found to yield an average accuracy for Cu in the individual steps of better than 17%. (Table A2 in the Electronic Annex).

2.4. Bulk analysis of digests and solutions

The concentrations of the main cations (Al, Ca, Fe, K, Mg, Mn, Na) and trace metals/metalloids (As, Cd, Co, Cu, Pb, V, Tl, Zn) in the total digests of soils, rocks, and tailing materials, as well as in the extracts (leachates from mine tailings materials, oxalate; and $BaCl_2$ extracts from soils, extracts from individual SEP steps) were determined using either inductively coupled plasma optical emission spectrometry (ICP-OES, iCAP 6500, ThermoScientific, Germany) or quadrupole inductively coupled plasma mass spectrometry (Q-ICP-MS, Xseries^{II}, ThermoScientific, Germany) under standard analytical conditions. The concentrations of the major anions (SO_4^{2-}, PO_4^{3-}, NO_3^-, F^-, Cl^-) in the mine tailing leachate were determined using ionic chromatography (ICS 2000, Dionex, USA). The alkalinity was determined by titration to pH 4.5 end-point with 0.05 mol l^{-1} HCl, using a Schott Titroline Easy (Schott, Germany) automatic titrator. Digestions were performed in duplicate.

2.5. Cu and Pb isotope analysis

The digests were used for the analyses to determine the isotope compositions of Cu and Pb after the separation steps. Copper was separated from the sample matrix using a slightly modified anion exchange chromatography procedure (Maréchal et al., 1999; Albarède, 2004; Dong et al., 2013). Samples were separated in Poly-Prep prefilled chromatography columns (Bio-Rad, AG1-X8 resin, chloride form, 200–400 mesh, 9 cm high, 2 ml resin), Bio-Rad catalogue number 7316212. After cleaning with 20 mL of 2% HNO_3, the resin was transformed into Cl^- form with 20 ml of 6 N ultrapure HCl (ROMIL-UpA™, ROMIL, UK) divided into two equal doses. A sample aliquot of 1 μg was reduced to dryness and then dissolved in 1 ml of HCl; then it was evaporated again and redissolved in another 1 ml of 6 N HCl + 0.001% H_2O_2. The sample was carefully loaded onto the column and the sample matrix was eluted with the first 4 ml of 6 N HCl + 0.001% H_2O_2. Then the matrix was washed out from the column with 4 ml 5 N HCl, and the Cu was subsequently eluted with 20 ml 5 N HCl. The pure Cu fraction was evaporated to dryness and dissolved in 5 ml 2% HNO_3. After this step, the column was cleaned with 0.5 N HNO_3 (ROMIL-UpA™, UK). The isotope composition of Cu was measured using a multi-collector inductively coupled plasma mass spectrometer (MC-ICP-MS Neptune and Neptune plus, Thermo Fisher Scientific, Germany) located at the Czech Geological Survey in Prague, and Faculty of Science in two repeated separations for each of the prepared solutions. The detector configuration layout was as follows: ^{60}Ni – L2, ^{61}Ni – L1, ^{62}Ni - C, ^{63}Cu - H1, ^{65}Cu – H2. The Cu concentration in the pure fraction and the contents of Na, K, Mn, Mg Fe and Ti were checked once again using Q-ICP-MS. The separation was repeated if the recovery of the Cu fraction was below 95% and the Ti/Cu ratio exceed a value of 0.05. Mass bias drift was eliminated using a Ni inter-element correction, where the ^{62}Ni/^{60}Ni isotope ratio is related to the raw ^{65}Cu/^{63}Cu data by the exponential mass-dependent fractionation law. For inter-element correction the SRM, NIST 986 Ni was added to all the samples and standards after purification, in equimolar ratios of the ^{63}Cu and ^{60}Ni isotopes. For the correction, the certified value of 0.1386 for the ^{62}Ni/^{60}Ni isotope ratio was used.

In this study, the isotope composition of Cu is presented as a delta notation:

$$\delta^{65}\mathrm{Cu}\ (‰) = (\mathrm{R_{measured}}/\mathrm{R_{standard}} - 1)^* 1000 \quad (1)$$

where the "R" values are the ^{65}Cu/^{63}Cu isotope ratios and the "measured" and "standard" indexes refer to the raw isotope data of an unknown sample and the ERM®-AE633 standard (Institute for Reference Materials and Measurements, IRMM, Belgium), respectively.

The mass bias on the Neptune spectrometer was corrected by sample-standard bracketing with ERM®-AE633 because the commonly used SRM NIST 976 (Cu) is not currently commercially available. The typical analytical sequence consisted of measuring the ERM®-AE633 standard after each fifth unknown sample. A blank solution containing 2% HNO_3 was measured before each sample solution. The total procedural blank for Cu isotope measurement was 4.8 ng ± 6.1 (2SD). This represents < 1% of the total Cu in the analyzed aliquots. The results for δ^{65}Cu in the analyzed standard reference materials are given in Table A2 in the Electronic Annex. Typical precision (external reproducibility) for the three replicates of BCR-2 certified reference material (Columbia River Basalt, USGS) was better than 0.08 (2SD).

The isotope compositions of Pb in the digests were determined from

solutions diluted to concentrations of < 10 μg L^{-1} Pb using Q-ICP-MS, under analytical conditions described elsewhere (Mihaljevič et al., 2011). Correction for the mass bias was performed using SRM NIST 981 (Common Lead) between measurements of the individual samples. The accuracy of the Pb isotope measurements was controlled by using repeated digestion and measurement of the BCR-2; this was in good agreement with the information values published by Wilson (1997) (< 0.5% RSD; Table A2 in the Electronic Annex). The isotope composition of Pb was also determined in the individual SEP fractions. Determinations of both the elemental concentration and the isotope ratio were conducted in duplicate.

2.6. Thermodynamic calculations and data treatment

The PHREEQC-2 geochemical code (Parkhurst and Appelo, 1999) was used for the speciation-solubility calculations in order to determine the element speciation in the aqueous leachates from the mine tailings materials (Table A3 in the Electronic Annex). The minteq.v4.dat thermodynamic database was used for all the calculations. STATISTICA software (StatSoft CZ, 2002, Czech Republic) was used to evaluate the data statistically, in particular for calculation of the correlation coefficients between the individual parameters. The Cu and Pb concentrations in the A horizons of soils P2 to P5 and P10 to P13 were compared using the non-parametrical Mann-Whitney test. The SigmaPlot 12 graphical software (Systat Software, USA) was used for the drawing the plots and for regression curve fitting with calculation of the 95% confidence and prediction bands.

3. Results

3.1. Mine tailings

The Kombat mine tailing materials were mainly composed of carbonates [particularly Fe dolomite, $Ca(Mg,Fe)CO_3$ and calcite, $CaCO_3$], quartz (SiO_2), and goethite (FeOOH). The materials were free of primary sulphide ores and only contained small amounts of their alteration products [malachite, $Cu_2(OH)_2CO_3$ and cerussite, $PbCO_3$]. The mine tailing materials exhibited significantly higher concentrations of Cu (average 2515 mg kg^{-1}) compared to Pb (average 1013 mg kg^{-1}) (Table 1). The total concentration of the two metals increased with depth in the "wet" profile (K2); the "dry" (K1) core exhibited a decrease in their concentration at the middle part of the profile. In terms of chemical forms, Cu in the tailing materials was mostly extracted into fraction 2 during SEP (reducible fraction; average 45%), followed by: fraction 1 (acid extractable; average 29%), fraction 3 (oxidizable fraction; average 17%), and the residual fraction (average 9%). In contrast, Pb was bound in the more "labile" fractions, and its concentration gradually decreased from fractions 1 to 4 (averages 37, 32, 19, and 12%) (Table A4 in the Electronic Annex). The isotope composition of Cu ($\delta^{65}Cu$) varied from 0.144 to 0.820‰ (average 0.550, $n = 6$). The isotope compositions of Pb ($^{206}Pb/^{207}Pb$ ratio) clustered around an average of 1.150 ($n = 6$), with values varying from 1.149 to 1.153.

The leaching tests performed on the mine tailings materials indicated that the Cu concentrations varied between 17.4 and 103 μg L^{-1}, and the Pb concentrations between 21.0 and 45.3 μg L^{-1}. The PHREEQC-2 calculation of metal speciation in the leachate (K1 0–20 cm, Table A3 in the Electronic Annex) demonstrated that neutral carbonate species ($MeCO_3^0$) predominated for both of the metals studied, accounting for 85.3% (Cu) and 75.0% (Pb) of the total concentrations, respectively. The sum of the positively charged species (Me^{2+}; $MeOH^+$; $MeHCO_3^+$) accounted for 19.2% of the total Pb concentration; for Cu, these species represented only 9.9% of the total speciation (Table A3 in the Electronic Annex).

3.2. Soils

The major soil types found in the immediate vicinity, as well as at greater distances from the tailings were: (i) Luvisols (profiles P2, P4, P5, and P10) with lower CEC (6.5–24.3 $cmol^+ kg^{-1}$), lower pH (pH_{H2O} 5.7–8.2, pH_{KCl} 5.1–7.4), and higher total Fe concentration (1.7–1.9 wt %); (ii) Chernozems (profiles P3 and P11), soils with higher CEC (17–39 $cmol^+ kg^{-1}$), mainly resulting from the higher total carbon content (2.6–5.3 wt%) and higher pH (pH_{H2O} 7.8–8.5, pH_{KCl} 7.1–7.7); and (iii) transition types having some basic properties similar to Chernozems (Kastanozem, profile P13) and Luvisols (profile P12) (Table 2, Table A5 in the Electronic Annex). Most of the soils had from neutral to slightly alkaline pH values ($pH_{H2O} \approx 7.0–8.5$); only profile P10 (Luvisol) exhibited $pH_{H2O} < 6.2$. The sandy fraction predominated in the soils (average 54%) (Table 2). Soil granulometry influenced by deposition from tailings can be clearly observed only in soil profile P5. Top soil horizon A is highly enriched in a sand fraction compared to lower lying horizons. The TOC concentration in the soils varied in the range from 1.75 to 35.3 g kg^{-1}, with higher values in the uppermost soil horizons.

The mineralogical composition of the soils is rather uniform, with quartz (SiO_2) predominating, plus minor amounts of: kaolinite [$Al_2Si_2O_5(OH)_4$], muscovite/illite [$KAl_2Si_3AlO_{10}(OH)_2/(K,H_3O)Al_2Si_3AlO_{10}(OH)_2$], Mg calcite ($(Ca,Mg)CO_3$), chlorite [$(Mg,Al)_6(Si,Al)_4O_{10}(OH)_8$], and hematite ($Fe_2O_3$) (Table 2).

The total concentrations of Al, Fe, and Mn exhibited similar

Table 1
Total concentrations of Fe, Mn, Cu and Pb, $\delta^{65}Cu$ (‰, mean and 2 standard deviations), $^{206}Pb/^{207}Pb$ and $^{208}Pb/^{206}Pb$ ratio (mean and standard deviation), and mineralogical composition of the tailing materials.

Sample	Depth	Fe_{tot}	Mn_{tot}	Cu	$\delta^{65}Cu$	2SD	Pb	$^{206}Pb/^{207}Pb$	SD	$^{208}Pb/^{206}Pb$	SD
	(cm)	(mg kg^{-1})	(mg kg^{-1})	(mg kg^{-1})	(‰)		(mg kg^{-1})				
K1 wet	0–20	4174	3811	1711	0.67	0.06	552	1.153	0.003	2.113	0.007
	40–60	4452	5335	2625	0.82	0.06	827	1.152	0.003	2.107	0.005
	160–180	13,370	4038	4794	0.38	0.06	1904	1.151	0.003	2.107	0.006
K2 dry	0–20	7965	4349	1851	0.68	0.06	989	1.148	0.003	2.114	0.009
	40–60	5670	2810	1199	0.61	0.06	689	1.150	0.004	2.119	0.006
	160–180	4921	3664	2915	0.14	0.06	1120	1.149	0.004	2.119	0.004
Sample	Depth	TC[a]	TS[b]	Mineralogy							
	(cm)	(%)	(mg kg^{-1})								
K1 wet	0–20	9.37	< 100	Fe-dolomite, calcite, quartz, apatite, malachite, hematite rutile, muscovite							
	40–60	10.2	< 100	Fe-dolomite, calcite, quartz, goethite, malachite, hematite, muscovite							
	160–180	10.1	< 100	goethite, apatite, malachite, Fe-dolomite, calcite, quartz, hematite, rutile, muscovite							
K2 dry	0–20	10.3	200	Fe-dolomite, calcite, goethite, apatite, malachite, quartz, hematite, muscovite							
	40–60	8.97	100	Fe-dolomite, apatite, calcite, goethite, quartz, rutile, malachite, hematite, muscovite, cerusite							
	160–180	9.23	300	fe-dolomite, apatite, calcite, quartz, rutile, cerusite, goethite, malachite, hematite, muscovite							

[a]TC = total inorganic carbon; [b] TS = total sulphur.

Table 2
Selected properties of the studied soils.

Code	Horizon	Depth	Clay	Silt	Sand	CEC[a]	pH_{H2O}	pH_{KCl}	Mn_{tot}	Mn_{ox}	Fe_{tot}	Fe_{ox}	Al_{ox}	TOC[b]	TIC[c]	TS[d]	Mineralogy[e]
		(cm)	(%)	(%)	(%)	(cmol + kg^{-1})			(mg kg^{-1})	(mg kg^{-1})	(mg kg^{-1})	(mg kg^{-1})	(mg kg^{-1})	(mg kg^{-1})	(mg kg^{-1})	(mg kg^{-1})	
P2 - Cutanic Luvisol	Ap	0–20	24.2	24.4	51.4	19.5	7.3	6.5	2050	1670	24,500	923	906	15,800	< 100	121	Qz, Kln, Ms./Ilt
Manganiferric Chromic Siltic	AB	20–40	28.2	23.4	48.4	17.3	7.4	6.7	2990	1210	28,300	963	954	6580	< 100	63.5	
Irrigated, contaminated	Bt1	40–60	31.0	22.3	46.8	20.0	7.2	6.3	1750	1200	29,500	877	1053	4670	< 100	57.9	
	Bt2	60–110	31.7	19.4	49.0	20.0	7.2	6.6	1780	1100	29,800	661	917	4600	< 100	49.3	
	BC	110–140	32.9	19.0	48.1	20.8	7.3	6.7	3710	1150	31,600	717	1001	3340	< 100	48.4	
	C	> 140	30.7	17.4	52.0	24.3	7.0	6.0	4160	4210	31,500	910	1044	3300	< 100	39.9	Qz, Ms./Ilt, Kln, Ttn
P3 - Petrocalcic Chernozem	Ap	0–20	9.1	34.5	56.4	29.3	7.8	7.1	690	421	18,100	541	1169	22,300	3810	12.5	Qz, Mg Cal, Kln, Cl, Ms./Ilt
Irrigated, contaminated	A	20–45	10.8	34.9	54.3	30.5	8.0	7.2	639	370	19,600	390	1367	18,600	7470	371	
	AC	45–60	27.9	30.2	42.0	27.0	7.9	7.2	789	250	19,000	485	1724	19,300	25,400	5.50	Qz, Ms./Ilt, Cal
P4 - Cutanic Luvisol	Ap	0–25	4.9	13.9	81.1	6.5	8.2	7.4	2260	1100	12,000	664	304	5990	53.2	< 50	Qz, Ms./Ilt, Kln
Chromic	Bt1	25–65	9.0	13.2	77.7	7.5	8.2	7.4	5250	2060	22,200	847	514	2340	< 100	< 50	
Irrigated, contaminated	Bt2	65–90	10.8	16.6	72.6	8.0	8.1	7.3	5740	1870	21,900	827	569	1980	< 100	< 50	
	BC	90–120	12.2	20.7	67.1	11.0	8.0	7.3	9320	2040	31,800	664	514	1750	< 100	< 50	Qz, Ms./Ilt, Kln
P5 - Cutanic Luvisol	O	1–0	2.6	41.2	56.2	9.3	7.9	7.3	2830	666	12,300	601	177	35,300	43,500	43,700	Qz, Ms./Ilt, Cal, Dol
Manganiferric Chromic	Ae	0–20	6.8	27.8	65.4	11.3	7.9	7.1	964	755	15,200	405	367	4200	5421	481	
Not irrigated, contaminated	Bt1	20–60	17.0	26.2	56.7	15.3	7.8	7.2	671	399	27,100	687	777	4790	< 100	< 50	
	Bt2	60–100	17.8	27.6	54.6	13.8	8.0	7.2	690	396	27,000	748	867	3670	< 100	< 50	
	BC	100–140	19.8	21.1	59.2	14.5	7.4	6.7	602	354	26,700	640	828	3000	< 100	< 50	
	C	> 140	24.9	20.8	54.3	14.8	6.5	6.0	645	341	26,800	583	705	2570	< 100	< 50	Qz, Ms./Ilt, Kln
P10 - Cutanic Luvisol	A	0–10	15.1	31.2	53.7	17.3	6.1	5.6	840	428	50,000	801	468	21,100	< 100	< 50	Qz, Mg cal, Kln, Hem
Not irrigated, uncontaminated	Bt1	10–40	37.6	11.8	50.6	21.3	5.7	5.1	783	514	60,200	2230	1064	9500	< 100	< 50	
	Bt2	40–80	22.6	26.3	51.1	22.3	5.7	5.8	722	418	62,400	1630	1007	6600	< 100	< 50	
	BC	80–100	33.6	23.1	43.3	18.5	6.2	5.4	733	407	66,100	1340	999	5160	< 100	< 50	Qz, Ms./Ilt, Kln, Ttn, Hem, Gth
P11 - Calcic Chernozem	Ac1	0–40	21.0	32.9	46.2	22.3	8.4	7.6	488	72	19,130	156	670	12,600	18,000	17,800	Qz, Mg cal, Kln, Ms./Ilt
Not irrigated, uncontaminated	Ac2	40–60	31.2	29.4	39.5	17.3	8.5	7.7	642	52	18,270	102	438	13,500	31,200	31,200	
	AC	60–70	5.5	33.8	60.8	38.5	8.3	7.6	916	104	17,455	160	740	13,900	39,400	39,400	Qz, Ms./Ilt, Ttn
P12 - Cutanic Luvisol	A	0–25	26.8	24.0	49.2	22.3	7.0	6.1	497	295	34,700	893	900	11,600	< 100	< 50	Qz, Ms./Ilt, Ttn
Not irrigated, uncontaminated	Bt	25–65	37.6	19.4	43.0	34.0	7.2	6.4	477	268	47,900	1320	1853	9400	< 100	< 50	
	BC	65–75	41.3	21.0	37.7	37.0	7.4	6.9	995	446	57,300	1370	1814	9680	< 100	< 50	Qz, Ms./Ilt, Kln
P13 - Kastanozem	A	0–30	31.2	20.7	48.1	33.5	7.5	6.9	434	197	34,400	1400	1261	18,300	< 100	77.4	Qz, Ms./Ilt, Dol, Kln, Ttn
Not irrigated, uncontaminated	Bt	30–60	24.9	23.5	51.6	39.8	7.6	6.9	475	236	39,900	1220	1573	10,400	< 100	< 50	
	BC	> 60	29.7	24.7	45.6	39.3	7.5	6.9	540	330	40,700	1310	1861	10,500	< 100	< 50	Qz, Ms./Ilt, Kln

[a]CEC = cation exchange capacity; [b] TOC = total organic carbon; [c] TIC = total inorganic carbon; [d] TS = total sulphur.
[e]Abbreviations of minerals: Qz, quartz; Kln, kaolinite; Mg cal, Mg calcite; Ms./Ilt, muscovite/illite; Ttn, titanite; Dol, dolomite; Hem, hematite; Gth, goethite.

Table 3
Bulk concentrations of Cu and Pb, δ^{65}Cu (‰, mean and 2 standard deviations), ^{206}Pb/^{207}Pb and ^{208}Pb/^{206}Pb ratio (mean and standard deviation) in the studied soil profiles.

Soil	Horizon	Cu (mg kg^{-1})	δ^{65}Cu (‰)	2SD	Pb (mg kg^{-1})	^{206}Pb/^{207}Pb	SD	^{208}Pb/^{206}Pb	SD
P2- Cutanic Luvisol Manganiferric Chromic, Siltic, irrigated, contaminated	Ap	64.1	0.05	0.06	69.7	1.170	0.004	2.085	0.007
	AB	85.5	0.00	0.06	78.8	1.167	0.003	2.091	0.006
	Bt1	61.5	−0.13	0.06	68.5	1.171	0.003	2.083	0.006
	Bt2	66.1	−0.08	0.06	69.2	1.169	0.003	2.088	0.005
	BC	70.8	−0.05	0.06	77.4	1.172	0.002	2.085	0.004
	C	75.5	−0.13	0.06	102	1.172	0.002	2.089	0.002
P3 - Petrocalcic Chernozem, irrigated, contaminated	Ap	51.5	0.11	0.06	41.6	1.166	0.004	2.086	0.008
	A	48.7	0.07	0.06	39.2	1.169	0.004	2.084	0.007
	AC	44.5	0.00	0.06	38.5	1.168	0.005	2.085	0.005
	rock	23.0	−1.03	0.06	35.8	1.179	0.002	2.090	0.006
P4 - Cutanic Luvisol Chromic, irrigated, contaminated	Ap	92.9	0.26	0.06	69.6	1.157	0.003	2.104	0.005
	Bt1	117	0.12	0.06	87.9	1.162	0.003	2.102	0.008
	Bt2	115	0.18	0.06	81.8	1.160	0.002	2.102	0.005
	BC	201	0.38	0.06	183	1.162	0.002	2.100	0.006
Ferromanganese nodules		402	0.46	0.06	482	1.159	0.003	2.106	0.005
P5 - Cutanic Luvisol Manganiferric Chromic, not irrigated, contaminated	O	757	0.56	0.06	815	1.150	0.003	2.113	0.003
	Ae	81.6	0.42	0.06	57.5	1.166	0.004	2.089	0.005
	Bt1	55.7	0.22	0.06	45.9	1.172	0.006	2.077	0.006
	Bt2	55.3	0.08	0.06	47.3	1.176	0.003	2.073	0.009
	BC	57	0.14	0.06	49.6	1.172	0.004	2.081	0.008
	C	58.5	0.03	0.06	47.9	1.174	0.004	2.080	0.007
P10 - Cutanic Luvisol, not irrigated, uncontaminated	A	34.6	−0.04	0.06	23.2	1.202	0.005	2.049	0.007
	Bt1	41.2	0.05	0.06	24.4	1.211	0.005	2.032	0.005
	Bt2	42.2	0.08	0.06	25.4	1.206	0.004	2.035	0.009
	BC	45.3	0.11	0.06	28.2	1.207	0.002	2.039	0.006
P11 - Calcic Chernozem, not irrigated, uncontaminated	Ac1	24.0	−0.10	0.08	30.5	1.175	0.002	2.078	0.006
	Ac2	22.5	−0.10	0.08	26.2	1.178	0.003	2.073	0.007
	AC	21.9	−0.10	0.08	26.1	1.178	0.004	2.069	0.008
	rock	26.3	−0.77	0.08	23.4	1.181	0.002	2.081	0.004
P12 - Cutanic Luvisol, not irrigated, uncontaminated	A	28.6	−0.32	0.06	18.6	1.189	0.003	2.062	0.007
	Bt	40.0	−0.36	0.08	21.4	1.193	0.004	2.053	0.011
	BC	54.1	−0.24	0.06	28.2	1.191	0.005	2.058	0.006
P13 – Kastanozem, not irrigated, uncontaminated	A	36.5	−0.24	0.06	34.6	1.161	0.002	2.109	0.004
	Bt	35.8	−0.37	0.06	20.7	1.192	0.005	2.056	0.007
	BC	38.3	−0.32	0.06	22.5	1.187	0.005	2.063	0.008

distribution patterns, with a general concentration increase with depth (with the exception of Chernozems and Luvisol profile P5) (Table 2 and Table A5 in the Electronic Annex). Selective oxalate extraction indicated that only a small part of the total Al and Fe corresponded to amorphous and/or low-crystalline oxides (< 6%; the average for both Al and Fe was 3%) (Table 2). In contrast, oxalate-extractable Mn corresponded to 8–99% of the total Mn content (average for all soils 50%) (Table 2). Abundant ferromanganese concretions (diameters 0.2–1.5 cm), containing 6.6 wt% MnO and 7.25 wt% Fe_2O_3 were also observed at the base of profile P4; these nodules were composed of quartz, rancieite (a birnessite group-mineral with the composition $(Ca,Mn)Mn_4O_9{\cdot}3H_2O$), todorokite ($NaMn_6O_{12}{\cdot}3H_2O$), goethite, and kaolinite.

Based on statistical comparison of the total concentrations of Cu and Pb in the A horizons of the soils (Mann-Whitney test), we divided the soil profiles into “contaminated” in the immediate vicinity of the tailings dams (P2 to P5), and “uncontaminated”, which corresponded to profiles at greater distances from the tailings (P10-P13). The total Cu contents in the contaminated soils varied in the range from 44.5 to 757 mg kg^{-1} (average 75.0 mg kg^{-1}, O horizon P5 was not included in the calculation of the average), whereas, uncontaminated soils yielded significantly lower Cu concentrations (range 21.9–54.1; average 35.1 mg kg^{-1}) (Table 3; Fig. 2). The Pb concentrations in the contaminated soils varied in the range from 38.5 to 815 mg kg^{-1} (average 68.0 mg kg^{-1}, O horizon P5 was not included in the calculation of the average); substantially lower values were found in soils from uncontaminated areas (18.6–34.6 mg kg^{-1}; average 25.3 mg kg^{-1}) (Table 3; Fig. 2). Whereas Chernozems (and also Kastanozem) either have their maximum Cu and Pb concentrations in the upper horizons or the two metals are evenly distributed throughout the entire profile, Luvisols from both contaminated and uncontaminated areas exhibited higher Cu and Pb concentrations in the lower horizons (Table 3; Fig. 2). The only exception was Luvisol profile P5 sampled in an uncultivated (unirrigated) area in the immediate vicinity of the mine tailings, which was overgrown by bush (grass, acacia), where the maximum Cu and Pb concentrations occurred in the uppermost horizon O (757 and 815 mg kg^{-1}, respectively).

Most Cu from contaminated soils was extracted in fraction 4 (residual: 55%), followed by: fraction 2 (reducible: 24%), fraction 3 (oxidizable: 17%), and finally fraction 1 (acid extractable: 4%) (Fig. 3; Table A6 in the Electronic Annex, averages for soils P2–P5). The selective extractability of Cu from uncontaminated soils gradually decreased in fractions 4, 3, 2 and 1 (65%, 21%, 13% and 1%, respectively) (Fig. 3; Table A6 in the Electronic Annex, averages for samples P10–P13). The chemical forms of Pb were similar for soils from both contaminated and uncontaminated areas, with predominant binding in fraction 2 (reducible), followed by: fractions 4, 3, and 1 (71%, 16%, 11% and 2% in the contaminated soils, and 48%, 28%, 23% and 1% in the uncontaminated soils) (Fig. 3; Table A6 in the Electronic Annex). The SEP results indicated that, in contrast to Pb, more Cu was bound in a “labile” pool (exchangeable/acid-extractable fraction 1), especially in contaminated soils. While the “labile” Cu concentration in the uncontaminated soils corresponded to a maximum value of 1.10 mg kg^{-1} (2.67% of total Cu, sample P10, BC horizon), it attained a maximum value of 83.8 mg kg^{-1} (11.7% of total Cu, sample P5, O horizon) in the contaminated soils (Fig. 3; Table A6 in the Electronic Annex). The maximum concentration of “labile” Pb was 0.51 mg kg^{-1} (1.71% of total Pb, sample P10, BC horizon) in the uncontaminated soils and

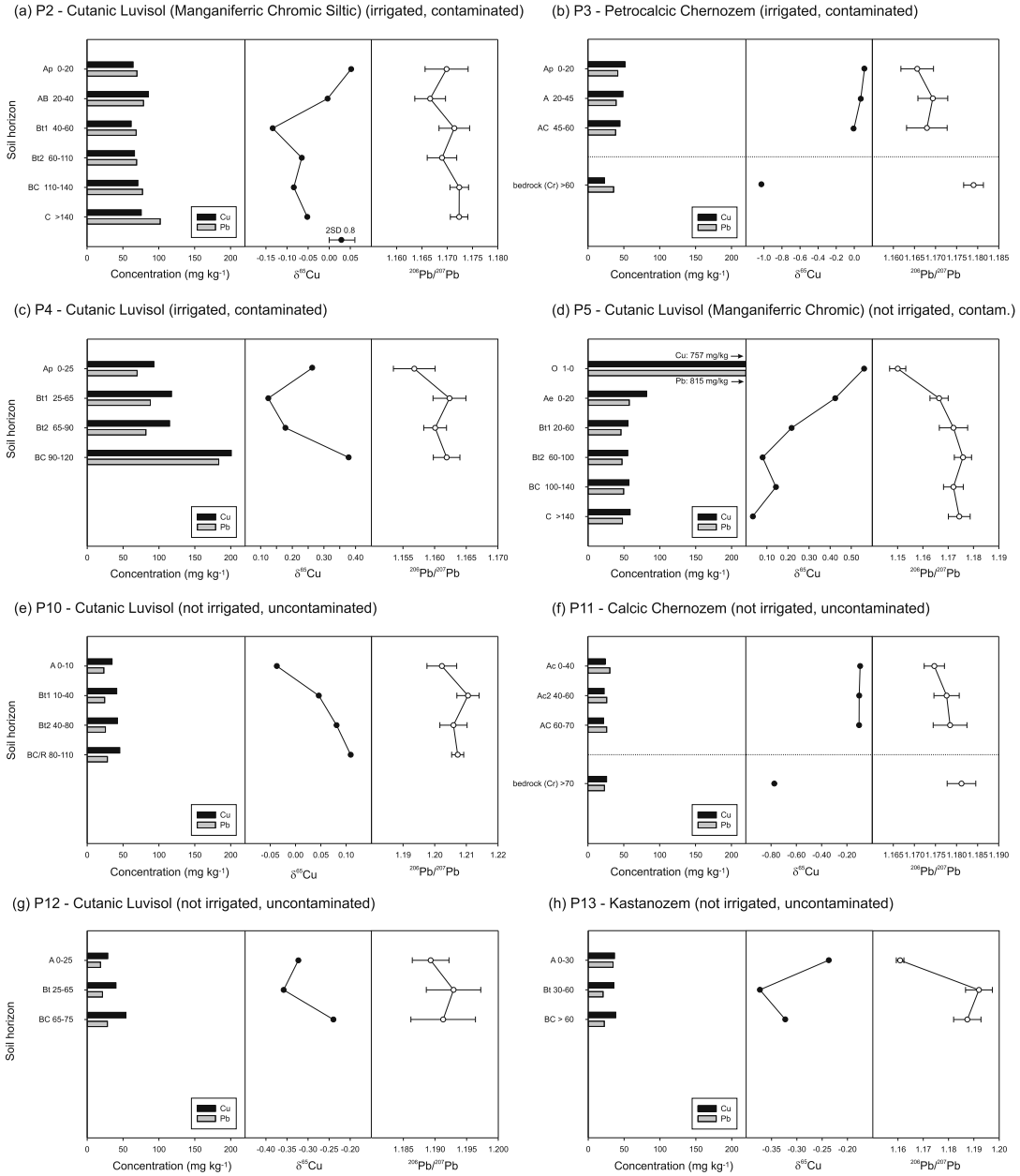

Fig. 2. Total concentrations of Cu a Pb, δ^{65}Cu (‰) and ^{206}Pb/^{207}Pb ratios in the studied soils. Values are given as the mean and SD from duplicate analyses.

equalled 65.2 mg kg^{-1} (8.56% of total Pb, sample P5, O horizon) in the contaminated soils (Fig. 3; Table A6 in the Electronic Annex).

Carbonates, taken as bedrocks from profiles P3 and P11 (Chernozems) and from rock materials from the drill cores in the Kombat area, contained isotopically light Cu (δ^{65}Cu = −1.08 to −0.37‰) (Tables 3 and 4). The δ^{65}Cu in the contaminated soil samples varied in the range from −0.134 to +0.561‰ (Table 3; Fig. 2). The value of δ^{65}Cu in the uncontaminated soils varied in the range − 0.373 to +0.109‰ (Table 3; Fig. 2). Whereas Chernozems exhibited a uniform Cu isotope composition as a function of depth, more complicated Cu isotope patterns were observed for Luvisols (Fig. 2; Table 3). In contaminated Luvisols, either a general decrease in δ^{65}Cu (profiles P2 and P5) or a decrease in δ^{65}Cu only in the central part of the profile (P4) was observed (Fig. 2; Table 3). The ^{206}Pb/^{207}Pb ratio, most often used in pollution tracing in the environmental sciences (Komárek et al., 2008), varied in the range 1.156–1.172 for contaminated soils and

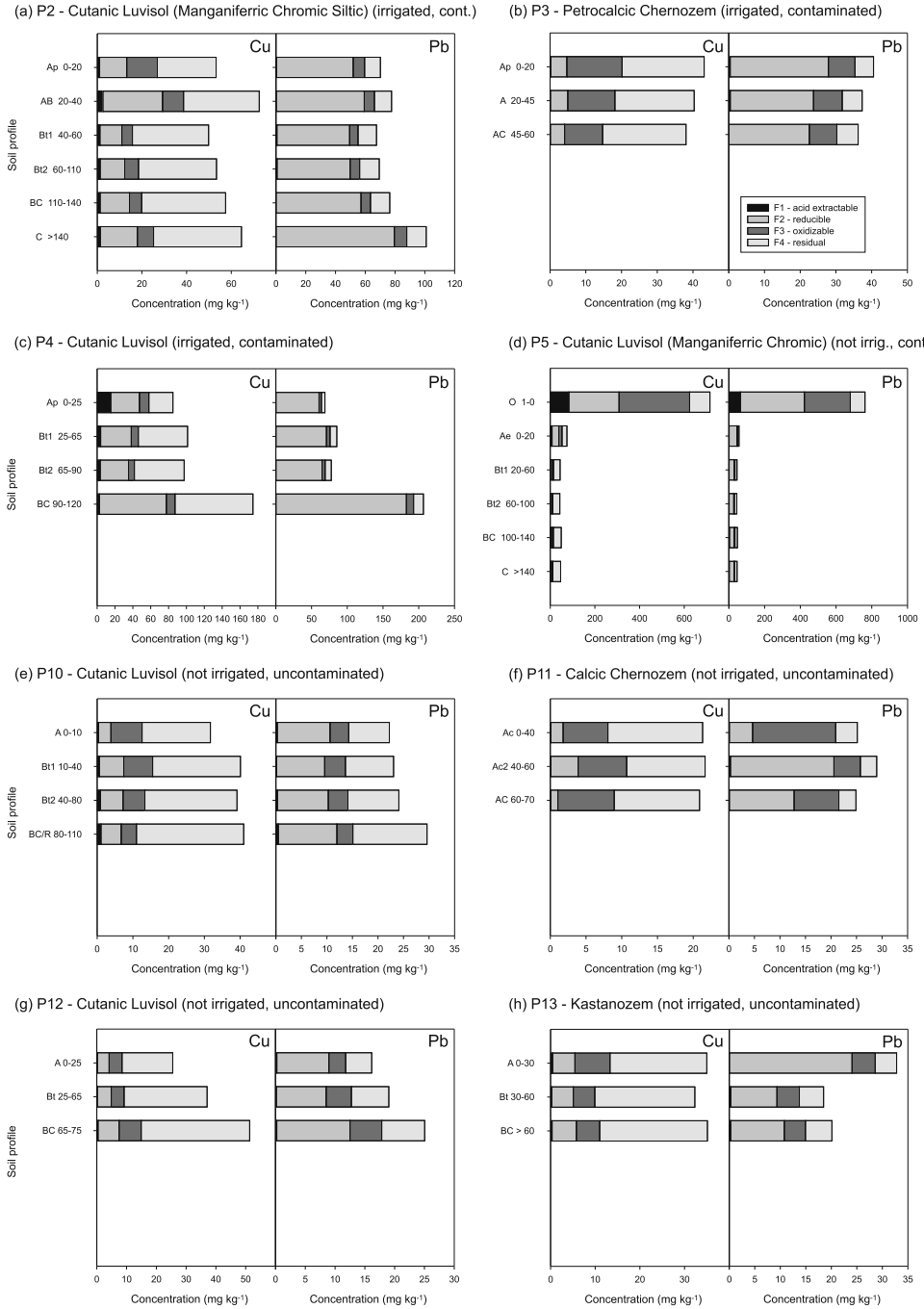

Fig. 3. Chemical forms of Cu and Pb in the studied soils as obtained by the sequential extraction procedure.

1.150–1.210 for uncontaminated soils. Similar to the Cu isotope composition, Chernozems exhibited uniform patterns as a function of depth and Luvisols generally had lower $^{206}Pb/^{207}Pb$ ratios in the uppermost portions of the profiles, with slightly increasing values as a function of depth (Fig. 2; Table 3).

4. Discussion

4.1. Distribution and chemical forms of Cu and Pb in soils

The character of soil contamination in the vicinity of mining and

Table 4
Bulk concentrations of Mn, Fe, Cu, Pb, δ^{65}Cu (‰, mean and 2 standard deviations), $^{206}Pb/^{207}Pb$ ratio, and $^{208}Pb/^{206}Pb$ (mean and standard deviation) in rocks from the Kombat area, and bedrocks of profiles P3 and P11.

Rock	Borehole	Mn (mg kg $^{-1}$)	Fe (mg kg $^{-1}$)	Cu (mg kg $^{-1}$)	δ^{65}Cu (‰)	2SD	Pb (mg kg $^{-1}$)	$^{206}Pb/^{207}Pb$	SD	$^{206}Pb/^{206}Pb$	SD
Calcareous dolostone	KBK 1 mine	1817	241	20.7	−0.98	0.08	80.9	1.149	0.003	2.128	0.004
Dolostone (laminated)	HFW 195/2 mine	216	164	1.44	−0.43	0.08	4.58	1.175	0.007	2.077	0.011
Oolitic limestone	HFW 195/2 mine	2555	707	7.05	−1.06	0.08	8.85	1.158	0.004	2.105	0.008
Dolomitic limestone (oolitic)	AW 86E 744 m	1218	1400	2.29	−1.08	0.08	3.5	1.212	0.003	1.999	0.006
Calcareous dolostone	AFM 195/2148 m Soil profile	1826	773	12.9	−0.37	0.08	3.75	1.244	0.004	1.950	0.004
Limestone	P3	4203	15,250	23	−1.03	0.08	35.8	1.179	0.002	2.074	0.005
Magnesium limestone	P11	1963	1193	26.3	−0.77	0.08	23.4	1.181	0.003	2.081	0.004

metallurgical facilities is dependent on the types of soils, the characteristics of the vegetation and also the land use, including irrigation and its intensity (e.g. Sterckeman et al., 2000). The Cu and Pb levels in soils in the vicinity of Kombat are presumably derived from their contents in the local rocks (Table 4) – rocks and soils have the same contents of Cu and Pb. Another source of metals in the soils consists in wind-dispersed materials from the tailings. Dust from the tailings settles on the surface of the soils and is leached, when precipitation is higher, into the soil solutions. From the soil solutions, the mobilized metals are partially bound to the colloids of the sorbent that are present and which can move through the soil profile with the solutions.

Luvisol and Chernozem located both in the vicinity of the tailing dump and at more distant and unaffected localities are completely different types of soil. Vertical translocation of a colloidal fraction in the profile is typical for the formations of Luvisols. The Chernozems were studied for comparison and represent a soil without significant translocation of colloids in the profile.

The heavy mineral fraction of the tailing materials contained malachite and cerussite as major hosts of Cu and Pb, respectively. Corresponding to the observation of Castillo et al. (2013) in a different dry mining district in Spain, wind-blown dusts from the mine tailing dam is deposited in soils, and these metal-bearing minerals can be dissolved (they were not detected in the heavy mineral fraction of our soils, Table 2); subsequently, both metals can be released into the soil. Nevertheless, in the area studied, a portion of these metals can also be derived from intensive irrigation (especially relevant for profiles P2, P3, and P4). The mine water, which was used for agriculture in the past and which was pumped into the Grootfontain-Omatako canal, contained 0.59 mg L^{-1} Cu, 1 mg L^{-1} Mn and 1.21 mg L^{-1} Pb at the exit from the Kombat mine pipeline (Schwartz and Ploethner, 1999). After flooding of the mine, this water has been used for the irrigation of fields, mainly near the village of Kombat (K. H. van Biljon, personal communication, 2012).

An interesting feature is that the concentrations of the two metals are quite similar in the soils and do not reflect the differences observed for the tailing materials (Table 3). Although Cu predominates over Pb in the tailing materials (Table 1), its effect on the soil contamination is indicated by the extraction test (Lin, 1997). The average Cu and Pb concentrations in the tailings were 2515 mg kg^{-1} and 1013 mg kg^{-1}, respectively (Table 1). Nevertheless, the leachates obtained from the tailing materials, simulating what can happen to materials when present in a humid environment, indicate similar dissolved concentrations of Cu and Pb (K1 0–20 cm: 17.4 µg L^{-1} Cu and 21.0 µg L^{-1} Pb; Table A3 in the Electronic Annex). Similar concentrations of Cu and Pb in the extract caused similar concentrations of Cu and Pb in the soil horizons.

Moreover, on the basis of SEP carried out on soils, it is apparent that Cu is extracted from generally stronger bonds than Pb (with the predominant residual fraction), but that larger amounts of the "labile" forms were observed for Cu compared to Pb (Fig. 3). Based on sequential extractions, Sipos et al. (2008) reported for Calcic and Haplic Luvisols that Cu has a general tendency to be bound to clay minerals (and can thus be extracted in the exchangeable fraction); whereas Pb prefers bonding to Fe oxides, which is in agreement with our results (Fig. 3). Moreover, the speciation calculation using PHREEQC-2 indicated that Cu forms neutral complexes to a greater extent than Pb (Table A3 in the Electronic Annex). Neutral complexes can be substantially more mobile, because they are not adsorbed onto the charged surfaces of inorganic sorbents and soil organic matter (Appelo and Postma, 2005). Therefore, Pb, which to a greater degree forms positively charged complexes (Pb: 19.2% of the total concentration; Cu: 9.9% of the total concentration; Table A3 in the Electronic Annex), can be more efficiently retained by adsorption onto the negatively charged surfaces of clay minerals, and also oxides or soil organic matter under the given pH conditions (Appelo and Postma, 2005). Higher affinities of Pb towards binding to soil constituents compared to Cu were also observed by Sipos (2009) for a Calcic Luvisol profile. In relation to the ionic diameters of Cu^{2+} (0.87 Å) and Pb^{2+} (1.43 Å) and the kinetics of the actual sorption on inorganic sorbents and soil organic matter, a difference has previously been observed between the two metals in their binding strength (Cu > Pb) compared to their sorption intensity (Pb > Cu) (Scheinost et al., 2001; Shi et al., 2013).

Both metals exhibit a marked affinity for bonding to Fe and Mn oxides (fraction 2 of the SEP) (Fig. 3; Table A6 in the Electronic Annex). The strong binding of these two metals to various Fe and Mn oxides has been extensively studied during the last two decades using a combination of different analytical methods (e.g. Matocha et al., 2001; Scheinost et al., 2001). Fig. 4 shows the statistically significant relationship between total Mn concentration and metals in the soil (the uppermost horizon O from profile P5 with extremely high metal concentrations was not included, because it was considered as an outlier). Ettler et al. (2017) described Fe – Mn concentric nodules (0.5–2 cm in size) in Cutanic Luvisols at this locality, which sequestered most of the contaminants. Based on the sequential extractions, Ettler et al. (2017) considered that the majority of the Cd, Ba, Co, Ni, Pb and REE is bound to Mn (oxyhydr)oxide phases, with slightly lower values for Cu and Zn, which are significantly sequestered within the Fe (oxyhydr)oxides. The SEP results of our study and the speciation calculations also agree with the fact that the sorption affinity of birnessite for Pb is significantly higher than for Cu (Wang et al., 2012). Similarly as for bulk soils and soil organic matter, greater affinity for adsorption of Pb compared to Cu was observed in competitive adsorption (e.g., Gao et al., 1997; Covelo et al., 2007; Sipos, 2009).

The subsequent fates of both metals are affected by the soil properties and pedogenetic processes. Luvisols are generally formed in more intense flushing regimes, compared to Chernozems. Leaching and intense movements of soil colloids are also effective during the development of Luvisols. While Chernozems are formed on limestone, the parent rocks of Luvisols in the Kombat area are mostly Quaternary sediments (Kříbek and Kamona, 2006). Uncontaminated Luvisols also exhibited lower pH than Chernozems, which can slightly increase the downward movement of metals. In soils with higher pH and higher basic saturation of the exchange complex (Chernozems), the colloidal

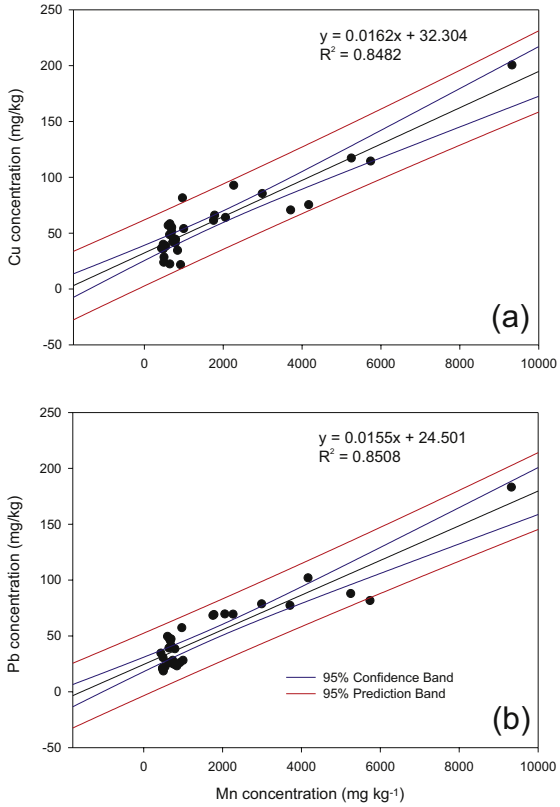

Fig. 4. Relationships between the Cu (a) and Pb (b) concentrations and total Mn.

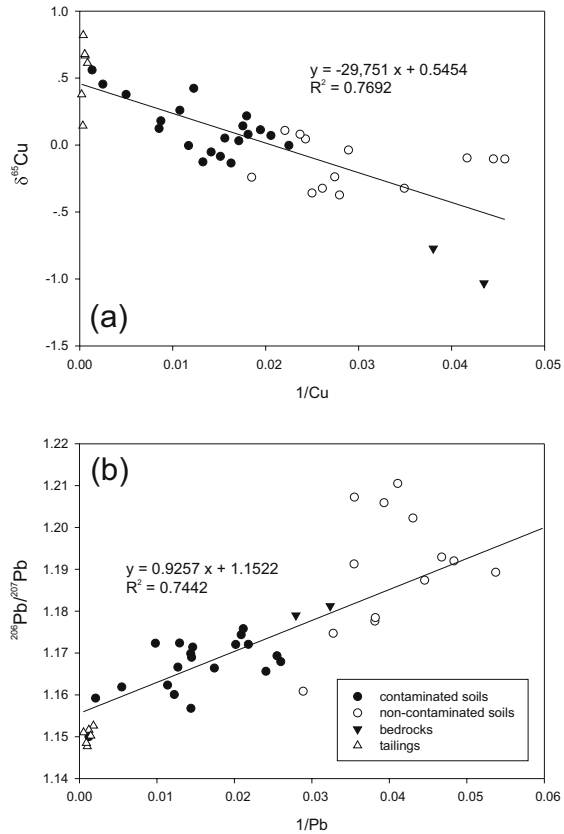

Fig. 5. a) Relationship between $\delta^{65}Cu$ and 1/Cu; b) relationship between $^{206}Pb/^{207}Pb$ and 1/Pb in soils, bedrocks, and tailing materials. Data from ore zone are not included in the figure.

fraction coagulates into larger particles. This process prevents movement of the colloidal fraction in the profile. However, in contaminated areas, the pH of the Luvisols was also controlled by carbonates from the tailings and/or the alkalinity of the water used for irrigation and the formation of neutral carbonate complexes can also influence the transport of metals in the profile. In most cases, Luvisols in both contaminated and uncontaminated areas (with the exception of profile P5 in the uncultivated area) exhibited an increase in the metal concentrations with depth. In contrast, Chernozems only exhibited slightly higher metal concentrations in the surface portions of the soil; however, both metals are more or less homogeneously distributed in the profiles below. Overall, the observed data indicate that the metal distribution patterns for both soil types could be the result of the downward migration of the metals in the soil solutions and colloids (Citeau et al., 2003).

4.2. Variations in $\delta^{65}Cu$

Variations of the isotope composition of Cu reflect both the soil type and are thus different for Luvisol and Chernozem, and are also dependent on the overall content of Cu (Fig. 5a). After eliminating outlying values (samples from the ore zone were not included in the dataset because of their heterogeneity and distance from the sampled soils), a marked linear dependence is apparent between the content of Cu and the isotope composition of Cu ($R^2 = 0.769$). This linear dependence would correspond to mixing of the two sources of Cu, where the contaminated dust derived from the tailings contains Cu predominantly in the form of the heavy isotope ($\delta^{65}Cu > 0.14‰$, Table 1) and the bedrock contains predominantly light Cu ($\delta^{65}Cu < -0.77‰$, Table 3). Nonetheless, the variation in the values of $\delta^{65}Cu$ in the soil profiles exhibits a V shape and it is thus apparent that the isotope composition of Cu affects both the mixing of Cu from the tailings and simultaneously the fractionation of the isotopes of Cu during pedogenesis of the individual profiles.

The patterns of the $\delta^{65}Cu$ values are different for the studied Luvisols and Chernozems. In most Luvisol profiles with lower Cu contents (with the exception of profile P10), the $\delta^{65}Cu$ value decreases with the depth of the profile to horizon Bt, where this value reaches a minimum. Similar trends with decrease of $\delta^{65}Cu$ from surface to deeper horizons were observed in Albeluvisol (Fekiacova et al., 2015) and Retisol (Kusonwiriyawong et al., 2017). Subsequently, the $\delta^{65}Cu$ value increases (P2, P4, P12 and P13) or $\delta^{65}Cu$ does not change substantially (P5) (Fig. 2). Profiles with higher Cu contents (P4, P5) have higher $\delta^{65}Cu$ values in the surface horizons (P5, O horizon $\delta^{65}Cu = 0.56‰$; P4 Ap horizon $\delta^{65}Cu = 0.26‰$), which can be affected by Cu contents from the tailing material material ($\delta^{65}Cu = +0.14$ to $+0.82‰$) (Table 1), but the dependence is the same as for the contamination of the only slightly affected Luvisol profiles. The formation of Luvisols is characterized by the dispersion and suspension of colloids in soil solutions in the surface horizons and their subsequent movement through the soil profile. Colloids accumulate in the pore spaces in horizon Bt, stopping or greatly retarding movement of soil solutions in the profile

(Dixit, 1978). The increase in the clay content in the Bt horizons is apparent from the clay content in the samples (Table 2).

The observed patterns δ^{65}Cu could have resulted from the following process: the surface of the soils contains Cu with characteristic δ^{65}Cu, which could correspond to the tailing materials or bedrock, which on interaction with the infiltrating water can form uncharged mobile Cu complexes, which migrate from the surface to deeper parts of the soil profiles (as also predicted by speciation calculations for the leachates, see above). When interactions occur between the water and soil particles, isotopically lighter Cu is preferentially accumulated in the solutions (as has been experimentally documented by Pokrovsky et al., 2008). The soil solutions containing isotopically light Cu move downwards and form a decreasing δ^{65}Cu pattern in this part of the profile.

The movement of the soil solutions is retarded in the Bt horizons and the mobilized Cu is bonded to the absorbents present. The intensity of the sorption in the Bt horizon is manifested in an increase in the Cu content in this and deeper parts of the profiles (Fig. 3) and the δ^{65}Cu value increases in the BC horizons of these profiles. Pokrovsky et al. (2008) calculated a similar magnitude of enrichment in ^{65}Cu through sorption of Cu on gibbsite (δ^{65}Cu 1 ± 0.25‰) and goethite (δ^{65}Cu 0.78 ± 0.2‰). Nevertheless, it is important to emphasise that we were not able to sample (and analyse) Quaternary sediments corresponding to the underlying bedrocks for Luvisols; therefore, the effect of their signature on the Cu isotope patterns in the soil profiles could not be determined. As mentioned above, the Cu concentration in the studied soils is highly correlated with the total Mn concentration (R^2 = 0.85) (Fig. 4), the amount of Mn in the oxalate extract (R^2 = 0.77), and the Mn extracted in the SEP fraction 2 (R^2 = 0.84). Increases in total Mn concentration (as well as high oxalate-extractable Mn) with depth were observed in the Luvisol profile. At the base of profile P4, we observed ferromanganese nodules which contained 400 mg kg^{-1} Cu and 480 mg kg^{-1} Pb (Table 3) and were also composed of rancieite and todorokite. Luvisol profile P4 exhibited a decrease in δ^{65}Cu from 0.26‰ (Ap horizon) to 0.12‰ (Bt1 horizon), followed by an increase to 0.38‰ in the BC horizon. Furthermore, the BC horizon was found to contain ferromanganese nodules, which exhibited even higher δ^{65}Cu values (0.46‰).

It has been demonstrated that Mn-oxide-based concretions commonly form in Mn-rich tropical soils (Dowding and Fey, 2007; Ettler et al., 2017) and precipitation of Mn oxides is especially easy in media with pH > 8 (Vodyanitskii, 2009), corresponding well to our data (Table 2). We hypothesize that the increase in δ^{65}Cu with depth in the profile could occur through intense sorption on secondary Mn oxides, with the preferential bonding of heavier ^{65}Cu.

Chernozems have a different variation of the δ^{65}Cu values in the profile. In Chernozems, uniform δ^{65}Cu values in the soil horizons are clearly distinct from the isotope signature of the underlying bedrock. This trend is typical for both contaminated and uncontaminated soils (P3 and P11, respectively). The isotope signatures of the bedrocks for profiles P3 and P11 were −1.03‰ and −0.77‰, respectively, corresponding well to the limestones from the area (Table 4). The soil horizons of chernozems had significantly higher δ^{65}Cu values. In profile P3, which was clearly affected by the tailing materials, the δ^{65}Cu values decreased from 0.11‰ (horizon Ap) to 0.0‰ (horizon AC). For profile P11, the δ^{65}Cu values clustered around −0.10‰, but also indicated that even this profile might have been slightly affected by the wind-blown tailing materials, despite its distance from the dam. Another possible explanation for the content of heavier Cu in Chernozems compared to the source carbonate materials could be the fractionation process connected with the uptake of Cu by plants. The studied Chernozems are intensely used in agriculture for growing grains. The fractionation of the Cu isotopes between the soil and a plant is accompanied by uptake of the lighter isotopes through the effect of diffusion processes, while the heavier Cu is accumulated at the root surface (Jouvin et al., 2012; Mihaljevič et al., 2018). In a study of the isotope composition of grasses in the Tsumeb area (Namibia) in a Cu-uncontaminated area, Kříbek et al. (2018) observed isotope lightening compared to the soil, where $\Delta\ \delta^{65}Cu_{plant\text{-}soil}$ = −0.15 to −0.22‰. Because the above-ground biomass containing isotopically lighter Cu is removed from the field during harvesting, in contrast to the roots, the less mobile and heavier ^{65}Cu isotope accumulates in the soil. The entire profile is then homogenized during ploughing or by uniform adsorption to yield similar δ^{65}Cu values.

4.3. Variation in the Pb isotope composition

While the basement carbonates in the Kombat area (limestone, dolomite) had variable Pb isotope compositions (^{206}Pb/^{207}Pb = 1.14–1.24), the tailing materials exhibited a very uniform Pb isotope signature (^{206}Pb/^{207}Pb = 1.14–1.15) (Tables 1 and 4). Regional pollution by Pb in Namibia (aerosol, Namib Desert) exhibits ^{206}Pb/^{207}Pb = 1.141, resulting from a combination of the Pb composition from leaded gasoline (Windhoek aerosols: ^{206}Pb/^{207}Pb = 1.076), as well as the Pb derived from the mining and metallurgy at Tsumeb (^{206}Pb/^{207}Pb = 1.143) (Bollhöfer and Rosman, 2000). The isotope composition of gasoline sampled in Tsumeb (Engen station, June 2012, Namibia leaded gasoline LRP 93) exhibited a slightly higher average ^{206}Pb/^{207}Pb = 1.150 ± 0.003 and ^{208}Pb/^{206}Pb = 2.120 ± 0.005). However, compared to the amounts and composition of the dust from the tailings in the studied area (Kříbek and Kamona, 2006), we estimate that these Pb sources can be considered to be negligible.

Fig. 5b depicts the dependence of ^{206}Pb/^{207}Pb on 1/Pb, generally used for the determination of end-members (Le Roux et al., 2008), which is linear for the given dataset (R^2 = 0.74). This mixing line has two end-members: a low ^{206}Pb/^{207}Pb ratio (~1.15), corresponding to 552–1900 mg kg^{-1} Pb (i.e. tailings); and a high ^{206}Pb/^{207}Pb ratio (1.24), corresponding to approx. 3.75 mg kg^{-1} of lithogenic Pb (Tables 1 and 4).

In most cases, Pb contamination of soils in the vicinity of important sources is primarily concentrated in the surface and subsurface horizons, dependent on the amounts of organic matter and Fe-, Mn- and Al-oxides, and also potentially dependent on the amounts and characteristics of the clay minerals (Erel, 1998; Teutsch et al., 2001; Emmanuel and Erel, 2002; Mihaljevič et al., 2011; Ettler et al., 2011). In the studied Luvisols (with the exception of profile P5), the Pb concentration increased with depth in the soil profiles, and only Chernozems and Kastanozem exhibited a slightly higher Pb content in the upper portions of the profiles (Fig. 2).

The Pb concentration, similar to that of Cu, is correlated with the total Mn concentration (Fig. 4); the Pb was found to be predominantly bound in the reducible fraction in the sequential extraction. The Pb isotope composition of most soils clustered around ^{206}Pb/^{207}Pb = 1.165 (range 1.150–1.180) (Fig. 2; Table 3). Only in the uncontaminated profiles P10 and P13 (Luvisols) and in the Bt horizon in P13 (Kastanozem), did the soil samples have ^{206}Pb/^{207}Pb ratios ranging from 1.19 to 1.21. Most soils exhibited a small difference in the ^{206}Pb/^{207}Pb ratio between the individual horizons (mostly within the analytical error of the measurements); however, this indicated a slight increasing trend as a function of depth (Fig. 2). Only the contaminated profile P5 (horizon O: ^{206}Pb/^{207}Pb = 1.15; horizon C: ^{206}Pb/^{207}Pb = 1.17) and profile P13 (horizon A: ^{206}Pb/^{207}Pb = 1.16; horizon Bt: ^{206}Pb/^{207}Pb = 1.19) exhibited larger differences within the profile. However, these two profiles were not located on cultivated land, thus the individual horizons were probably not mixed by ploughing. Smaller differences between the surface and subsurface horizons of the studied profiles could be caused by Pb with a relatively low ^{206}Pb/^{207}Pb ratio in the basement carbonates (Table 4). Profiles in (sub)tropical soils that are not affected by ploughing generally exhibit substantially greater differences in the ^{206}Pb/^{207}Pb isotope compositions between the surface and deeper horizons (Ettler et al., 2011; Mihaljevič et al., 2011).

Selected examples of the ^{206}Pb/^{207}Pb isotope ratio in the individual

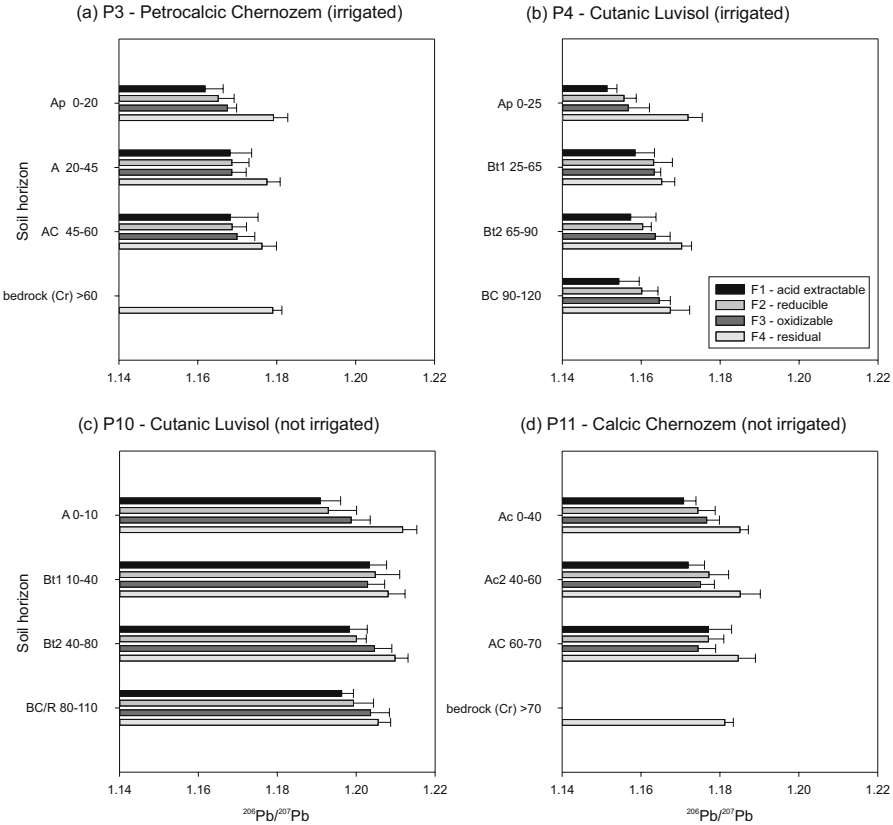

Fig. 6. Patterns of Pb isotope composition ($^{206}Pb/^{207}Pb$) in different fractions of the sequential extraction procedure and their changes with depth in selected contaminated and uncontaminated soils.

extracts of the SEP are depicted in Fig. 6 (all data are reported in Table A7 in the Electronic Annex). In contaminated and uncontaminated Luvisols and Chernozems, the value of the $^{206}Pb/^{207}Pb$ ratio increased slightly or stagnated, dependant upon the strength of the extraction agent. The contaminated soils had a lower value of the $^{206}Pb/^{207}Pb$ ratio compared to uncontaminated soils in all the fractions (Fig. 6). No noticeable differences were apparent between the surface and deeper horizons and simultaneously there were no substantial differences in the $^{206}Pb/^{207}Pb$ ratio dependant on the strength of the extraction agent. This observation is in clear contrast with other research dealing with contaminated soils in semi-arid areas, e.g. smelter-affected soils from Zambia (Ettler et al., 2011) or Mediterranean soils near roads with heavy traffic (Teutsch et al., 2001). These two studies showed clear differences in the Pb isotope composition of individual SEP fractions between the polluted topsoils and the lower parts of the profiles, which in turn contained very low Pb concentrations of anthropogenic origin, bound to "labile" fractions (expressed by lower $^{206}Pb/^{207}Pb$ ratios). However, most of the Pb in these deep soil layers was bound in the residual fraction, with a clear lithogenic character, i.e. with a higher $^{206}Pb/^{207}Pb$ ratio (Teutsch et al., 2001; Ettler et al., 2011). The observed uniform Pb isotope trends in the SEP fractions in soils from the Kombat area (Fig. 6; Table A7 in the Electronic Annex) are probably indicative of tailings-related contamination which can travel through the profiles of contaminated soils (Figs. 3 and 6). Manganese oxides are assumed to be the most efficient Pb sorbent in the studied soils (Fig. 4b). Lead in these secondary minerals can be derived either from "natural" long-term weathering of the basement rocks (whose Pb isotope signal is quite variable, see Table 4) or directly from anthropogenic (i.e. tailings-derived) contamination. During the sequential extraction, the Mn-oxide phases are presumably extracted in the reducible fraction (fraction 2) because of their high contents in the soils and also in subsequent steps in the SEP (see Tables A6 and A7 in the Electronic Annex). Thus, their signature may contribute to the subsequent $^{206}Pb/^{207}Pb$ compositions of the individual fractions.

4.4. Environmental implications

The application of isotope systems to trace contamination is one of the most exciting new areas of environmental geochemistry. Bullen and Walczyk (2009) used combined Cd–Zn isotope systems (original data from Cloquet et al., 2008 and Weiss et al., 2007) to better trace the sources of soil pollution, emphasizing the usefulness of this isotope "multitracing" in the environmental sciences, where multiple sources of pollution occur and where each of the coupled isotope systems can be useful in the understanding of distinct geochemical processes occurring in the environmental compartments. In their footsteps, we plotted the Pb–Cu isotope compositions of the studied materials in one graph (Fig. 7), which clearly demonstrates that the Pb isotope data are a convincing indication of simple mixing between the individual end-members; however, the Cu isotope compositions reflect mixing and also a combination of biogeochemical processes affecting the Cu distribution in the soils (e.g., sorption onto the soil constituents, effect of plants

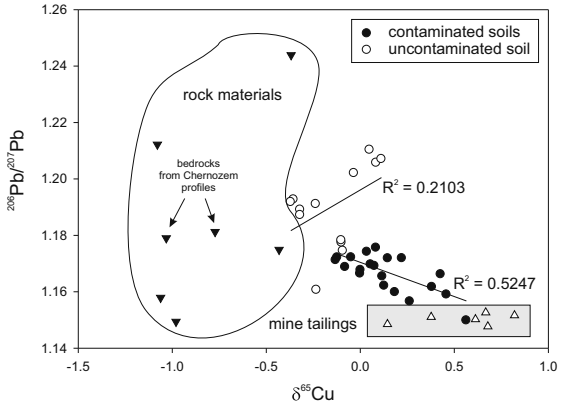

Fig. 7. Pb–Cu isotope systematics for contaminated and uncontaminated soil samples, mine tailing materials and bedrocks from Chernozem soil profiles and rock samples from boreholes in the Kombat area.

cultivated in the area). The tailing materials have a relatively uniform Pb isotope signal and the contaminated soils seem to cluster around a line connecting this source of pollution and "uncontaminated" soils/rocks. Similarly, the Cu isotope composition of the contaminated soils is also very close to the δ^{65}Cu range of the tailings (Fig. 7), indicating that tailings-related Cu occurs in most of them and confirming the fact that the Cu contaminant migrates vertically in the profile. In contrast, uncontaminated soils exhibit the opposite trend regarding Cu isotope clustering, with some samples exhibiting "tailings-derived" Cu signatures, however, mostly within the range of the background Pb isotope signal (Fig. 7). Thus, the increase in δ^{65}Cu towards higher values (the low-end signature of the tailings) may not be caused by wind-blown dust from the tailings as suggested above, but may result from other and possibly more pronounced biogeochemical processes. Another explanation for these opposite trends may be related to the contrasting behaviours of Cu and Pb in the soils (coming both from anthropogenic and geogenic sources). It has been suggested that manganese oxides play a key role in the contaminant dynamics in these semi-arid soils. The changes in the Cu isotope composition of solids and the remaining solutions during Cu sorption onto Mn oxides should be investigated experimentally in the future to better understand whether the trends in isotope fractionation are similar to those observed during Cu sorption onto Fe oxy(hydro)xides (Balistrieri et al., 2008; Pokrovsky et al., 2008). Moreover, the sorption onto omnipresent clays and the role of plants (Weinstein et al., 2011; Jouvin et al., 2012; Kříbek et al., 2018) in Cu isotope fractionation in soils should be clarified, in order to better understand the processes affecting the dynamics and biogeochemical cycles of Cu in semi-arid environments.

5. Conclusions

We studied eight soil profiles near the mine-tailings dams located near the Cu-Pb-(Zn)-Ag mine located at Kombat (Namibia) in order to understand the subsequent fates of Cu and Pb in a semi-arid soil system. The combination of bulk chemical composition, leaching/extraction tests and combined Cu and Pb isotope measurements indicated that both metals moved through the soil profiles. The migration of forms of Cu and Pb through the profile is dependent on their speciation in solutions, the character of bonding to the soil particles and also the soil type.

Copper forms more neutral complexes than Pb in the solutions formed during the interaction of water with the tailing material. It follows from soil extraction experiments that Cu is bonded more strongly in soils than Pb. As a consequence of these two phenomena, the binding strength of Cu is higher than that of Pb, but the sorption intensity of Pb is higher than that of Cu. The movement of soil colloids is apparent in Luvisols, with accumulation in the Bt horizons. The immobility of colloids in Chernozem profiles is caused by the higher pH and greater saturation of the exchange complex by basic cations. These parameters cause coagulation of colloids and their settling down as larger and immobile species. The behavior of metals and solutions in soils is manifested in the soil isotope compositions of Cu and Pb.

Whereas Luvisols were mostly characterized by an increase in Cu concentration with changing δ^{65}Cu value as a function of depth, Chernozems exhibited uniform Cu concentrations and isotope compositions in all the soil horizons, clearly contrasting with the isotopically lighter composition of the carbonate bedrocks. Whereas the Cu isotope composition of soils resulted not only from a combination of the two signatures (tailings vs. bedrock), but was also highly affected by geochemical processes (e.g., sorption to soil constituents), the Pb composition of soils is a result of simple mixing between the end-members.

Acknowledgements

This study was supported by Czech Science Foundation grant 16-13142S and by the Center for Geosphere Dynamics (UNCE/SCI/006). Part of the equipment used for this study was purchased under the Operational Programme Prague –Competitiveness (Project CZ.2.16/3.1.00/21516). We would like to thank K.H. van Biljon and E. DuToit for allowing us to take soil samples on their farms. Dr. Madeleine Štulíková and Dr. Peter Lemkin are thanked for reviewing the English in the manuscript. Dr. Richard Wanty of USGS kindly supplied the standards ERM®-AE633, ERM®-AE647 and SRM NIST 976 (Cu). A number of colleagues helped with the analytical work: Marie Fayadová and Věra Vonásková (chemical analyses and SEP), Lenka Jílková (HPLC), Ondřej Šebek (ICP-OES), František Veselovský (heavy mineral separation). The reviews of anonymous reviewers greatly assisted in improving the original manuscript.

Appendix A. Supplementary data

Supplementary data to this article can be found online at https://doi.org/10.1016/j.chemgeo.2019.03.026.

References

Albarède, F., 2004. The stable isotope geochemistry of copper and zinc. Rev. Mineral. Geochem. 55, 409–427.
Appelo, C.A.J., Postma, D., 2005. Geochemistry, Groundwater and Pollution, 2nd Edition, A. A. Balkema Publishers, Leiden.
Balistrieri, L.S., Borrok, D.M., Wanty, R.B., Ridley, W.I., 2008. Fractionation of Cu and Zn isotopes during adsorption onto amorphous Fe(III) oxyhydroxide: Experimental mixing of acid rock drainage and ambient river water. Geochim. Cosmochim. Acta 72, 311–328.
Bigalke, M., Weyer, S., Wilcke, W., 2010a. Stable copper isotopes: a novel tool to trace copper behavior in hydromorphic soils. Soil Sci. Soc. Am. J. 74, 60–73.
Bigalke, M., Weyer, S., Kobza, J., Wilcke, W., 2010b. Stable Cu and Zn isotope ratios as tracers of sources and transport of Cu and Zn in contaminated soils. Geochim. Cosmochim. Acta 74, 6801–6813.
Bigalke, M., Weyer, S., Wilcke, W., 2010c. Copper isotope fractionation during complexation with humic acid. Environ. Sci. Technol. 44, 5496–5502.
Bigalke, M., Weyer, S., Wilcke, W., 2011. Stable Cu isotope fractionation in soils during oxic weathering and podzolization. Geochim. Cosmochim. Acta 75, 3119–3134.
Bollhöfer, A., Rosman, K.J.R., 2000. Isotopic source signatures for atmospheric lead: the Southern Hemisphere. Geochim. Cosmochim. Acta 64, 3251–3262.
Borrok, D.M., Nimick, D.A., Wanty, R.B., Ridley, W.I., 2008. Isotopic variations of dissolved copper and zinc in stream waters affected by historical mining. Geochim. Cosmochim. Acta 72, 329–344.
Bullen, T.D., Walczyk, T., 2009. Environmental and biomedical applications of natural metal stable isotope variations. Elements 5, 381–385.
Castillo, S., de la Rosa, J.D., de la Campa, A.M.S., González-Castanedo, Y., Fernández-Caliani, J.C., Gonzalez, I., Romero, A., 2013. Contribution of mine waste to atmospheric metal deposition in the surrounding area of an abandoned heavily polluted mining district (Rio Tinto mines, Spain). Sci. Total Environ. 449, 363–372.
Chisholm, E.I., Sircombe, K.N., DiBugnara, D.L., 2014. Handbook of Geochronology Mineral Separation Laboratory Techniques. Record 2014/46. Geoscience Australia, Canberra. https://doi.org/10.11636/Record.2014.046.

Citeau, L., Lamy, I., van Oort, F., Elsass, F., 2003. Colloidal facilitated transfer of metals in soils under different land use. Colloids Surf. A Physicochem. Eng. Asp. 217, 11–19.
Cloquet, C.H., Carigan, J., Lehman, M.F., Vanhaecke, F., 2008. Variation in the isotopic composition of zinc I the natural environment and the use of zinc isotopes in the biogeosciences: a review. Anal. Bioanal. Chem. 390, 451–463.
Covelo, E.F., Vega, F.A., Andrade, M.L., 2007. Competitive sorption and desorption of heavy metals by individual soil components. J. Hazard. Mater. 140, 308–315.
Csavina, J., Field, J., Taylor, M.P., Gao, S., Landázuri, A., Betterton, E.A., Sáez, A.E., 2012. A review on the importance of metals and metalloids in atmospheric dust and aerosol from mining operations. Sci. Total Environ. 433, 58–73.
Dixit, S.P., 1978. Measurement of the mobility of soil colloids. J. Soil Sci. 29, 557–566.
Dong, S.F., Weiss, D.J., Strekopytov, S., Kreissig, K., Sun, Y., Baker, A.R., Formenti, P., 2013. Stable isotope ratio measurements of Cu and Zn in mineral dust (bulk and size fractions) from the Taklimakan Desert and the Sahel and in aerosols from the eastern tropical North Atlantic Ocean. Talanta 114, 103–109.
Dowding, C.E., Fey, M.V., 2007. Morphological, chemical and mineralogical properties of some manganese-rich oxisols derived from dolomite in Mpumalanga province, South Africa. Geoderma 141, 23–33.
Ehrlich, S., Ben-Dor, L., Halicz, L., 2004. Precise isotope ratio measurement by multi-collector-ICP-MS without matrix separation. Can. J. Anal. Sci. Spectrosc. 49, 136–147.
Emmanuel, S., Erel, Y., 2002. Implications from concentrations and isotopic data for Pb partitioning processes in soils. Geochim. Cosmochim. Acta 66, 2517–2527.
Erel, Y., 1998. Mechanisms and velocities of anthropogenic Pb migration in Mediterranean soils. Environ. Res. 78, 112–117.
Ettler, V., Mihaljevič, M., Komárek, M., 2004. ICP-MS measurements of lead isotopic ratios in soils heavily contaminated by lead smelting: tracing the sources of pollution. Anal. Bioanal. Chem. 378, 311–317.
Ettler, V., Mihaljevič, M., Kříbek, B., Majer, V., Šebek, O., 2011. Tracing the spatial distribution and mobility of metal/metalloid contaminants in Oxisols in the vicinity of the Nkana copper smelter, Copperbelt province, Zambia. Geoderma 164, 73–84.
Ettler, V., Chren, M., Mihaljevič, M., Drahota, P., Kříbek, B., Veselovský, F., Sracek, O., Vaněk, A., Penížek, V., Komárek, M., Mapani, B., Kamona, F., 2017. Characterization of Fe-Mn concentric nodules from Luvisol irrigated by mine water in semi-arid agricultural area. Geoderma 299, 32–42.
FAO, 2006. Guidelines for Soil Description. Food and Agriculture Organization of the United Nations, Rome.
Fekiacova, Z., Cornu, S., Pichat, S., 2015. Tracing contamination sources in soils with Cu and Zn isotopic ratios. Sci. Total Environ. 517, 96–105.
Gale, N.H., Woodhead, A.P., Stos-Gale, Z.A., Walder, A., Bowen, I., 1999. Natural variations detected in the isotopic composition of copper: possible applications to archeology and geochemistry. Int. J. Mass Spectrom. 184, 1–9.
Gao, S., Walker, W.J., Dahlgren, R.A., Bold, J., 1997. Simultaneous sorption of Cd, Cu, Ni, Zn, Pb and Cr on soils treated with sewage sludge supernatant. Water Air Soil Pollut. 93, 331–345.
Gee, G.W., Or, D., 2002. Particle-size analysis. In: Dane, J.H., Topp, G.C. (Eds.), Methods of Soil Analysis, Part 4 – Physical Methods. Soil Science Society of America, Madison, pp. 255–294.
Grösslová, Z., Vaněk, A., Oborna, V., Mihaljevič, M., Ettler, V., Trubac, J., Drahota, P., Penížek, V., Pavlů, L., Sracek, O., Kříbek, B., Voegelin, A., Göttlicher, J., Drábek, O., Tejnecký, V., Houška, J., Mapani, B., Zádorová, T., 2018. Thallium contamination of desert soil in Namibia: Chemical, mineralogical and isotopic insights. Environ. Pollut. 239, 272–280.
Hayes, S.M., Webb, S.M., Bargar, J.R., O'Day, P.A., Maier, R.M., 2012. Geochemical weathering increases lead bioaccessibility in semi-arid mine tailings. Environ. Sci. Technol. 46, 5834–5841.
Innes, J., Chaplin, R.C., 1986. Ore bodies of the Kombat mine, Sout West Africa/Namibia. In: Anhaeusser, C.R., Maske, S. (Eds.), Mineral Deposits of Southern Africa. Geological Society of South Africa, pp. 1789–1805.
Jackson, M.L., Lim, C.H., Zelazny, L.W., 1986. Oxides, hydroxides, and aluminosilicates. In: Klute, A. (Ed.), Methods of Soil Analysis, Part 1, Physical and Mineralogical Methods. Am. Soc. Agron.-Soil Sci. Soc. Am., Madison, WI, pp. 101–150 Agronomy Monograph no. 9. Chap. 6.
Jouvin, D., Weiss, D.J., Mason, T.F.M., Bravin, M.N., Louvat, P., Zhao, F., Ferec, F., Hinsinger, P., Benedetti, M.F., 2012. Stable isotopes of Cu and Zn in higher plants: evidence for Cu reduction at the root surface and two conceptual models for isotopic fractionation processes. Environ. Sci. Technol. 46, 2652–2660.
Kamona, A.F., Günzel, A., 2007. Stratigraphy and base metal mineralization in the Otavi Mountain Land, Northern Namibia-a review and regional interpretation. Gondwana Res. 11, 396–413.
Kimball, B.E., Mathur, R., Dohnalkova, A.C., Wall, A.J., Runkel, R.L., Brantley, S.L., 2009. Copper isotope fractionation in acid mine drainage. Geochim. Cosmochim. Acta 73, 1247–1263.
Komárek, M., Ettler, V., Chrastný, V., Mihaljevič, M., 2008. Lead isotopes in environmental sciences: a review. Environ. Int. 34, 562–577.
Kříbek, B., Kamona, F., 2006. Assessment of the Mining and Processing of Ores on the Environment in Mining District of Namibia. - Final Report. Czech Geological Survey, Prague (166 pp).
Kříbek, B., Majer, V., Veselovský, F., Nyambe, I., 2010. Discrimination of lithogenic and anthropogenic sources of metals and sulphur in soils of the central-northern part of the Zambian Copperbelt Mining District: a topsoil vs. subsurface soil concept. J. Geochem. Explor. 104, 69–86.
Kříbek, B., Šípková, A., Ettler, V., Mihaljevič, M., Majer, V., Knésl, I., Mapani, B., Penížek, V., Vaněk, A., Sracek, O., 2018. Variability of the copper isotopic composition in soil and grass affected by mining and smelting in Tsumeb, Namibia. Chem. Geol. 493, 121–135.
Kusonwiriyawong, Ch., Bigalke, M., Cornu, S., Montagne, D., Fekiacova, Z., Lazarov, M., Wilcke, W., 2017. Response of copper concentration and stable isotope ratios to artificial drainage in a French Retisol. Geoderma 300, 44–54.
Le Roux, G., Sonke, J.E., Cloquet, C., Aubert, D., de Vleeschouwer, F., 2008. Comment on "the biosphere: a homogeniser of Pb-isotope signals" by C. Reimann, B. Flem, A. Arnoldussen, P. Englmaier, T. E. Finne, F. Koller and Ø. Nordgulen. Appl. Geochem. 23, 2789–2792.
Lin, Z., 1997. Mobilization and retention of heavy metals in mill-tailings from Garpenberg sulfide mines, Sweden. Sci. Total Environ. 198, 13–31.
Mapaure, I., Chimwamurombe, P.M., Mapani, B.S., Kamona, F.A., 2011. Impact of mine dump pollution on plant species diversity, composition and structure of a semiarid savannah in Namibia. Afr. J. Range Forage Sci. 28, 149–154.
Maréchal, C., Albarède, F., 2002. Ion exchange fractionation of copper and zinc isotopes. Geochim. Cosmochim. Acta 66, 1499–1509.
Maréchal, C.N., Télouk, P., Albarède, F., 1999. Precise analysis of copper and zinc compositions by plasma-source mass spectrometry. Chem. Geol. 156, 251–273.
Markl, G., Lahaye, Y., Schwinn, G., 2006. Copper isotopes as monitors of redox processes in hydrothermal mineralization. Geochim. Cosmochim. Acta 70, 4215–4228.
Mathur, R., Jin, L., Prush, V., Paul, J., Ebersole, C., Fornadel, A., Williams, J.Z., Brantley, S., 2012. Cu isotopes and concentrations during weathering of black shale of the Marcellus Formation, Huntingdon County, Pennsylvania (USA). Chem. Geol. 304–305, 175–184.
Matocha, C.J., Elzinga, E.J., Sparks, D.L., 2001. Reactivity of Pb(II) at the Mn(III,IV) (hydr)oxide-water interface. Environ. Sci. Technol. 35, 2967–2972.
Mendelsohn, J., Jarvis, A., Roberts, C., Robertson, T., 2002. Atlas of Namibia: A Portrait of the Land and its People. David Philip Publishers, Cape Town.
Mihaljevič, M., Ettler, V., Šebek, O., Sracek, O., Kribek, B., Kyncl, T., Majer, V., Veselovsky, F., 2011. Lead isotopic and metallic pollution record in tree rings from the Copperbelt mining-smelting area, Zambia. Water Air Soil Pollut. 216, 657–668.
Mihaljevič, M., Jarošíková, A., Ettler, V., Vaněk, A., Penížek, V., Kříbek, B., Chrastný, V., Sracek, O., Trubač, J., Svoboda, M., Nyambe, I., 2018. Copper isotopic record in soils and tree rings near a copper smelter, Copperbelt. Sci. Total Environ. 621, 9–17.
Mileusnic, M., Mapani, B.S., Kamona, F.A., Ružičić, S., Mapaure, I., Chimwamurombe, P.M., 2014. Assessment of agricultural soil contamination by potentially toxic metals dispersed form improperly disposed tailings, Kombat mine, Namibia. J. Geochem. Explor. 144, 409–420.
Miller, R.McG., 1983. The Pan-African Damara Orogen of South West Africa/Namibia. In: Miller, R.McG. (Ed.), Evolution of the Damara Orogen of Sout West Africa/Namibia. Spec. Publ. Geol. Soc. S. Afr.pp. 431–515 11pp.
Parkhurst, D.L., Appelo, C.A.J., 1999. User's Guide to PHREEQC (Version 2) - a Computer Program for Speciation Batch-Reaction, One Dimensional Transport and Inverse Geochemical Calculations. U. S. Geological Survey Report, Denver, Colorado. pp. 99–4259.
Pokrovsky, O.S., Viers, J., Emnova, E.E., Kompantseva, E.I., Freydier, R., 2008. Copper isotope fractionation during its interaction with soil and aquatic microorganism and metal oxy(hydr)oxides: possible structural control. Geochim. Cosmochim. Acta 72, 1742–1757.
Rauret, G., López-Sanchez, J.F., Sahuquillo, A., Rubio, R., Davidson, C., Ure, A., Quevauviller, P., 1999. Improvement of the BCR three step sequential extraction procedure prior to the certification of new sediment and soil reference materials. J. Environ. Monit. 1, 57–61.
Romero, F.M., Armienta, M.A., Gonzalez-Hernandez, G., 2007. Solid-phase control on the mobility of potentially toxic elements in an abandoned lead/zinc mine tailings impoundment, Taxco, Mexico. Appl. Geochem. 22, 109–127.
Ryan, B.M., Kirby, J.K., Degryse, F., Harris, H., McLaughlin, M.J., Scheiderich, K., 2013. Copper speciation and isotopic fractionation in plants: uptake and translocation mechanism. New Phytol. 199, 367–378.
Scheinost, A.C., Abend, S., Pandya, K.I., Sparks, D.L., 2001. Kinetic controls on Cu and Pb sorption by ferrihydrite. Environ. Sci. Technol. 35, 1090–1096.
Schwartz, M.O., Ploethner, D., 1999. Removal of heavy metals from mine water by carbonate precipitation in the Grootfontein-Omatako canal, Namibia. Environ. Geol. 39, 1117–1126.
Shi, Z., Di Toro, D.M., Allen, H.E., Sparks, D.L., 2013. A general model for kinetics of heavy metal adsorption and desorption on soils. Environ. Sci. Technol. 47, 3761–3767.
Sipos, P., 2009. Single element and competitive sorption of copper, zinc and lead onto a Luvisol profile. Cent. Eur. J. Geosci. 1, 404–415.
Sipos, P., Németh, T., Kovács Kis, V., Mohai, I., 2008. Sorption of copper, zinc and lead on soil mineral phases. Chemosphere 73, 461–469.
Sracek, O., Mihaljevič, M., Kříbek, B., Majer, V., Veselovský, F., 2010. Geochemistry and mineralogy of Cu and Co in mine tailings at the Copperbelt, Zambia. J. Afr. Earth Sci. 57, 14–30.
Sracek, O., Mihaljevič, M., Kříbek, B., Majer, V., Filip, J., Vaněk, A., Penížek, V., Ettler, V., Mapani, B., 2014. Geochemistry of mine tailings and behavior of arsenic at Kombat, northeastern Namibia. Environ. Monit. Assess. 186, 4891–4903.
Sterckeman, T., Douay, F., Proix, N., Fourrier, H., 2000. Vertical distribution of Cd, Pb and Zn in soils near smelters in the North France. Environ. Pollut. 107, 377–389.
Sutherland, R.A., Tack, F.M.G., 2002. Determination of Al, Cu, Fe, Mn, Pb and Zn in certified reference materials using the optimized BCR sequential extraction procedure. Anal. Chim. Acta 454, 249–257.
Teutsch, N., Erel, Y., Halicz, L., Banin, A., 2001. Distribution of natural and anthropogenic lead in Mediterranean soils. Geochim. Cosmochim. Acta 65, 2853–2864.
Vaněk, A., Ettler, V., Skipalová, K., Novotný, J., Penížek, V., Mihaljevič, M., Sracek, O., Drábek, O., Tejnecký, V., Mapani, B., 2014. Environmental stability of the processing waste from sulfide mining districts of Namibia — a model rhizosphere solution approach. J. Geochem. Explor. 144, 421–426.

Vodyanitskii, Y.N., 2009. Mineralogy and geochemistry of manganese: a review of publications. Eurasian Soil Sci. 42, 1170–1180.
Wang, Y., Feng, X., Villalobos, M., Tan, W., Liu, F., 2012. Sorption behaviour of heavy metals on birnessite: Relationship with its Mn average oxidation state and implications for types of sorption sites. Chem. Geol. 292-293, 25–34.
Weinstein, C., Moynier, F., Wang, K., Paniello, R., Foriel, J., Catalano, J., Pichat, S., 2011. Isotopic fractionation of Cu in plants. Chem. Geol. 286, 266–271.
Weiss, D.J., Rausch, N., Mason, T.F.D., Coles, B.J., Wilkinson, J.J., Ukonmaanaho, L., Arnold, T., Nieminen, T.M., 2007. Atmospheric deposition and isotope biogeochemistry of zinc in obrotrophic peat. Geochim. Cosmochim. Acta 71, 3498–3517.
Wiederhold, J.G., 2015. Metal Stable Isotope Signatures as Tracers in Environmental Geochemistry. Environ. Sci. Technol. 49, 2606–2624.
Wilson, S.A., 1997. The collection, preparation, and testing of USGS reference material BCR-2, Columbia River, Basalt: U.S. In: Geological Survey Open-File Report 98-Xxx.
Zhu, X.K., O'Nions, R.K., Guo, Y., Belshaw, N.S., Rickard, D., 2000. Determination of natural Cu-isotope variation by plasma-source mass spectrometry: implications for use as geochemical tracers. Chem. Geol. 163, 139–149.

Journal of African Earth Sciences 181 (2021) 104246

Contents lists available at ScienceDirect

Journal of African Earth Sciences

journal homepage: www.elsevier.com/locate/jafrearsci

Depicting the historical pollution in a Pb–Zn mining/smelting site in Kabwe (Zambia) using tree rings

Rafael Baieta [a], Martin Mihaljevič [a,*], Vojtěch Ettler [a], Aleš Vaněk [b], Vít Penížek [b], Jakub Trubač [a], Bohdan Kříbek [c], Josef Ježek [d], Miroslav Svoboda [e], Ondra Sracek [f], Imasiku Nyambe [g]

[a] Institute of Geochemistry, Mineralogy and Mineral Resources, Faculty of Sciences, Charles University, Albertov 6, CZ-128 43, Prague 2, Czech Republic
[b] Department of Soil Science and Soil Protection, Faculty of Agrobiology, Food, and Natural Resources, Czech University of Life Sciences Prague, Kamýcká 129, 165 21, Prague 6, Czech Republic
[c] Czech Geological Survey, Geologická 6, Prague, 152 00 5, Czech Republic
[d] Institute of Applied Mathematics and Information Technologies, Faculty of Sciences, Charles University, Albertov 6, CZ-128 43, Prague 2, Czech Republic
[e] Forest Ecology Department, Faculty of Forestry and Wood Sciences, Czech University of Life Sciences Prague, Kamýcká 129, 165 21, Prague 6, Czech Republic
[f] Department of Geology, Faculty of Science, Palacky University in Olomouc, 17. listopadu 1192/12, 771 46, Olomouc, Czech Republic
[g] University of Zambia, School of Mines, Department of Geology, POB 32 379, Lusaka, Zambia

ARTICLE INFO

Keywords:
Pollution
Soils
Lead
Lead isotopes
Carbon isotopes

ABSTRACT

Historical Pb–Zn mining and smelting in Kabwe in Zambia have made it one of the most polluted cities in the world. Four soil profiles were collected around the smelter and in remote locations, and two pine trees (*Pinus montezumae* L.) were sampled for tree ring cores. These were analyzed for Pb, Zn and Cu contents and Pb isotopic ratio. Furthermore, the C isotopic composition of tree rings was also assessed. High concentrations of metals are present only in the top layers of soil and are higher in soils closer to the smelter (up to 16000 mg kg^{-1} Pb; 14000 mg kg^{-1} Zn; 600 mg kg^{-1} Cu) compared to remote soils (up to 194 mg kg^{-1} Pb; 438 mg kg^{-1} Zn; 46 mg kg^{-1} Cu). Metals are also present in trees and the one located furthest from the slag dump contains higher metal concentrations (up to 6.48 mg kg^{-1} Pb; 10.6 mg kg^{-1} Zn; 10.2 mg kg^{-1} Cu), possibly due to the deposition of wind-blown particles. Results of a sequential extraction procedure (SEP) showed that metal contaminants are not available for tree root uptake and the above-ground processes must be more important. The Pb isotopic ratios of slags, tree rings, and topsoils average at $^{206}Pb/^{207}Pb = 1.15$, corresponding to the signature of local ores and smelting slags, thus confirming that the mine and smelter are the main sources of contamination in the area. The results were compared to the historical records of smelter production. Tree ring Pb and Zn concentrations, $\delta^{13}C$ and $^{206}Pb/^{207}Pb$ reveal linear dependence on production with different statistical significance.

1. Introduction

Kabwe town in central Zambia is known to be one of the most polluted sites in the world due to its historical lead (Pb) and zinc (Zn) ore mining and processing. The local mine was active from 1906 to 1994. In total it produced 0.8 Mt of Pb and 1.8 Mt of Zn as well as other by-products: silver (Ag), 79 t; fused V_2O_5, 7820 t; cadmium (Cd), 235 t; and copper (Cu), 64 t (Kamona and Friedrich, 2007). It has created a regional environmental anomaly that poses a significant health risk (Bose-O'Reilly et al., 2018; Kříbek et al., 2019; Tembo et al., 2006). Studies have focused on determining how former ore mining and smelting activities have affected the local population, especially children (Yabe et al, 2015, 2018) and cattle (Yabe et al., 2011). Another study (Nakata et al., 2016) found high concentrations of Pb in farm animals and determined, using a Pb stable isotopes approach, that the smelter is the source of the contamination. All the studies confirmed the need for remediation. Elevated concentrations of Pb, Zn, and Cd in the soils found close to the smelter have been reported and these soils were classified as highly polluted (Tembo et al., 2006). Recently, some authors have proposed soil remediation measures to mitigate the effects on the local population (Kříbek et al., 2019; Mwandira et al., 2019). Kříbek et al. (2019) have also determined the bioaccessibility of the

* Corresponding author.
E-mail address: mihal@natur.cuni.cz (M. Mihaljevič).

https://doi.org/10.1016/j.jafrearsci.2021.104246
Received 13 August 2020; Received in revised form 15 February 2021; Accepted 4 May 2021
Available online 18 May 2021
1464-343X/

contaminants in topsoil, pointing out that high concentrations alone do not necessarily imply a hazardous nature for living beings and that the contaminant speciation and particle size could have greater relevance (Trapp, 2004).

Lead isotopes are a useful tool for tracing sources of contamination: e.g., chronological marker (Renberg et al., 2001), migration velocities (Erel, 1998; Puchelt et al., 1993), contamination source determination (Monna et al., 1997; Shirahata et al., 1980), among others; Komárek et al. (2008) compiled a comprehensive review on this aspect. Tree rings have been used as an approximate environmental archive of anthropogenic Pb emissions by several authors (e.g., Mihaljevič et al., 2015; Tommasini et al., 2000; Zuna et al., 2011); however, studies have shown that several factors can hinder their applicability, e.g., climatic variations (Kirdyanov et al., 2007; Time et al., 2018), radial mobility in the xylem (Cutter and Guyette, 1993; Prohaska et al., 1998), soil acidity (metal mobility) fluctuations not caused by pollution sources, different elements having distinct roles in the tree and different species of trees behaving differently (Patrick and Farmer, 2006; Watmough, 1999). Some authors, following the work of Satake et al. (1996), have shown that it is advantageous to use bark pockets instead of tree rings (Bellis et al, 2002a, 2002b, 2004, 2002a); however, the nature of these samples sometimes prevents their collection and use. Metal uptake by trees is also an above-ground process, i.e. the roots are not the only entry-point, but the bark and leaves also play an important role (Klaminder et al., 2005; Watmough and Hutchinson, 2003).

Ore mining/smelting had been carried out for almost 100 years in Kabwe, but slag dumps and mine tailings remain an important source of pollution to the present day. Thus, this site represents a suitable geochemical laboratory for investigating the use of tree rings to study the dispersion of contaminants and their historical record in a humid subtropical environmental setting. We investigated the soil profiles and tree rings using a combination of bulk contaminant (Pb, Zn, Cu) measurements and determination of Pb and C isotopes to depict the potential sources and mobility of metals in time and space and to compare these records with the historical production of the mine and smelter.

2. Materials and methods

2.1. Study area and sampling

Kabwe is the fourth largest town in Zambia, with a population of more than 200,000 inhabitants (2010 census) and is the capital of the Central Province (Fig. 1). Town coordinates: 14°26′S 28°27′E.

Carbonate-hosted mineralization in this area is linked to the Kabwe Dolomite Formation consisting of a massive dolomitic marble. Five members compose the Formation: arenaceous dolomite; micaceous dolomite; schistose dolomite (bedrock for soil profiles P1 and P2, see below); carbonaceous dolomite (area of soil profile P4) and massive dolomite. To the north, the Formation is bordered by granitic gneiss of the Basement Complex, composed of feldspars (such as orthoclase, plagioclase), quartz (SiO_2), and accessory minerals. Conglomerate and schist, intercalated with arkose and quartzite overlay the Basement Complex (soil profile area P3) (Kamona and Friedrich, 2007). The mineralization is structurally controlled along the NE-SW faults (pipe--like orebodies). The major ore minerals are galena (PbS), pyrite (FeS_2), sphalerite (ZnS), and chalcopyrite ($CuFeS_2$). Bornite (Cu_5FeS_4), covellite (CuS), chalcocite (Cu_2S), and tetrahedrite [$Cu_6(Cu_4X_2)Sb_4S_{13}$; X = Fe, Zn] are of minor importance. Other, non-sulfide, ores are represented by cerussite ($PbCO_3$), willemite (Zn_2SiO_4), smithsonite ($ZnCO_3$) and V, As, Mo and Cu minerals.

2.2. Sampling and sample processing

Four soil-sampling sites were selected in contaminated and uncontaminated areas according to the regional screening study recently published by Kříbek et al. (2019). Two of these soil profiles were located

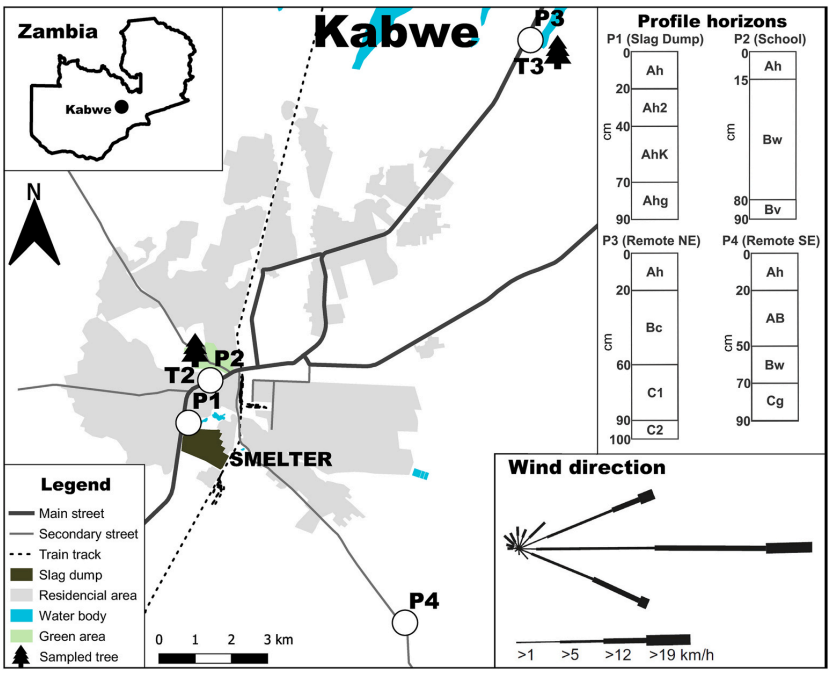

Fig. 1. Location of soil pits (P1–P4), trees (T2 and T3) and former smelter area in Kabwe (Zambia). Local mean wind directions (meteoblue.com, 2019) and soil profile horizons are indicated.

in areas where trees were also available for sampling tree ring cores (Fig. 1). Two sites were located in the vicinity of the mine/smelter (P1, near the slag dumps, and P2, close to a primary school) and the other two were in remote locations to the NE (P3, close to the highway) and the SE (P4). The latter two sites were used as controls (presumably less contaminated). Soil samples were collected from 1 m deep pits in June 2017. The soil horizons were described (Table S1) and soils were classified according to the IUSS Working Group WRB (2014) as Vertisol (P1), Ferralsol (P2), Regosol (P3) and Phaeozem (P4). Samples corresponding to 5-cm thick segments were stored in PE bags and transported to the laboratory. The soil samples were dried to constant weight in the air at room temperature and then sieved (2 mm mesh size). An aliquot was then milled to analytical fineness in an agate ball mill (Fritsch, Pullverissette, Germany). The granulometry of the soils was measured using the hydrometer method (Gee and Or, 2002). Digests for elemental and isotopic analysis were prepared using HF and $HClO_4$. A weighed amount of 0.2 g of the sieved sample was dissolved using 0.5 ml of $HClO_4$ (70–72% v/v) and 10 ml HF (50% v/v) and then evaporated to dryness at 170 °C for 2 h. The evaporated sample was then re-dissolved with 0.5 ml $HClO_4$ (70–72% v/v) and 5 ml HF (50% v/v) and evaporated once more. Finally, it was dissolved in 2 ml HNO_3 (v/v) and transferred to a 100 ml volumetric flask. The samples for dendrochemical studies were collected from two pine trees (*Pinus montezumae* L.*)* in July 2017 using a Haglof incremental borer (diameter 5 mm). For the sake of simplicity, the tree rings are designated as T2 and T3, as they were drilled next to profiles P2 and P3 respectively (Fig. 1). Three cores were collected at chest height from each tree at relative angles of 120°. The tree ring samples were cut in 3-year segments and dried to constant weight. The individual segments were digested overnight in PTFE Savillex® beakers (Minnetonka, USA) in 10 ml of concentrated HNO_3 at 150 °C.

Five representative slag samples corresponding to waste materials from smelting processes used at Kabwe (ISF smelting and Waelz) were collected from the local dump, which now represents the major source of dust contamination (Fig. 1). The slag samples were crushed, milled to analytical fineness and digested in mineral acids. The detailed digestion procedure is described elsewhere (Ettler et al., 2009).

The solutions were prepared and diluted using analytical grade HNO_3 (Merck, Germany), which was additionally purified by sub-boiling distillation, and deionized water (DI) obtained from a Milli-Q Academic purifying system (Millipore®, USA).

2.3. Analytical procedures

2.3.1. Determination of soil properties and mineralogy

The soil pH (H_2O and 1 M KCl) was measured for the <2 mm soil fraction using a soil-to-extract ratio of 1:5 (v/v) after 1 h agitation (ISO 10390, 2005) using a Schott Handylab pH-meter (Schott, Germany). The cation exchange capacity (CEC) was calculated as the sum of the basic cations and Al extracted using a 0.1 M $BaCl_2$ solution (Hendershot and Duquette, 1986). The extracts in $BaCl_2$ were analyzed by inductively coupled plasma optical emission spectroscopy (ICP-OES, iCAP 6500 radial, Thermo Scientific, Germany) under the conditions recommended by the manufacturer.

2.3.2. Determination of bulk concentrations

The total carbon (TC) and total sulfur (TS) contents were determined by catalytic oxidation at 1250 °C using an ELTRA CS 500 element analyzer (ELTRA, Germany). Soils, tree rings, and slag digests were then analyzed for trace elements (Cu, Zn and Pb) using quadrupole-based inductively coupled plasma mass spectrometry (Q-ICP MS, XSeries 2, Thermo Scientific) and/or ICP OES under the conditions described elsewhere (Mihaljevič et al., 2011). The quality of the elemental analysis procedure for soils, tree rings and slags was controlled using reference materials (NIST 2710, Montana soil; NIST 1575, Pine needles and NIST 1515, Apple leaves). The accuracy of the measurements was <5% RSD.

2.3.3. Sequential extraction procedure

The sequential extraction procedure (SEP) was performed following the BCR scheme described in Rauret et al. (1999) to determine the chemical fractionation of the metal/metalloid contaminants. The extractions were conducted in duplicate in 100-ml PE reactors (P-lab, Czech Republic), centrifuged after each step, with washing steps (when defined in the original procedure), diluted to 2% (v/v) HNO_3 and immediately analyzed by Q-ICPMS for the total concentrations Cu, Pb and Zn, and Pb isotopes. The SEP consisted of the following steps: Step 1 – exchangeable/acid extractable fraction (targeting soluble/exchangeable metals and carbonates), 0.11 M CH_3COOH; Step 2 – reducible (targeting Fe–Mn oxyhydroxides), 0.5 M $NH_2OH{\cdot}HCl$ at pH 1.5; Step 3 – oxidizable (targeting organic matter and sulfides), H_2O_2 (85 °C) then 1 M CH_3COONH_4; Step 4 – residual, total digestion (targeting metals bound to silicates) (for a more detailed description of the preparation of the extraction solutions and procedure, see e.g. (Bacon and Davidson, 2008; Rauret et al., 1999). We applied the method to a representative sample of each soil horizons to determine operationally defined solid speciation of contaminants and their potential plant availability/"lability".

2.3.4. Pb isotopic determinations

The Pb isotopic composition was determined using Q-ICP MS, under conditions described elsewhere (Mihaljevič et al., 2011). The solutions for Pb isotopic determination were diluted to a concentration of <25 μg l^{-1} Pb. The mass bias was corrected using a reference material (NIST 981, Common lead) measured between the individual samples. The standard errors for measurement of the $^{206}Pb/^{207}Pb$ and $^{208}Pb/^{206}Pb$ ratios were <0.4% RSD and <0.5% RSD, respectively. A BCR-2 (Basalt, Columbia River; USGS) certified reference material was used to test the accuracy of the digest measurements.

2.3.5. Carbon isotopic determinations

The stable isotopic composition of carbon was determined using a Thermo Flash 2000 elemental analyzer connected to a Thermo Delta V Advantage isotope ratio mass spectrometer in a Continuous Flow IV system (ThermoFisher Scientific). The minimum sample weight depends on the wt. % amount of elemental carbon. Samples wrapped in tin capsules were combusted. The released gases (CO_2) separated in a GC column were transferred through a capillary to an MS source. The isotope ratios are reported as delta (δ) values and expressed relative to VPDB for $\delta^{13}C$. The delta values are normalized to a calibration curve based on IAEA-CH-6, IAEA-CH-3 and IAEA 600 international standards.

3. Results and discussion

3.1. Metals and Pb isotopic composition of slags

The five collected slags contain high levels of metals. The slags have metal concentration ranges of 834–1730 mg kg^{-1} Cu; 29300–154000 mg kg^{-1} Zn and 6700–17100 mg kg^{-1} Pb. The slag Pb isotopic signatures range from $^{206}Pb/^{207}Pb = 1.142$ to 1.157 averaging at 1.148 ± 0.0064 (n = 5). The 95% prediction interval for individual values of $^{206}Pb/^{207}Pb$ (mean ± 2 standard deviations) is [1.135, 1.161]. This signature range of the contamination derived from the smelter is henceforth referred to as the contamination signature.

3.2. Soil properties and metal contaminant concentrations

In all the soil profiles, the pH is stable with depth ($6.11 \leq pH \leq 7.66$), except for P1, located near the slag dump, where it increases from 7.16 at the surface to 9.35, stabilizing at a depth of 65 cm (Table S1). The CEC, TC, and TS values are reported in detail in Table S1.

The highest concentrations of contaminants were found in the two profiles collected in the vicinity of the mine/smelter, with up to 16000 mg kg^{-1} Pb, 140000 mg kg^{-1} Zn and 600 mg kg^{-1} Cu in profile P1

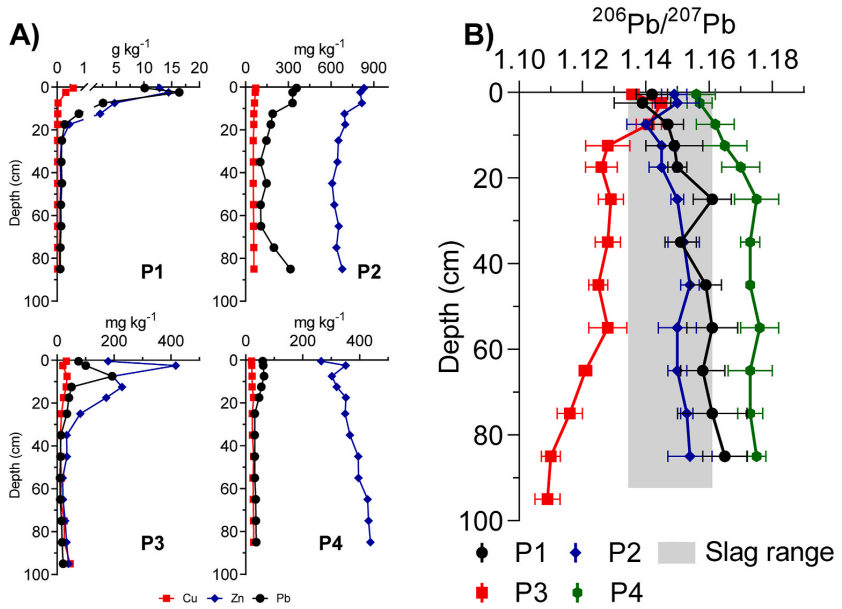

Fig. 2. A) Total Cu, Zn and Pb concentrations in the studied soil profiles. Note the different scales on the x-axis. B) Isotopic $^{206}Pb/^{207}Pb$ ratios in the studied soil profiles and slags.

(Fig. 2A and Table S2). Soils close to smelters are commonly contaminated (e.g. Ettler, 2016; Kříbek et al., 2019; Li et al., 2015; Rieuwerts et al., 1999). The remote sites have substantially lower concentrations (up to 194 mg kg^{-1} Pb; 438 mg kg^{-1} Zn; 46 mg kg^{-1} Cu, Fig. 2A and Table S2). The highest concentrations are found in the topsoil and tend to decrease with depth. At a maximum depth of 40 cm, the metal concentrations in most soils stabilize, suggesting that, below this depth, they are mostly controlled by the geochemical characteristics of the underlying bedrocks. Interestingly, the Zn concentration in P4 continues to increase with depth, reaching its highest values in the deepest part of the profile (up to 438 mg kg-1), this can most likely be explained by the different geology at this site (Fig. 2). Unfortunately, it was not possible to obtain local bedrock samples or find previous analyses in the literature to confirm this hypothesis. The concentration of Zn in the P2 profile does not decrease substantially and the Pb trend behaves erratically, first decreasing unpredictably, stabilizing and then increasing once again in

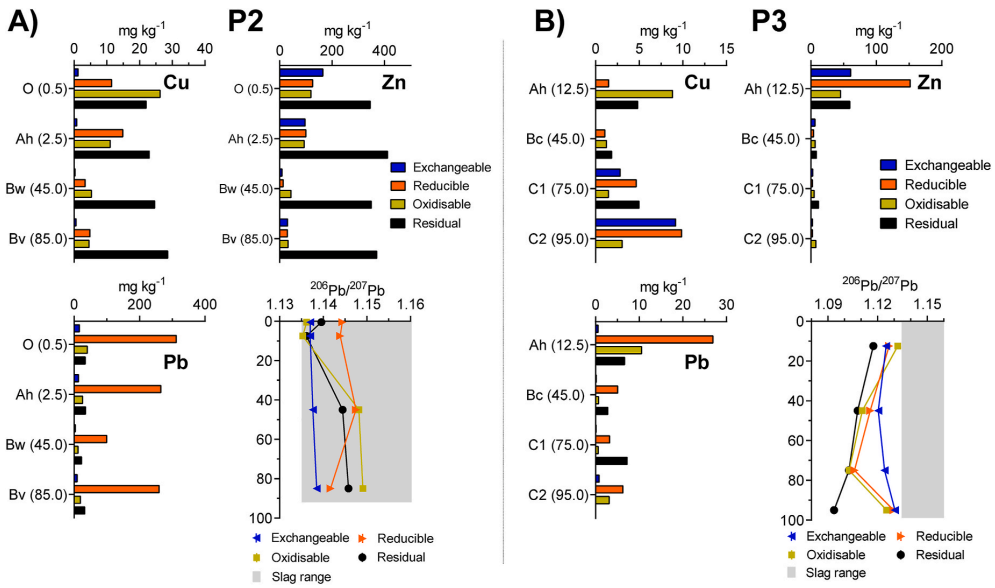

Fig. 3. Cu, Zn and Pb concentrations and $^{206}Pb/^{207}Pb$ ratios in the P2 (A) and P3 (B) soil profiles in the SEP fraction.

deeper layers (Fig. 2). During the soil collection of profile P2, it was noticed that the material had seemingly been turned and might not represent natural conditions. This could explain the behavior of the contaminants. Previous studies concluded that anthropogenic contamination in Kabwe affects only the upper 5–10 cm thick surficial soil layer (Kříbek et al., 2019). All the three studied contaminants, i.e. Pb, Zn, and Cu exceed the concentrations in soils recommended by the World Health Organization (WHO) (Cu 30 mg kg^{-1}, Zn 90 mg kg^{-1}, Pb 35 mg kg^{-1}, Tembo et al., 2006) and the Canadian Soil Quality Guidelines (residential) (Cu 63 mg kg^{-1}, Zn 200 mg kg^{-1}, Pb 140 mg kg^{-1}; Canadian Council of Ministers of the Environment, 2007).

The chemical fractionations of Cu, Zn and Pb were determined to assess the metal availability for root uptake (Fig. 3, Table S3). We suggest that only metals bound in the exchangeable fraction of the soil can be considered accessible. Only the results for P2 and P3 are discussed and the results for P1 and P4 can be found in the supplement (Table S3) since no trees were collected near these profiles. Copper is mostly not accessible for root uptake in either of the soil profiles (P2 and P3, Fig. 3). In the P2 profile, this element is mostly bound to the oxidizable and reducible fractions across all the horizons, with barely any presence in the exchangeable fraction (up to 2%, 1.21 mg kg^{-1} in the O-horizon, Fig. 3A). In the P3 profile, Cu becomes more mobile as the C horizons are reached and is increasingly bound in the reducible and exchangeable fractions of the soil. However, the labile Cu corresponds to a relatively low concentration (9.17 mg kg^{-1}, up to 41.5% of the total, Fig. 3B) and is probably too deep (˃ 70 cm) to be accessible for plants.

The SEP showed that, for both soils, Zn is available in the O (P2: 165 mg kg^{-1}, 21.8% of the total) and Ah (P2: 96.4 mg kg^{-1}, 13.8%; P3: 60.9 mg kg^{-1}, 19.2%) horizons (Fig. 3). However, Zn is mostly bound in the residual fraction in deeper horizons in P2, and there is not enough of this metal in P3 for it to be considered an important source for tree uptake.

In both soils, Pb is the most labile contaminant, as most of it is bound almost exclusively in the reducible fraction across nearly all the horizons, from 72.5 to 81.1% of the total, 99.5–312 mg kg^{-1} in the P2 profile (Fig. 3A) and from 28.9 to 61.6%, 3.22–26.9 mg kg^{-1} (Fig. 3B). A low amount of Pb is found in the exchangeable fraction, corresponding to up to 15.9 mg kg^{-1} (4.0%) in the O-horizon in P2. In P3, only up to 0.80 mg kg^{-1} (7.8%) is found in the C2-horizon, indicating that this metal is also not very available for root uptake.

3.3. Soil Pb isotopic ratios

Isotopic $^{206}Pb/^{207}Pb$ ratios in profiles P1 and P2 closer to the smelter have similar patterns (Fig. 2B, Table S4). The $^{206}Pb/^{207}Pb$ ratios in topsoil (P1, $^{206}Pb/^{207}Pb = 1.142$; P2, $^{206}Pb/^{207}Pb = 1.149$) increase constantly with depth (up to 1.165 and 1.154, for P1 and P2 respectively). These soils are located on top of the same geological structure as the Kabwe mines and, as expected, the Pb signature doesn't vary much with depth. In the southeast remote location (P4), the topsoil signature ($^{206}Pb/^{207}Pb = 1.157$) is higher than at the contaminated sites but still within the contamination range. The ratio increases with depth down to 17.5 cm, where it stabilizes at a value of 1.175. This ratio is higher than the ones found in the lower layers of the P2 and P3 profiles (Fig. 2B). This could be due to the P4 profile soil developing on slightly different geology than P2 and P3: carbonaceous dolomite as opposed to schistose dolomite. The P3 profile signature in the topsoil (up to $^{206}Pb/^{207}Pb = 1.145$) is similar to the other profiles and is once again within the contamination range. However, it decreases rapidly with depth to $^{206}Pb/^{207}Pb = 1.128$ and stabilizes at a depth of 55 cm, after which it decreases once again to a minimum value of 1.109. This contrasting trend, together with the difference in deep metal concentrations, is compatible with the completely different nature of the underlying soil-forming bedrocks, the Basement Complex as opposed to the Dolomite Formation, on which every other studied profile was formed.

The Pb isotopic analysis of the sequential extraction leachate reveals very different behaviors in all the soil profiles, reflecting the different geologies and the distance to the slag dump (Fig. 3). The P1 profile is characterized by an increase in $^{206}Pb/^{207}Pb$ with depth for all the SEP steps. The topsoil signatures range from $^{206}Pb/^{207}Pb = 1.136$ (oxidizable) to $^{206}Pb/^{207}Pb = 1.140$ (residual) (Table S3). These values are within the standard deviation of the measurement (SD = 0.004; n = 72) and are slightly below the low-end of the contamination range. From the Ah horizon, the trend is stabilized and all the SEP steps seem to reflect geogenic concentrations.

In the P2 profile, the exchangeable fraction has a constant $^{206}Pb/^{207}Pb = 1.137$ to 1.138 signature at depth, while the residual and oxidizable fractions increase from similar values to the geogenic signature (Fig. 3A). Interestingly, the reducible fraction has a slightly higher topsoil value ($^{206}Pb/^{207}Pb = 1.144$) and decreases with depth to regular values ($^{206}Pb/^{207}Pb = 1.142$); these values are still well within the slag range of isotopic values.

The lead isotopic ratios in P3 are much lower, reflecting the different geology, as already discussed above (Fig. 3B). The $^{206}Pb/^{207}Pb$ values in the Ah-horizon range from 1.117 (residual fraction) to 1.132 (oxidizable fraction). The isotopic signature in the exchangeable, reducible and oxidizable fractions decreases with depth (down to $^{206}Pb/^{207}Pb$: 1.120, exchangeable; 1.106, reducible; 1.103 oxidizable) and then increases to a depth of 95 cm to very similar values to those found at the surface. The signature of the residual fraction continues to decrease to $^{206}Pb/^{207}Pb = 1.094$, confirming the geogenic origin of this Pb.

In the P4 profile (Table S3), the $^{206}Pb/^{207}Pb$ trend is very similar in the exchangeable, reducible and oxidizable fractions. The topsoil shows the same signature as the other soils. There is a steep increase in $^{206}Pb/^{207}Pb$ (1.14–1.16, in all profiles) down to the Ah horizon, where the trends in all 4 fractions exhibit the same behavior, increasing only slightly in deeper horizons.

In short, the measured $^{206}Pb/^{207}Pb$ ratios confirm that the anthropogenic contamination penetrates the soil layers to a maximum depth of 25 cm. The $^{206}Pb/^{207}Pb$ ratios in the lower horizons probably tend towards the assumed signature of the bedrock underlying the soils and are stable after a mean depth of 25 cm, except for the NE remote location. The surface ratios all trend towards the $^{206}Pb/^{207}Pb$ signature of the contamination ($^{206}Pb/^{207}Pb = 1.142$ to 1.157). All soil ratios in P1 and P2, except for one value in P2, fall within the prediction interval of the slag ratios [1.135, 1.161]. Additionally, topsoil values in P3 and P4 also do so, suggesting the slag dump to be the source of pollution. It can be assumed that the whole area may have its topsoil contaminated by the dust released from the dump, even at sites like P4, which are not in the direction of the preferential wind direction (Fig. 1). Furthermore, contamination could also be derived from mining activities in the past and local ore deposits, as the local Pb ore, galena (PbS), has the same isotopic signature ($^{206}Pb/^{207}Pb = 1.145$; Kamona et al., 1999) and it is known that smelting processes do not cause isotopic fractionation, or alter in any way the Pb isotopic signatures of geomaterials (Shiel et al., 2010). Therefore, the whole Pb cycle, from ore to processed geo-material to contamination in soils, can be traced using this specific isotopic ratio range. Ratios that are at the low end or even slightly below the contamination range may also be influenced by the atmospheric background characteristic of the region. Southern African atmospheric aerosols have a signature of $^{206}Pb/^{207}Pb = 1.067$ to 1.090 (Bollhöfer and Rosman, 1997), which could potentially lower the topsoil signature by mixing with the ore signature.

3.4. Trace elements in tree rings

Tree rings date back to 1963 (T2) and 1987 (T3) (Fig. 4). Thus, for T2, the mining and smelting activities had already been active for 61 years. The presented values are the calculated means of the metal concentrations (Table S5) and C and Pb isotopic ratios (Table S6) measured in the three collected cores. Interestingly, the tree farther from the source of contamination (T3) has a larger amount of Pb (up to 6.48 mg kg^{-1}) compared to the tree near the slag dump, T2 (up to 1.55 mg kg^{-1})

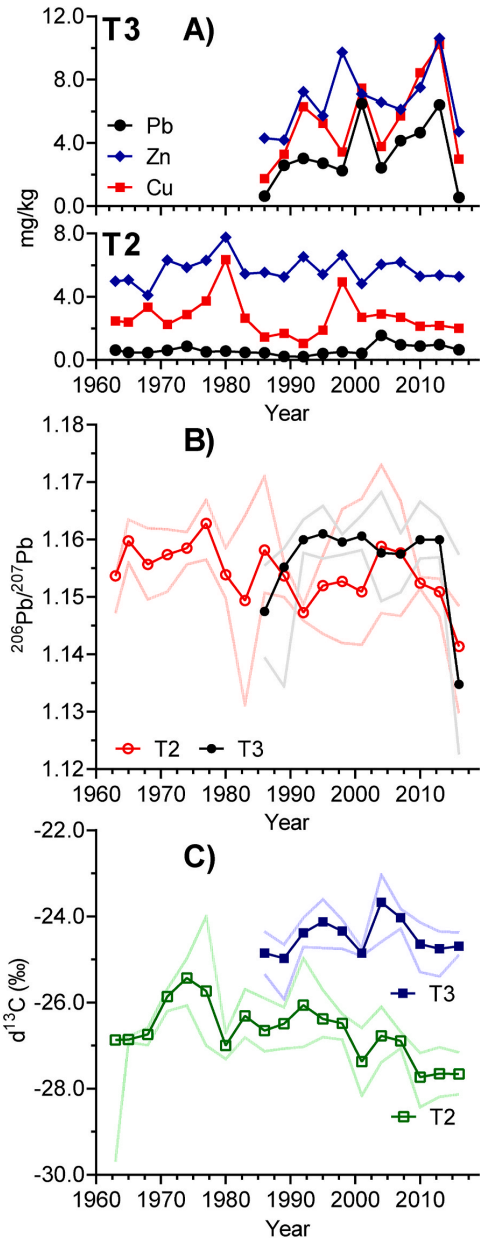

Fig. 4. A) Elemental concentrations of Cu, Zn, and Pb in the T1 and T2 tree rings. B) Isotopic $^{206}Pb/^{207}Pb$ ratios in the studied T2 and T3 tree rings. Lighter lines represent the range of observed values. C) Isotopic $\delta^{13}C$ ratios in the studied T2 and T3 tree rings. Lighter lines represent the range of observed values.

(Fig. 4A). The other elements, Cu and Zn, are also represented more in the remote tree biomass, although not to such a degree (maximum in T2: Cu, 6.35 mg kg^{-1}, Zn, 7.76 mg kg^{-1}; and in T3: Cu, 10.2 mg kg^{-1}, Zn, 10.6 mg kg^{-1}). The T3 tree is located close to one of the major highways in Zambia, meaning larger Pb levels could be caused by heavy traffic. No more trees were available for sampling around the whole region. Leaded gasoline is no longer in use, but dust carried from Kabwe (the road goes through the town) or the northern mining cities in the Copperbelt could greatly influence this tree ring record. A study by Mihaljevič et al. (2015) found similar results; the increased presence of Pb in remote locations. Perhaps the dimensions of the wind-blown particles at such distances are small enough to boost absorption by the trees compared to the closer site. A study by Csavina et al. (2014) has found that smelter-derived particles < 1 μm contain greater percentages of Pb than larger particles, which could potentially explain this phenomenon. However, Csavina et al. (2012) showed that, even for smaller particles, the contaminant concentration decreases rapidly with distance from the smelters. This phenomenon requires further investigation.

3.5. Pb isotopic ratios in tree rings

The lead isotopic compositions (Fig. 4B, Table S6) are very similar at both sites; the results have average values of $^{206}Pb/^{207}Pb = 1.536$ (T2) and $^{206}Pb/^{207}Pb = 1.558$ (T3). The ratio in T3 is more constant than in T2 and generally higher. This tendency is sustained after the smelter closed in 1994. There are several variations in the Pb isotope time-dependent pattern at the T2 site. Most noteworthy are the ratio increases in the 1970s from $^{206}Pb/^{207}Pb = 1.157$ to 1.163, with a subsequent sudden decrease to 1.149, followed by another peak in 1986 ($^{206}Pb/^{207}Pb = 1.158$). Again, there is an immediate decrease to 1.147 in 1992 followed by an unsteady increase until 2004, reaching $^{206}Pb/^{207}Pb = 1.158$. Finally, the ratio decreased to a value of 1.141 in 2016. All the values fall within the interval of contamination signature [1.135, 1.161], same as soils, closer to the high-end of the slag signature range in most of the data points, suggesting that this Pb originated from the mining/smelting activity. The sequential extraction procedure (SEP) showed that most of the Pb in the soils is bound in the reducible fraction (the mean value in the contaminated soils was 76% and, in remote soils, 54%, Fig. 3) proving it is not very accessible for root uptake. Utilizing a Pb isotope approach and comparing the signature of available Pb in the soils (mean $^{206}Pb/^{207}Pb = 1.144$, 1.120; in P2 and P3 respectively) with the Pb present in the tree biomass (mean $^{206}Pb/^{207}Pb = 1.154$; T2 and T3) supports the idea that an above-ground uptake must be the preferred route for Pb assimilation in these trees. Metals can only enter the tree biomass either through root uptake or above-ground processes, since the Pb available for root uptake is shown not to share the signature of the Pb in the tree biomass, and there is no noticeable fractionation of Pb in this process, this uptake method is eliminated. Wind-blown particles from the smelter will share the signature of the slags and will be falling on the trees and absorbed into the biomass either through breathing or other processes. Other studies have also shown that Pb found in wood mostly originates from above-ground uptake processes (Lepp and Dollard, 1974; Watmough, 1999).

3.6. Carbon isotopic ratios in tree rings

Mean $\delta^{13}C$ values (Fig. 4C, Table S6) are always higher in the remote site (T3: mean $\delta^{13}C = -24.58$‰) compared to the contaminated site (T2 mean $\delta^{13}C = -26.8$‰). In tree T2, the ratio rapidly increases from 1970, culminating in 1974 ($\delta^{13}C = -25.4$‰), followed by a steady decrease back to mean values ($\delta^{13}C = -27.0$‰) in 1980; this is the most notable trend in the record. The T3 record begins in 1987 and both records have had similar trends since then. Pearson's correlation coefficient ($r = 0.77$, $p < 0.001$) shows a very strong correlation between these two trees, in these years. Similar peaks appear in the early 1990s and early 2000s, with a depression in 2001. This suggests that both trees are part of a system that affects both records.

3.7. Smelter production vs. tree rings record

Smelter yearly production amounts were compiled from the USGS annual reports (U.S. Geological Survey, Bureau of Mines, 1964–1993,

Table S7). Unfortunately, it was not possible to find earlier records than those for 1959. The mine had been active for 53 years prior to this date. The earliest record available shows the smelter producing 15 Mt of Pb and 30 Mt of Zn in 1959. Production peaked in the mid-1970s (28 Mt of Pb in 1971 and 58 Mt of Zn in 1974; Fig. 5). It is noteworthy that the Zn and Pb productions correlate with an $r = 0.93$ ($p = 4 \times 10^{-16}$; Spearman coefficient) and that the Zn production exceeds Pb more than twice.

In previous studies, it was observed that apparent correlations between the tree ring record and the smelter production records can be blurred or smoothed out and may suffer a delay of up to 10-years (Lageard et al., 2008; Watmough and Hutchinson, 2002). This effect is present also in our data (Fig. 5). Major trends and long periods of increase and decrease in production seem to be recorded in the tree data, but short bursts do not. The data interpretation is complicated by the fact that the tree data represents 3-year sums while production is known for each year.

We have investigated if the presence of Pb in the trees is controlled by smelter production. It makes sense to compare tree-data to a moving average or to equivalent summation of production over several previous years with some time delay, evaluated at years to which tree data corresponds to. We considered combinations of summation from 1 to 10 years (denoted as parameter ny) and delays of 0–6 years (parameter nd). For all these combinations we examined linear dependence of the Pb content in the T2 tree on time-averaged and delayed Pb production by means of linear regression.

The linear regression of the tree on production is significant, with a coefficient of determination $R^2 = 0.67$ ($r = 0.82$, $p = 0.001$). This result means that 67% of variability of Pb in the T2 tree can be explained by a linear dependence on 3 previous years of production delayed by 1 year. Figure S1 shows the result of a 3-years summation (ny = 3) delayed 1 year (nd = 1).

More combinations of the averaging parameters (ny, nd) provided statistically significant results, some of them having similar R-squared coefficient, as in the previous example. Formally, the best one was found for averaging 5 previous years without any delay (ny = 5, nd = 0) with $R^2 = 0.68$. Given the size of data, it makes no sense to state that, for such a small difference in R^2, one of the models is preferred. Nevertheless, we can conclude that Pb in the T2 tree significantly reflects the cumulative effect of several previous years of production.

Carbon isotopes have proven to be a useful tool for describing environmental conditions affecting tree behavior; a review on this subject can be found in van der Sleen et al. (2017) and references therein. In this study, $\delta^{13}C$ is used as a stress indicator for tree growth. Variations in $\delta^{13}C$ are caused by environmental factors like water availability, light and nutrient availability (van der Sleen et al., 2017). The premise is that greater smelter activity leads to larger amounts of SO_2 in the atmosphere, which through both wet and dry deposition, would suppress the tree assimilation process. When subject to stress, plants can partially or totally close their stomata, which decreases the partial pressure of CO_2 into the leaf and, in turn, decreases discrimination of ^{13}C (Time et al., 2018). This information, coupled with Pb isotopes and the Pb and Zn content in the tree biomass, was compared to the yearly smelter production of Pb and Zn, in an attempt to assess the environmental archive potential of these trees.

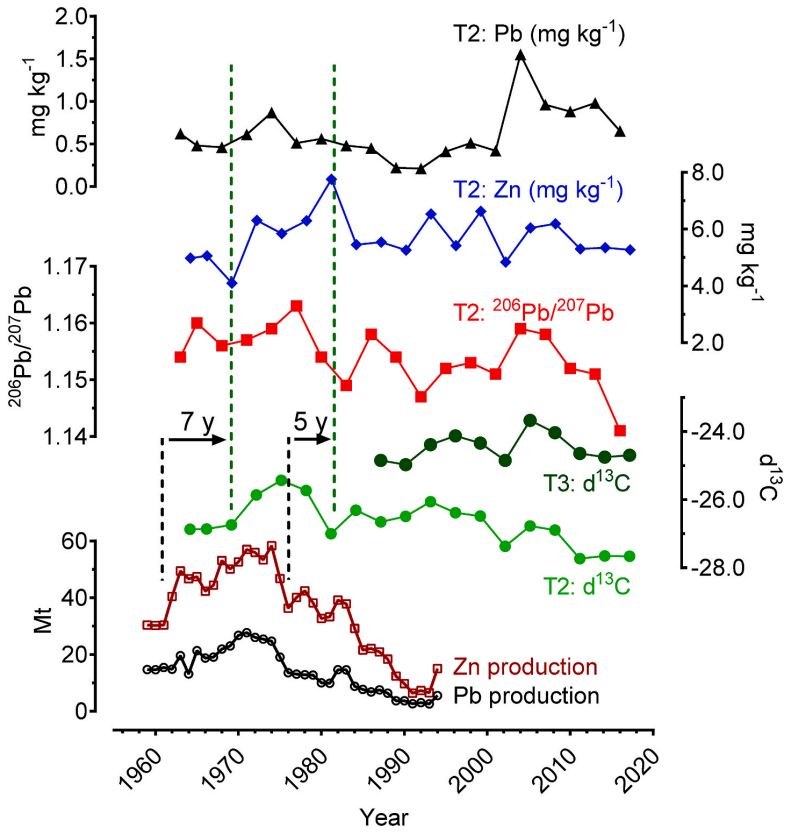

Fig. 5. Kabwe smelter historical Pb and Zn production records compared to tree ring $\delta^{13}C$ and $^{206}Pb/^{207}Pb$ values and the elemental Pb and Zn record.

The $\delta^{13}C$ record in T2 seems to have a relation to Zn and Pb production (Fig. 5). The increase in $\delta^{13}C$ from 1968 to 1974 and the subsequent decrease until 1980 reflects the increased smelter production from 1961 to 1976. Later, there are two smaller peaks in 1983 and 1992. Nevertheless, linear regression of $\delta^{13}C$ in T2 on the time-averaged and delayed sum of Pb and Zn productions (similar as in the above described case of Pb) don't show up statistically significant dependence. Only the first part of the record up to 1986 can be explained by linear regression on the total production ($R^2 = 0.53$), with a 5-year summation and no delay in tree response. Comparing only $\delta^{13}C$ to Zn production produces a similar value of $R^2 = 0.51$. Therefore, only up to this date, the $\delta^{13}C$ record in pines can be used as a proxy for high industrial activity. Note that post-1987, both tree $\delta^{13}C$ records behave similarly.

In the case of the Pb isotopes, linear dependence on Pb production was found. A summation over 5 years with a delay of 2 years produces significant regression with $R^2 = 0.56$. This is indicated in Fig. 5 where periods of higher smelter production seem to increase the $^{206}Pb/^{207}Pb$ ratio and periods of lower production result in smaller ratios. The background aerosol signature ($^{206}Pb/^{207}Pb = 1.067$ to 1.090 (Bollhöfer and Rosman, 1997), could play a more significant role, leading to a decrease of the ratio.

Total Zn concentrations in the trees also seems to be linked to smelter production (Fig. 5). The sudden increase in production in 1963 matches an increase in Zn in the tree biomass in 1971. The major increases and decreases are also recorded until the end of the production boom. When production suddenly decreased in 1976, so did the Zn concentration in the tree biomass in 1983. Nevertheless, linear regression of Zn in T2 on summed and delayed production, shows only weak relation with low R^2(the best value found $R^2 = 0.319$). Therefore, Zn recorded in T2 doesn't show such simple and relatively strong relation to the course of production as Pb.

From 2000 to 2010, there was a pronounced increase across all the variables, which is not caused by active smelting since the production had ceased long before this time (Fig. 5). This must either be justifiable by some natural or anthropogenic phenomenon or it throws doubt on all the other discussed correlations between smelter production and the tree ring record. Perhaps either the tree reacted with a greater delay than previously to the final increase in 1994 or it is somehow connected with an increase in traffic and overall atmospheric pollution. We were not able to find a weather phenomenon, which could cause this trend, such as a year with intense rain or lack thereof or even stronger winds, which could blow more dust from the dumps. This phenomenon calls for more trees to be studied around Kabwe and the involvement of other isotopic systems like Zn and Cu to elucidate the reason(s) for these variations.

4. Conclusions

Here, the impact of the historical Pb–Zn mining and smelting in Kabwe, Zambia was assessed in local soils and trees. We concluded that the whole area is contaminated by the smelter's historical activities and still in the present day due to the wind-blown particles coming from the completely unprotected massive slag dump and already contaminated soils. Extreme contamination is only found in the topsoils up to a depth of about 10 cm, but the contamination extends down to a depth of 40 cm, as indicated by Pb isotopes. The presence of Pb in the tree biomass is also significant (up to 6.48 mg kg^{-1} Pb) and we concluded its origin not to be from root uptake but rather from the deposition of the wind-blown particles on the bark and leaves of these trees. Interestingly, the presence of Pb in the remote tree was much higher than in the tree close to the slag dump, a trend not shared by the other metals. Possibly, this is due to smaller particles, aerosols, having greater Pb concentrations and traveling to greater distances. This phenomenon invites further investigation.

Finally, local pine trees are sensitive to changes in smelter production throughout time and a massive increase in production in the 1970s is well documented in both tree records. Both trees belong to the same system as their respective $\partial^{13}C$ trends always behave in the same way. The record of Pb production is more reliable than that of Zn production. Carbon and Pb isotopes also are good indicators of smelter production.

Declaration of competing interest

The authors declare that they have no known competing financial interests or personal relationships that could have appeared to influence the work reported in this paper.

Acknowledgments

This study was supported by the Czech Science Foundation Project (GAČR 19-18513S), received institutional funding from the Center for Geosphere Dynamics (UNCE/SCI/006), and a student grant awarded to Rafael Baieta from the Grant Agency for Charles University (GAUK 946120). Part of the equipment used for this study was purchased from Operational Program Prague - Competitiveness (Project CZ.2.16/3.1.00/21516). Dr. Roman Businský (Silva Tarouca Research Institute for Landscape and Ornamental Gardening) for precise taxonomic identification of the studied pine trees. In addition, the authors would like to thank the contributions from Marie Fayadová, Vera Vonásková and Lenka Jílková with sample handling and treatment. The reviews of anonymous reviewer and editor assisted in improving the original manuscript.

Electronic Annex as MS Excel file: RB_2020_annex.

Appendix A. Supplementary data

Supplementary data to this article can be found online at https://doi.org/10.1016/j.jafrearsci.2021.104246.

References

Bacon, J.R., Davidson, C.M., 2008. Is there a future for sequential chemical extraction? Analyst 133, 25–46. https://doi.org/10.1039/b711896a.

Bellis, D.J., McLeod, C.W., Satake, K., 2002a. Pb and $^{206}Pb/^{207}Pb$ isotopic analysis of a tree bark pocket near Sheffield, UK recording historical change in airborne pollution during the 20th Century. Sci. Total Environ. 289, 169–176. https://doi.org/10.1016/S0048-9697(01)01037-3.

Bellis, D.J., Satake, K., McLeod, C.W., 2004. A comparison of lead isotope ratios in the bark pockets and annual rings of two beech trees collected in Derbyshire and South Yorkshire, UK. Sci. Total Environ. 321, 105–113. https://doi.org/10.1016/j.scitotenv.2003.08.030.

Bellis, D.J., Satake, K., Noda, M., Nishimura, N., McLeod, C.W., 2002b. Evaluation of the historical records of lead pollution in the annual growth rings and bark pockets of a 250-year-old Quercus crispula in Nikko. Japan. Sci. Total Environ. 295, 91–100. https://doi.org/10.1016/S0048-9697(02)00054-2.

Bollhöfer, A.B., Rosman, K.J.R., 1997. Isotopic source signatures for atmospheric lead: the Southern Hemisphere. Geochem. Cosmochim. Acta 64, 3251–3262. https://doi.org/10.1016/S0016-7037(00)00436-1.

Bose-O'Reilly, S., Yabe, J., Makumba, J., Schutzmeier, P., Ericson, B., Caravanos, J., 2018. Lead intoxicated children in Kabwe, Zambia. Environ. Res. 165, 420–424. https://doi.org/10.1016/j.envres.2017.10.024.

Canadian Council of Ministers of the Environment, 2007. Canadian Soil Quality Guidelines for the Protection of Environmental and Human Health: Summary Tables.

Csavina, J., Field, J., Taylor, M.P., Gao, S., Landázuri, A., Betterton, E.A., Sáez, A.E., 2012. A review on the importance of metals and metalloids in atmospheric dust and aerosol from mining operations. Sci. Total Environ. 433, 58–73. https://doi.org/10.1016/j.scitotenv.2012.06.013.

Csavina, J., Taylor, M.P., Félix, O., Rine, K.P., Eduardo Sáez, A., Betterton, E.A., 2014. Size-resolved dust and aerosol contaminants associated with copper and lead smelting emissions: implications for emission management and human health. Sci. Total Environ. 493, 750–756. https://doi.org/10.1016/j.scitotenv.2014.06.031.

Cutter, B.E., Guyette, R.P., 1993. Anatomical, chemical, and ecological factors affecting tree species choice in dendrochemistry studies. J. Environ. Qual. 22, 611–619. https://doi.org/10.2134/jeq1993.00472425002200030028x.

Erel, Y., 1998. Mechanisms and velocities of anthropogenic Pb migration in Mediterranean soils. Environ. Res. 78, 112–117. https://doi.org/10.1006/enrs.1997.3811.

Ettler, V., Johan, Z., Kříbek, B., Šebek, O., Mihaljevič, M., 2009. Mineralogy and environmental stability of slags from the Tsumeb smelter, Namibia. Appl. Geochem. 24, 1–15. https://doi.org/10.1016/j.apgeochem.2008.10.003.

Ettler, V., 2016. Soil contamination near non-ferrous metal smelters: a review. Appl. Geochem. 64, 56–74. https://doi.org/10.1016/j.envpol.2014.04.035.
Gee, G.W., Or, D., 2002. Particle-size analysis. In: Methods of Soil Analysis: Part 4 – Physical Methods. Soil Science Society of America, Madison. https://doi.org/10.2136/sssabookser5.4.frontmatter.
Hendershot, W.H., Duquette, M., 1986. A simple barium chloride method for determining cation exchange capacity and exchangeable cations. Soil Sci. Soc. Am. J. 50, 605–608. https://doi.org/10.2136/sssaj1986.03615995005000030013x.
ISO 10390, 2005. Soil quality. Determination of pH ISO Geneva. https://www.iso.org/stan-dard/40879.html.
IUSS Working Group WRB, 2014. World Reference Base for Soil Resources 2014. International Soil Classification System for Naming Soils and Creating Legends for Soil Maps. World Soil Resources Reports No. 106. FAO, Rome.
Kamona, A.F., Friedrich, G.H., 2007. Geology, mineralogy and stable isotope geochemistry of the Kabwe carbonate-hosted Pb-Zn deposit, Central Zambia. Ore Geol. Rev. 30, 217–243. https://doi.org/10.1016/j.oregeorev.2006.02.003.
Kamona, A.F., Lévêque, J., Friedrich, G., Haack, U., 1999. Lead isotopes of the carbonate-hosted Kabwe, tsumeb, and Kipushi Pb-Zn-Cu sulphide deposits in relation to Pan African orogenesis in the Damaran-Lufilian fold Belt of central Africa. Miner. Depos. 34, 273–283. https://doi.org/10.1007/s001260050203.
Kirdyanov, A.V., Vaganov, E.A., Hughes, M.K., 2007. Separating the climatic signal from tree-ring width and maximum latewood density records. Trees Struct. Funct. 21, 37–44. https://doi.org/10.1007/s00468-006-0094-y.
Klaminder, J., Bindler, R., Emteryd, O., Renberg, I., 2005. Uptake and recycling of lead by boreal forest plants: quantitative estimates from a site in northern Sweden. Geochem. Cosmochim. Acta 69, 2485–2496. https://doi.org/10.1016/j.gca.2004.11.013.
Komárek, M., Ettler, V., Chrastný, V., Mihaljevič, M., 2008. Lead isotopes in environmental sciences: a review. Environ. Int. 34, 562–577. https://doi.org/10.1016/j.envint.2007.10.005.
Kříbek, B., Nyambe, I., Majer, V., Knésl, I., Mihaljevič, M., Ettler, V., Vaněk, A., Penížek, V., Sracek, O., 2019. Soil contamination near the Kabwe Pb-Zn smelter in Zambia: environmental impacts and remediation measures proposal. J. Geochem. Explor. 197, 159–173. https://doi.org/10.1016/j.gexplo.2018.11.018.
Lageard, J.G.A., Howell, J.A., Rothwell, J.J., Drew, I.B., 2008. The utility of Pinus sylvestris L. in dendrochemical investigations: pollution impact of lead mining and smelting in Darley Dale, Derbyshire, UK. Environ. Pollut. 153, 284–294. https://doi.org/10.1016/j.envpol.2007.08.031.
Lepp, N.W., Dollard, G.J., 1974. Studies on lateral movement of 210Pb in woody stems - patterns observed in dormant and non-dormant stems. Oecologia 16, 179–184. https://doi.org/10.1007/BF00345582.
Li, P., Lin, C., Cheng, H., Duan, X., Lei, K., 2015. Contamination and health risks of soil heavy metals around a lead/zinc smelter in southwestern China. Ecotoxicol. Environ. Saf. 113, 391–399. https://doi.org/10.1016/j.ecoenv.2014.12.025.
Mihaljevič, M., Ettler, V., Šebek, O., Sracek, O., Kříbek, B., Kyncl, T., Majer, V., Veselovský, F., 2011. Lead isotopic and metallic pollution record in tree rings from the copperbelt mining-smelting area, Zambia. Water, Air, Soil Pollut. 216, 657–668. https://doi.org/10.1007/s11270-010-0560-4.
Mihaljevič, M., Ettler, V., Vaněk, A., Penížek, V., Svoboda, M., Kříbek, B., Sracek, O., Mapani, B.S., Kamona, A.F., 2015. Trace elements and the lead isotopic record in marula (Sclerocarya birrea) tree rings and soils near the tsumeb smelter, Namibia. Water. Air. Soil Pollut 226, 177. https://doi.org/10.1007/s11270-015-2440-4.
Monna, F., Lancelot, J., Croudace, I.W., Cundy, A.B., Lewis, J.T., 1997. Pb isotopic composition of airborne particulate material from France and the southern United Kingdom: implications for Pb pollution sources in Urban areas. Environ. Sci. Technol. 31, 2277–2286. https://doi.org/10.1021/ES960870+.
Mwandira, W., Nakashima, K., Kawasaki, S., Ito, M., Sato, T., Igarashi, T., Banda, K., Chirwa, M., Nyambe, I., Nakayama, S., Ishizuka, M., 2019. Efficacy of biocementation of lead mine waste from the Kabwe Mine site evaluated using Pararhodobacter sp. Environ. Sci. Pollut. Res. 26, 15653–15664. https://doi.org/10.1007/s11356-019-04984-8.
Nakata, H., Nakayama, S.M.M., Yabe, J., Liazambi, A., Mizukawa, H., Darwish, W.S., Ikenaka, Y., Ishizuka, M., 2016. Reliability of stable Pb isotopes to identify Pb sources and verifying biological fractionation of Pb isotopes in goats and chickens. Environ. Pollut. 208, 395–403. https://doi.org/10.1016/j.envpol.2015.10.006.
Patrick, G.J., Farmer, J.G., 2006. A stable lead isotopic investigation of the use of sycamore tree rings as a historical biomonitor of environmental lead contamination. Sci. Total Environ. 362, 278–291. https://doi.org/10.1016/j.scitotenv.2005.12.004.
Prohaska, T., Stadlbauer, C., Wimmer, R., Stingeder, G., Latkoczy, C., Hoffmann, E., Stephanowitz, H., 1998. Investigation of element variability in tree rings of young Norway spruce by laser-ablation-ICPMS. Sci. Total Environ. 219, 29–39. https://doi.org/10.1016/S0048-9697(98)00224-1.
Puchelt, H., Kramar, U., Cumming, G.L., Krstic, D., Nöltner, T., Schöttle, M., Schweikle, V., 1993. Anthropogenic Pb contamination of soils, southwest Germany. In: Hitchon, B., Fuge, R. (Eds.), Applied Geochemistry, pp. 71–73. https://doi.org/10.1016/S0883-2927(09)80014-0. Uppsala, Sweeden.
Rauret, G., López-Sánchez, J.F., Sahuquillo, A., Rubio, R., Davidson, C., Ure, A., Quevauviller, P., 1999. Improvement of the BCR three-step sequential extraction procedure prior to the certification of new sediment and soil reference materials. J. Environ. Monit. 1, 57–61. https://doi.org/10.1039/a807854h.
Renberg, I., Bindler, R., Brännvall, M.L., 2001. Using the historical atmospheric lead-deposition record as a chronological marker in sediment deposits in Europe. Holocene 11, 511–516. https://doi.org/10.1191/095968301680223468.
Rieuwerts, J.S., Farago, M., Cikrt, M., Bencko, V., 1999. Heavy metal concentrations in and around households near a secondary lead smelter. Environ. Monit. Assess. 58, 317–335. https://doi.org/10.1023/A:1006058331453.
Satake, K., Tanaka, A., Kimura, K., 1996. Accumulation of lead in tree trunk bark pockets as pollution time capsules. Sci. Total Environ. 181, 25–30. https://doi.org/10.1016/0048-9697(95)04955-X.
Shiel, A.E., Weis, D., Orians, K.J., 2010. Evaluation of zinc, cadmium and lead isotope fractionation during smelting and refining. Sci. Total Environ. 408, 2357–2368. https://doi.org/10.1016/j.scitotenv.2010.02.016.
Shirahata, H., Elias, R.W., Patterson, C.C., Koide, M., 1980. Chronological variations in concentrations and isotopic compositions of anthropogenic atmospheric lead in sediments of a remote subalpine pond. Geochem. Cosmochim. Acta 44, 149–162. https://doi.org/10.1016/0016-7037(80)90127-1.
Tembo, B.D., Sichilongo, K., Cernak, J., 2006. Distribution of copper, lead, cadmium and zinc concentrations in soils around Kabwe town in Zambia. Chemosphere 63, 497–501. https://doi.org/10.1016/j.chemosphere.2005.08.002.
Time, A., Garrido, M., Acevedo, E., 2018. Water relations and growth response to drought stress of *Prosopis tamarugo* phil. A review. J. Soil Sci. Plant Nutr. 18, 329–343. https://doi.org/10.4067/S0718-95162018005001103.
Tommasini, S., Davies, G.R., Elliott, T., 2000. Lead isotope composition of tree rings as bio-geochemical tracers of heavy metal pollution: a reconnaissance study from Firenze. Italy. Appl. Geochemistry 15, 891–900. https://doi.org/10.1016/S0883-2927(99)00106-7.
Trapp, S., 2004. Plant uptake and transport models for Neutral and ionic chemicals. Environ. Sci. Pollut. Res. 11, 33–39. https://doi.org/10.1065/espr2003.08.169.
U.S. Geological Survey, 1963. n.d. Bureau of Mines Minerals Yearbook for the Federation of Rhodesia and Nyasaland. Rhodesia, (Southern Rodesia), Zambia, and Malawi (1964-1965); Zambia (1967-1993).
van der Sleen, P., Zuidema, P.A., Pons, T.L., 2017. Stable isotopes in tropical tree rings: theory, methods and applications. Funct. Ecol. 31, 1674–1689. https://doi.org/10.1111/1365-2435.12889.
Watmough, S.A., 1999. Monitoring historical changes in soil and atmospheric trace metal levels by dendrochemical analysis. Environ. Pollut. 106, 391–403. https://doi.org/10.1016/S0269-7491(99)00102-5.
Watmough, S.A., Hutchinson, T.C., 2003. Uptake of ^{207}Pb and 111Cd through bark of mature sugar maple, white ash and white pine: a field experiment. Environ. Pollut. 121, 39–48. https://doi.org/10.1016/S0269-7491(02)00208-7.
Watmough, S.A., Hutchinson, T.C., 2002. Historical changes in lead concentrations in tree-rings of sycamore, oak and Scots pine in north-west England. Sci. Total Environ. 293, 85–96. https://doi.org/10.1016/S0048-9697(01)01149-4.
Yabe, J., Nakayama, S.M.M., Ikenaka, Y., Muzandu, K., Ishizuka, M., Umemura, T., 2011. Uptake of lead, cadmium, and other metals in the liver and kidneys of cattle near a lead-zinc mine in Kabwe, Zambia. Environ. Toxicol. Chem. 30, 1892–1897. https://doi.org/10.1002/etc.580.
Yabe, J., Nakayama, S.M.M., Ikenaka, Y., Yohannes, Y.B., Bortey-Sam, N., Kabalo, A.N., Ntapisha, J., Mizukawa, H., Umemura, T., Ishizuka, M., 2018. Lead and cadmium excretion in feces and urine of children from polluted townships near a lead-zinc mine in Kabwe, Zambia. Chemosphere 202, 48–55. https://doi.org/10.1016/j.chemosphere.2018.03.079.
Yabe, J., Nakayama, S.M.M., Ikenaka, Y., Yohannes, Y.B., Bortey-Sam, N., Oroszlany, B., Muzandu, K., Choongo, K., Kabalo, A.N., Ntapisha, J., Mweene, A., Umemura, T., Ishizuka, M., 2015. Lead poisoning in children from townships in the vicinity of a lead-zinc mine in Kabwe, Zambia. Chemosphere 119, 941–947. https://doi.org/10.1016/j.chemosphere.2014.09.028.
Zuna, M., Mihaljevič, M., Šebek, O., Ettler, V., Handley, M., Navrátil, T., Goliáš, V., 2011. Recent lead deposition trends in the Czech Republic as recorded by peat bogs and tree rings. Atmos. Environ. 45, 4950–4958. https://doi.org/10.1016/j.atmosenv.2011.06.007.

Geoderma 414 (2022) 115760

Contents lists available at ScienceDirect

Geoderma

journal homepage: www.elsevier.com/locate/geoderma

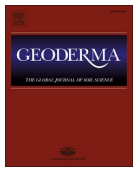

Effects of forest fires on soil lead elemental contents and isotopic ratios

Rafael Baieta *, Alda M.D. Vieira, Maria Vaňková, Martin Mihaljevič

Institute of Geochemistry, Mineralogy and Mineral Resources, Faculty of Science, Charles University, Albertov 6, CZ-128 43 Prague 2, Czech Republic

ARTICLE INFO

Handling Editor: Daniel Said-Pullicino

Keywords:
Volatile
Metals
Burning
Organic matter
Wildfire

ABSTRACT

This study described the behavior of Pb and its isotopes in forest soils affected by different temperature wildfires. We collected samples of burned (and unburned) soil and ash in Abiul, central Portugal, in areas affected by different temperatures. The different soil burned severities were assessed *in situ*.

The high-temperature fires consumed all organic matter in the topsoil (down to 5 cm), while lower temperatures did not. All the soil and ash samples were analyzed for their lead (Pb) contents and Pb isotopic compositions using inductively coupled plasma mass spectrometry.

The average Pb elemental concentration in the unburned topsoils was 10.7 mg kg^{-1}, and the isotopic composition ranged from $^{206}Pb/^{207}Pb = 1.167$ to 1.178. No significant accumulation of Pb was observed in the topsoil (and ash) affected by the high-temperature fire, but their respective ratios increased (soil $^{206}Pb/^{207}Pb = 1.197$; ash $^{206}Pb/^{207}Pb = 1.180$). However, there was a significant accumulation of Pb (15.3 mg kg^{-1}) in the topsoil and especially in the ash (Pb avg. = 21.8 mg kg^{-1}), affected by the low-temperature fire. The soil $^{206}Pb/^{207}Pb$ isotopic ratios remained stable but decreased in the ash ($^{206}Pb/^{207}Pb = 1.174$ and 1.166, respectively).

According to the isotopic composition, Pb in the topsoils was of mixed origin (natural and anthropogenic). We assumed that lithogenic Pb ($^{206}Pb/^{207}Pb > 1.19$) occurred in stable mineral forms while anthropogenic Pb mainly originated from leaded gasoline ($^{206}Pb/^{207}Pb < 1.16$). Anthropogenic Pb was more easily mobilized due to the volatile nature of the emitted compounds of vehicular Pb (oxyhalogenides). Hence, during the high-temperature burning of the soil, Pb with a lower isotopic signature would be preferentially released from the soil Pb pool. Consequently, resulting soils and ash exhibited an increase in $^{206}Pb/^{207}Pb$ isotopic ratios. However, ash and soils affected by low temperatures, which did not volatilize anthropogenic Pb, retained their isotopic signatures.

This work suggests that it may be possible to determine the temperature of a forest fire from the Pb isotopic signatures of the burned materials.

1. Introduction

The presence of Pb in soils and the pedosphere has extensively and continuously increased for the past millennia relative to its natural concentrations due to anthropogenic activities (Dickson et al., 1972; Nriagu, 1996). The first emissions date from 8000 years ago, when early smelting techniques were probably first used (Goodwin and Ponikvar, 2013). During the past century, Pb emissions derived from the combustion of leaded gasoline have massively impacted ecosystems (Nriagu and Pacyna, 1988). Due to the use of non-leaded gasoline and increasing environmental awareness, atmospheric levels of Pb have decreased in the past decades (Bollhöfer and Rosman, 2001). Consequently, we are now observing a decrease in Pb concentrations in topsoils and the environment in general (Friedland et al., 1992; Trefry et al., 1985). However, it will take a long time for restoration of the natural lower concentrations of Pb. This metal is very immobile and has a high retention time in the soil environment (Harrison et al., 1981).

Only recently has the use of leaded petrol been finally globally eradicated when Algeria stopped providing this product in August 2021 (Lobet, 2021). Nonetheless, the Pb that remains in the soil must be addressed and studied. Lead in the form of halogenides, the product of the combustion of leaded gasoline, is much more volatile than Pb in its mineral forms (Nriagu, 1990).

The mobilization of the Pb present in soils has been shown to contaminate water resources (Abraham et al., 2017; Ré et al., 2021; Trefry et al., 1985), plant life, even showing up in the blood and stool

* Corresponding author.
E-mail address: santosbaietar@natur.cuni.cz (R. Baieta).

https://doi.org/10.1016/j.geoderma.2022.115760
Received 27 October 2021; Received in revised form 2 February 2022; Accepted 4 February 2022
Available online 19 February 2022

samples of cattle (Bose-O'Reilly et al., 2018) and humans (Flegal and Smith, 1992; Zahran et al., 2013). Mobilization can occur in many different ways: root uptake (Bigalke et al., 2011; Jiang and Liu, 2010; Piechalak et al., 2002; Shahid et al., 2011), direct ingestion, wind-blown particles (Csavina et al., 2014), pulverization, dust inhalation (Zhao et al., 2021), among others. In the present study, the authors focused on post-fire mobilization, resulting from the loss of vegetation and organic matter in topsoils, converting metals to a labile state (Biswas et al., 2007; Certini, 2005).

In general, wildfires adversely affect the soil. For example, a portion or all topsoil organic matter is always lost (Giovannini et al., 2001). Some nutrients (organic N) in the topsoil can be lost due to volatilization (Fisher and Binkley, 2000) while others (P, K) may be concentrated as a result of the combustion of biomass and formation of ash (Kutiel and Shaviv, 1992). Also, the soil structure can be affected, causing a decrease in the porosity (Durgin and Vogelsand, 2011), which facilitates runoff and wind erosion (Martin and Moody, 2001). Fires do not directly affect particle size, but the release and loss of fine particles may lead to more coarse soil (Mermut et al., 1997). Additionally, the biological component is greatly affected. A review on these aspects was compiled by Certini (2005).

Understanding only the chemical and mineralogical position of Pb in soils is not sufficient for the exact evaluation of contamination sources (Komárek et al., 2008). Hence, the use of Pb isotopic systems has been introduced to trace contamination sources and is a well-established method for waste incineration (Monna et al., 1997), mining/smelting processes (Baieta et al., 2021), and leaded gasoline-related deposition (Hernandez et al., 2003), among many others.

To assess the behavior of Pb during and after forest fires, we collected soil and ash samples of both burned and unburned soils in a small region of Portugal after a wildfire. This paper describes the Pb isotopic composition of soils affected by forest fires and ash and compares it to unaffected soils. Very few studies have focused on this aspect of forest fires (Kristensen et al., 2014).

2. Materials and methods

2.1. Site description and sampling procedure

The samples were collected in the town of Abiul, Pombal, in Portugal (Fig. 1). The climate in this region was classified as Warm-summer Mediterranean, Csb according to the Köppen-Geiger classification (climate-data.org). This region was affected by a low to moderate intensity fire on 23 August 2019. It destroyed about 12.52 ha of forest, mainly composed of maritime pine trees (*Pinus pinaster* Ait.). These trees were scorched during the fire. The soil burn severity (SBS) was assessed in-situ using the method described by Vega et al. (2013). The SBS varied from level 1 to level 3. Level 5 was found exclusively at the base of the local pine trees. The sandy loam soils at the surface were covered by roughly 4 cm of organic soil with a large amount of litter at the control sites (C1 and C2). The fire affected only the top 5 cm of the soil. For reference, SBS: level 1 – when the Oa layer is found partially or intact and the mineral horizons are undisturbed; level 3 – when the forest floor is completely consumed and ash may be found while the mineral horizons are still undisturbed; level 5 – when the forest floor is completely consumed leaving no charred residue and the mineral horizons are affected: the soil structure is altered, the soil surface color shifts to reddish, the roots are burned and the SOM is consumed (Vega et al., 2013).

The campaign was carried out seven days after the fire. Four pits were dug to a depth of 1 m and soil samples were collected at incremental depths. Two pits were excavated in the burned area, while two others were dug in an unburned area. In the burned area, one pit was excavated at the top of a hill (B1) where the SBS was level 3, and the

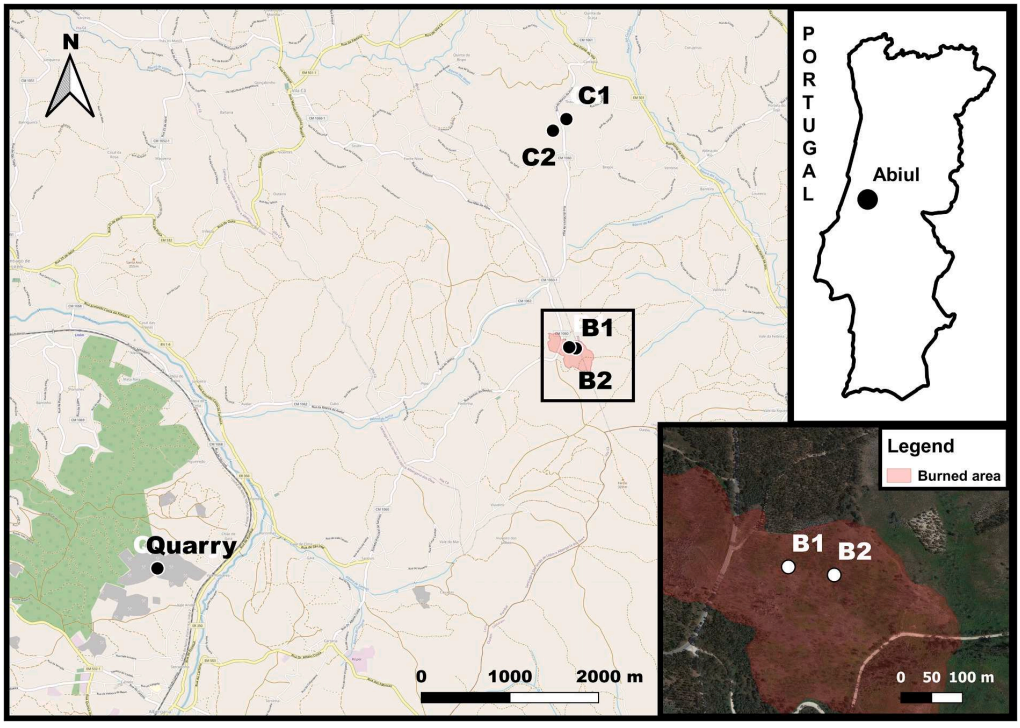

Fig. 1. Location of the soil pits (C1, C2, B1, B2) and the quarry where the fresh bedrock was collected. The studied burned area is designated by red shading.

second was in the middle of a small valley or water line, SBS = level 1 (B2, Fig. 2a, c).

Samples of fresh bedrock were collected from a local sandstone quarry since the 1 m depth pits were not deep enough to reach the bedrock (Fig. 1). Both burned sampling sites had been previously affected by two wildfires in 1990 and 2001 (ICNF, 2020).

2.2. Treatment of samples and analytical procedures

The samples were stored in PE bags. Later, they were air-dried to constant weight and transported to the laboratory, where they were sieved to 2 mm particle size and homogenized. Part of the < 2 mm fraction was milled to analytical fineness in an agate ball mill (Fritsch, Pullverissette, Germany). The granulometry of the sieved soil was measured using the hydrometer method (Gee and Or, 2002).

Digests were prepared for elemental and isotopic analysis using 0.2 g of the previously milled samples. These were then dissolved using 0.5 ml of $HClO_4$ (70–72 %) and 10 ml of HF (50 %) and evaporated to dryness at 170 °C for two hours. The second dissolution used 0.5 ml $HClO_4$ (70–72 % v/v) and 5 ml HF (50 %) and was evaporated for the second time. Finally, it was again dissolved in 2 ml analytical grade HNO_3 (Merck, Germany) (v/v), which was additionally purified by sub-boiling distillation, and deionized water (DI) obtained from a Milli-Q Academic purifying system (Millipore®, USA).

The soil pH was measured in a 1:2.5 (m/v) ratio of soil and deionized water suspension and 2 M solution of KCl. The cation exchange capacity (CEC) was determined using a Ba^{2+} solution (0.1 M $BaCl_2$ buffered at pH 8.1) to saturate soil cation exchange sites, followed by Ba^{2+} exchange with $MgSO_4$ (ISO 13536:1995). The crystalline Fe and Al oxide contents were obtained by acid oxalate extraction using 0.2 M ammonium oxalate at pH 3. The resulting solution was measured using an ICP-OES (Agilent 5110). Total carbon (TC) and total sulfur (TS) concentrations were determined using an ELTRA CS-500 analyzer (1450 °C). The accuracy of the results was verified using reference materials (SRM) NIST 1635 (Table 1S).

2.3. Trace element concentrations and determination of Pb isotopic ratios

Trace element concentrations and the Pb isotopic compositions of the samples were determined using a quadrupole-based inductively coupled plasma mass spectrometer (Q-ICP MS, XSeries 2, Thermo Scientific) under the recommended conditions. The accuracy of the trace element measurements was controlled using a reference material (SRM NIST 2711a - Montana II soil, Table 2S). The stock solutions were diluted to < 20 μg l^{-1} Pb for determination of the isotopic composition. Mass bias correction was carried out using a reference material (SRM NIST 981, Common lead, Table 3S) measured between the individual samples. The certified reference material BCR-2 (Basalt, Columbia River; USGS, $^{206}Pb/^{207}Pb = 1.2007 \pm 0.0007$, $^{208}Pb/^{206}Pb = 2.0635 \pm 0.0016$) was used to verify the accuracies of the measurements. The standard errors for measurement of the $^{206}Pb/^{207}Pb$ and $^{208}Pb/^{206}Pb$ ratios were <0.3 % RSD and <0.4 % RSD. The Pb procedural blank was below 0.03 μg l^{-1}.

3. Results and discussion

3.1. Basic properties

The soils were sandy loams. The unburned soil C1 was classified as Albic Podzol (Loamic), and the unburned C2, burned B1 and B2, all as Dystric Cambisol (Loamic). The pH values ranged from 3.99 to 5.01, indicating that these were acidic soils (Table 1). An increase in pH can be expected for fires with temperatures >450–500 °C (Arocena and Opio, 2003; Santana et al., 2018). No such increase was observed. Excluding the organic layers, the TC was low in all the soil horizons (max: 4.12 %, Table 1). However, the organic layers of the unburned soil had a higher TC value (avg: 22.7 %) than the organic or top layer (if no organic was found) of the burned soils (avg: 8.10 %). From the burned soils, only the B2 profile contained an organic layer. The organic matter can be expected to be substantially consumed in fires with temperatures > 200–250 °C and total consumption takes place at around 460 °C (Giovannini et al., 2001). Very low-intensity fires do not seem to affect the TC contents of the topsoil (Varela et al., 2015), while low-intensity fires may increase it. Other authors have explained this as the remains of burned vegetation and litter being deposited on the topsoil (Certini, 2005; Strømgaard, 1992). The burning of soil organic layers produces ash which contains mostly Ca, K, and Mg carbonates, lime (CaO), quartz (SiO_2), and P, mainly in the form of apatite [$Ca_5(PO_4)_3(Cl,F,OH)$; Yusiharni and Gilkes, 2012]. Excluding in the organic layers, CEC values ranged from 1.80 to 17.7 cmol+ kg^{-1}, fitting the soil classification (Table 1). The O-horizons of unburned soils C1 and C2 had a CEC of 48.9 and 77.2 cmol+ kg^{-1}, which was relatively high compared to the lower layers. Soil CEC decreases after the burning of the soil (Badía and Martí, 2003) as the cation exchange sites on organic matter are lost (Oswald et al., 1999).

Fig. 2. a) Dug pit where the B2 samples were collected. The burned topsoil was about 5 cm deep. b) Site where a pine tree burned, leaving white ash. c) "Valley" or water line near the B2 profile. d) Unburned analogous site (C1).

Table 1
Description and physicochemical properties of the studied soils.

Profile	Soil / Horizon		Depth	Granulometry (%)			Soil	pH H2O	pH KCl	CEC	FeOx	AlOx	TC	TS
			cm	Clay	Silt	Sand	Texture	std units	std units	cmol+ kg^{-1}	mg kg^{-1}	mg kg^{-1}	%	%
		O	−4–−2					4.46	3.43	48.9	1090	1160	21.3	0.099
			−2–0					4.32	3.11	57.6	763	831	22.8	0.105
C1	Albic	E	0–5	7.38	26.8	65.8	Sandy loam	4.06	3.24	11.9	1580	2600	3.34	0.018
(control)	Podzol	Bh	5–15	7.65	23.2	69.1		4.25	3.50	12.6	1860	2610	2.27	0.012
	(Loamic)	Bs	15–60	4.74	33.6	61.6		4.72	4.24	12.0	7950	4500	2.33	0.018
			60–90	6.11	36.5	57.4		4.77	4.43	5.97	6740	2390	0.99	0.014
		C	90–95	11.0	34.4	54.6		4.73	4.43	5.86	6050	2610	0.74	0.013
		O	−4–−2					4.63	3.55	71.2	1390	1310	23.9	0.102
C2	Dystric		−2–0					4.40	3.04	22.4	536	644	8.13	0.035
(control)	Cambisol	Ah	0–10	13.7	20.5	65.8	Sandy loam	4.19	3.12	11.8	902	1050	2.80	0.015
	(Loamic)	Bw	20–35	8.48	29.1	62.4		4.68	3.98	14.4	5850	8620	2.31	0.016
			35–50	4.41	20.0	75.6		4.89	4.26	17.7	13,100	6610	2.98	0.019
		C	55–65	4.82	20.8	74.3		5.00	4.44	10.8	14,200	3120	1.32	0.008
		Ah	0–10	8.40	21.6	70.0		4.90	3.96	12.3	5880	4940	3.50	0.014
B1	Dystric	Bw	10–25	6.19	29.9	63.9		4.89	4.20	15.0	12,300	6170	3.62	0.019
(burned)	Cambisol		25–40	4.70	30.6	64.7	Sandy loam	4.82	4.29	17.0	17,700	4970	3.63	0.022
	(Loamic)	C1	45–60	6.04	28.6	65.4		4.81	4.36	9.06	20,600	2540	1.67	0.010
		C2	65–70	4.02	22.7	73.2		5.01	4.74	1.80	6460	999	0.14	0.002
		O	−2–0					3.99	2.95	35.5	1550	1480	12.7	0.053
B2	Dystric	Ah	0–10	4.08	23.7	72.2	Sandy loam	4.10	3.20	12.0	2380	2800	4.12	0.019
(burned)	Cambisol	Bw	15–40	4.76	16.1	79.1	Loamy sand	4.51	3.94	10.8	4410	4780	2.02	0.011
	(Loamic)		40–70	9.57	9.39	79.8	Sandy loam	4.69	4.24	14.4	10,760	5340	2.36	0.016
		C	75–80	3.90	1.82	94.3	Sand	4.63	4.30	14.7	12,400	3270	2.13	0.016

3.2. Soil and ash Pb content

The bedrock was classified as sandstone and contained 10.2 mg kg^{-1} of Pb (Table 1, Fig. 3a). It is important to note that the quarry is approximately 5 km SW from the sampling sites (Fig. 1), which could cause a slight difference in properties compared to the bedrock found directly under the profiles.

All the studied soils were uncontaminated according to the maximum permitted amount of Pb (70 mg kg^{-1}) in soils for agricultural purposes (Canadian Council of Ministers of the Environment, 2007).

Lead concentrations in the C1 soil ranged from 8.28 to 13.9 mg kg^{-1} (Table 1, Fig. 3a). In the topsoil, Pb varied from an average of 11.3 mg kg^{-1} in the organic horizons to 9.83 mg kg^{-1} in the first mineral horizon. The concentration steadily increased to 13.9 mg kg^{-1} (Fig. 3a) in deeper layers. The highest concentration of Pb in the C2 soil was found in the organic topsoil and deeper layers at 12.4 mg kg^{-1}. Similar to C1, the organic horizons were richer in Pb compared to the top mineral layers, with mean values of 12.1 mg kg^{-1} to 7.37 mg kg^{-1} (Table 1, Fig. 3a). A higher concentration of metals in the organic horizons than the immediate mineral layers can be expected. The forest floor, characterized by a mixture of organic matter (OM) and minerals, acts as a metal reservoir (Shcherbov, 2012). The same behavior occurred for other elements, such as Zn, Ni, Co, for example (Table 2S). The Pb content increased with depth to a max of 12.5 mg kg^{-1} (Table 1, Fig. 3a). A steady increase in Pb with depth may be simply due to a richer bedrock or vertical migration in the soil. The studies of Miller and Friedland (1994) and Ettler et al. (2004) concluded that labile Pb (of anthropogenic origin) in soils migrates rapidly (8–20 mm y^{-1}, 30–36 mm y^{-1}, respectively) vertically through the mineral profile. This effect might be increased by frequent wildfires causing the release of metals accumulated in the organic layers of the soils. An increase in the content of total and bioavailable forms of heavy metals in soils exposed to fires has been well documented (Mitic et al., 2015; Stankov Jovanovic et al., 2011). Santorufo et al. (2021) reported that the availability of Pb increased after a wildfire and was still significant two years later, probably as a result of mineralization of the organic matter caused by the fire. Since the soils had been exposed to previous fires, faster vertical leaching might be occurring.

The burned B1 soil did not contain an O-horizon (Table 1), possibly due to the burning of its original one, implying temperatures ≥ 460 °C (Giovannini et al., 2001). In the top 65 cm of soil, the Pb content was mostly constant (mean: 10.38 mg kg^{-1}; SD = 0.56; n = 4). At 65 cm of

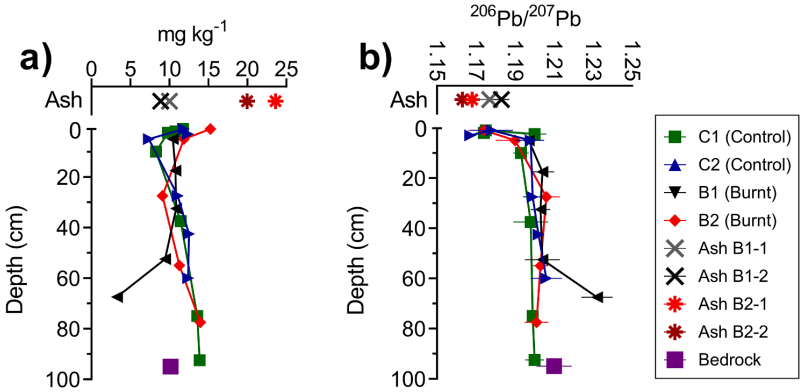

Fig. 3. a) Lead concentrations and b) isotopic $^{206}Pb/^{207}Pb$ ratios in the soil profiles, ashes, and bedrock.

depth, the deepest collected horizon contained only 3.29 mg kg^{-1} Pb. Ashes collected from the B1 profile had Pb concentrations of 10.0 and 8.89 mg kg^{-1}, similar to the topsoil (Fig. 3a).

In contrast, what was left of the O-horizon of the burned B2 profile contained more Pb (15.3 mg kg^{-1}) than any other layer in any profile (Table 1, Fig. 3a). A prediction with 95 % certainty for the concentration of Pb that can be expected in unburned topsoils gives an interval of [9.34; 13.28] mg kg^{-1}. Hence the accumulation of Pb (15.26 mg kg^{-1}) in B2 topsoil is statistically significant. The literature documents increased metal concentrations in topsoils affected by wildfires (Bartkowiak and Lemanowicz, 2017; Santorufo et al., 2021). Even burned, the CEC of this horizon was 35.4 cmol+ kg^{-1} and TC = 12.7 %. In-situ observations determined that the organic horizons were not fully consumed by the fire. Ash containing carbonates also lined the surface of the soil, contributing to the TC contents. The B1 profile was collected at the top of a hill and the B2 profile in the water line next to the same hill. The geographical distribution facilitates the accumulation of particles, organic matter, and litter visible in the B2 profile (Fig. 2c). Particles tend to be washed from the top of the hill to the valley through natural processes like wind, water drainage, or simply gravity. Erosion and transport of topsoils are facilitated after a wildfire and are a significant concern in the European Mediterranean countries, such as Portugal (Benito et al., 2014; Depountis et al., 2020; Shakesby, 2011; Varela et al., 2015, 2010).

The B2 ashes had a much higher concentration of Pb than the soil (23.6 and 20.0 mg kg^{-1}; Table 1, Fig. 3a). The accumulation of Pb, and other metals, in soils through ash deposition after a wildfire can be expected (Stankov Jovanovic et al., 2011). Ash is often richer in some metals (Pb in this case) compared to the original burned litter, organic matter, or vegetation (Campos et al., 2016; Kristensen et al., 2014; Odigie and Flegal, 2011).

3.3. Does the $^{206}Pb/^{207}Pb$ ratio change in burned soils?

The $^{206}Pb/^{207}Pb$ signature varied between 1.167 and 1.232 in the soil profiles and from 1.163 to 1.183 in the ashes. The local bedrock had a ratio of $^{206}Pb/^{207}Pb = 1.210$ (Table 2, Fig. 3b).

The $^{206}Pb/^{207}Pb$ ratio in the C1 soil was lower in the organic horizon, 1.174, relative to the top mineral horizon, $^{206}Pb/^{207}Pb = 1.200$. The ratio value stabilized with depth, between 1.193 and 1.200 (Table 2, Fig. 3b). Similarly, the ratio varied in the C2 profile between 1.167 and 1.178 in the organic horizons and from 1.198 to 1.206 in the mineral layers. The ratio increased slightly with depth in both profiles (Table 2, Fig. 3b). These ratios can be expected in soils not affected by wildfires in this region. In deeper layers, all the profiles ratios tended to the bedrock ratio ($^{206}Pb/^{207}Pb = 1.210$; Table 2, Fig. 3b).

The top layer of the first burned soil B1 had a ratio of $^{206}Pb/^{207}Pb = 1.197$, which increased continuously to 1.204 at −60 cm (Table 2, Fig. 3b). The deepest collected layer at −70 cm had a ratio of $^{206}Pb/^{207}Pb = 1.123$ (Fig. 4,*). One possible explanation is that the "1 m" depth of the profiles were located at different altitudes. A similar apparent outlier was noted in the concentration of Pb. On the other hand, it may simply be an outlier. For the sake of this work, it is irrelevant since forest fires do not directly affect soils that deep. Ashes collected near this soil had an average ratio of $^{206}Pb/^{207}Pb = 1.180$, lower than the ratio in the top horizon (Fig. 3b and 4) but higher than the typical unburned top horizons ($^{206}Pb/^{207}Pb = 1.173$).

The second burned soil, B2, at the bottom of the valley, retained its O-horizon, and it shared a similar isotopic ratio with the unburned ones ($^{206}Pb/^{207}Pb = 1.174$) while having a ratio of $^{206}Pb/^{207}Pb = 1.190$ to 1.206 in deeper layers. These values were also in agreement with the unburned soils. Ashes collected near this pit had an average ratio of 1.166. Ash (B2) had lower ratios than topsoils, suggesting a decrease in the lighter ^{206}Pb after burning (Fig. 3b and 4).

Why was there a decrease in $^{206}Pb/^{207}Pb$ in the B2 ash? Lead present in more volatile compounds, like halogenides from leaded gasoline, was released during the burning of the organic layers and litter more quickly than Pb in mineral form. Up to 85 % of the Pb can remobilize as airborne components during fires: fly ash and dust (Narodoslawsky and Obernberger, 1996; Nzihou and Stanmore, 2013). However, this did not seem to be the case, as there was an increase in Pb in the topsoils. This Pb must have had a lower $^{206}Pb/^{207}Pb$ ratio than the unburned soil organic

Table 2
Total Pb concentrations and $^{206}Pb/^{207}Pb$ and $^{208}Pb/^{206}Pb$ ratios in the studied soils, ashes, and bedrock.

Profile	Soil / Horizon		Depth	Pb		$^{206}Pb/^{207}Pb$		$^{208}Pb/^{206}Pb$	
			cm	mg kg^{-1}	SD	Ratio	SD	Ratio	SD
		O	−4–−2	10.8	0.34	1.174	0.004	2.102	0.012
			−2–0	11.7	0.13	1.175	0.006	2.104	0.008
C1	Albic	E	0–5	9.83	0.21	1.200	0.006	2.093	0.018
(control)	Podzol	Bh	5–15	8.28	0.27	1.193	0.004	2.097	0.012
	(Loamic)	Bs	15–60	11.4	0.19	1.198	0.009	2.087	0.012
			60–90	13.6	0.32	1.199	0.003	2.087	0.010
		C	90–95	13.9	0.47	1.200	0.005	2.082	0.005
		O	−4–−2	12.4	0.13	1.167	0.003	2.118	0.007
C2	Dystric		−2–0	11.8	0.06	1.178	0.011	2.104	0.015
(control)	Cambisol	Ah	0–10	7.37	0.04	1.198	0.007	2.093	0.016
	(Loamic)	Bw	20–35	11.1	0.37	1.199	0.005	2.082	0.009
			35–50	12.5	0.31	1.202	0.003	2.076	0.006
		C	55–65	12.4	0.25	1.206	0.008	2.068	0.014
		Ah	0–10	10.4	0.61	1.197	0.007	2.079	0.011
B1	Dystric	Bw	10–25	10.8	0.21	1.204	0.006	2.069	0.013
(burned)	Cambisol		25–40	10.9	0.20	1.203	0.005	2.068	0.010
	(Loamic)	C1	45–60	9.45	0.38	1.204	0.009	2.070	0.008
		C2	65–70	3.29	0.23	1.232	0.008	2.026	0.010
		O	−2–0	15.3	0.26	1.174	0.008	2.107	0.019
B2	Dystric	Ah	0–10	11.9	0.14	1.190	0.010	2.096	0.011
(burned)	Cambisol	Bw	15–40	9.11	0.23	1.206	0.007	2.069	0.008
	(Loamic)		40–70	11.3	0.02	1.203	0.004	2.068	0.007
		C	75–80	14.0	0.01	1.201	0.006	2.070	0.010
	Ash B11			10.0	0.54	1.177	0.006	2.107	0.011
	Ash B12			8.89	0.08	1.183	0.004	2.078	0.038
	Ash B21			23.6	0.22	1.168	0.005	2.116	0.012
	Ash B22			20.0	0.39	1.163	0.004	2.124	0.007
Bedrock	Sandstone			10.2	0.03	1.210	0.009	2.055	0.012

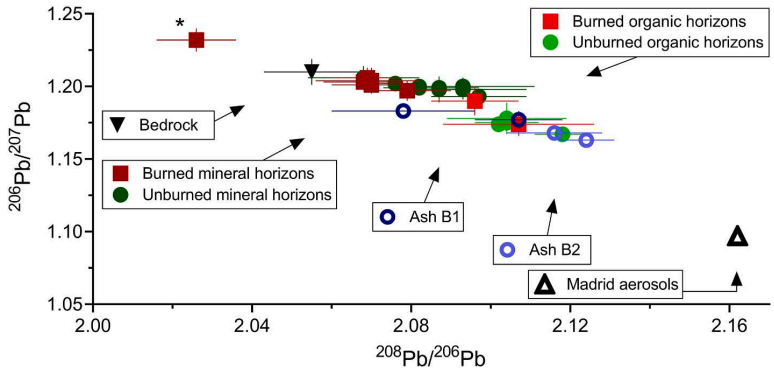

Fig. 4. A three-isotope plot ($^{206}Pb/^{207}Pb$ vs. $^{208}Pb/^{206}Pb$) showing the Pb isotopic compositions of soils and ash. The Madrid aerosol values were taken from (Bollhöfer and Rosman, 2001). *See the text for a comment on this sample.

layers. Tuhý et al. (2021) showed experimentally that Pb volatilization in soils exposed to high temperatures occurs significantly only at temperatures higher than 600–650 °C. In low-temperature fires, the anthropogenic Pb with lower $^{206}Pb/^{207}Pb$ is accumulated in the ash, lowering its isotopic ratio compared to the source (soil).

There was a clear linear decrease in $^{206}Pb/^{207}Pb$ (increase in $^{208}Pb/^{206}Pb$) upwards from the bedrock to the organic horizons at the surface (Fig. 4, Table 2). Burned organic horizons were more radiogenic than the unburned ones. Ash collected near the B1 profile had higher $^{206}Pb/^{207}Pb$ ratios than ash collected near the B2 profile (Fig. 4, Table 2).

The combustion of leaded gasoline accounted for approx. 75 % of global Pb aerosol during the second half of the twentieth century (Dunlap et al., 2008; Nriagu and Pacyna, 1988). Kristensen et al. (2014) found that ash originating in Australian bushfires contained a mixture of natural Pb and a legacy of industrial Pb depositions, such as leaded petrol combustion. One of the sites they studied was located at a distance of 340 km from any important source of contamination. Other studies found similar results in the ash produced in the 2012 California wildfires; the isotopic composition of the excess Pb found in the ash fell between the local natural Pb signature and that of the leaded gasoline used in that region in the previous century (Odigie and Flegal, 2014) or for Pb released from the combustion of trees in Australian wildfires (Isley and Taylor, 2020). Unfortunately, to our knowledge, the specific signature of leaded gasoline used in Portugal during the last century is not known. However, the literature can suggest a range of values. A survey of the Pb ratios in the ocean during the 1980s determined that $^{206}Pb/^{207}Pb = 1.167$ near the Portuguese west coast (Weiss et al., 2003). In a study in the Golf of Cadiz (Company et al., 2011), the authors also could not find available data from the nearby countries: Morroco, Algeria, Portugal, Tunisia. They assumed that an average Western European leaded-petrol emission ratio would be a good approximation $^{206}Pb/^{207}Pb \sim 1.093$ to 1.141 (ratio calculated; Monna et al., 1997). Bollhöfer and Rosman (2001) composed an extensive compilation of Pb isotopic ratios of aerosols in the Northern Hemisphere. The closest (and relevant) location would be Madrid with: $^{206}Pb/^{207}Pb = 1.097 \pm 0.001$; $^{208}Pb/^{206}Pb = 2.162$ (calculated ratio, Fig. 4). This data is from 1995 and, by then most of Western Europe had banned the use of lead additives in gasoline. The authors admit that these values should reflect a mixture of leaded gasoline and industrial Pb.

The present work assumed that the $^{206}Pb/^{207}Pb$ ratio of leaded gasoline in Portugal fell within the given literature values. Hence, the emissions would have had ratios well below the ones we observe today in the topsoils.

The B1 topsoil suffered a higher intensity fire, hence higher temperatures, which consumed all the organic matter. Lead-bearing particles originating in leaded gasoline use are more volatile than geogenic ones. These must have been mobilized into the atmosphere and dispersed, leaving the residual Pb in the soils with a more geogenic, higher isotopic signature ($^{206}Pb/^{207}Pb = 1.197$; Fig. 3b and 4). The B2 profile suffered a lower intensity fire that would not volatilize as much Pb, accumulating the element. Ash isotopic data seems to corroborate this finding. Ash collected near the B1 profile had an isotopic signature much closer to the geogenic one (Ash: $^{206}Pb/^{207}Pb = 1.177$, 1.183 to bedrock $^{206}Pb/^{207}Pb = 1.210$) when compared to ash collected in the B2 profile ($^{206}Pb/^{207}Pb = 1.168$, 1.163), which was similar to, even if slightly lower than the signature of the organic layers ($^{206}Pb/^{207}Pb =$ 1.167 to 1.178; Fig. 3b and 4). The B2 topsoil was also richer in Pb compared to the other topsoils. A study (Mihaljevič et al., 2011) that looked into Pb isotopic ratios in topsoils and trees found little evidence for gasoline-induced soil contamination. However, local trees possessed Pb with this signature. Knowing that the studied region was often affected by vegetation fires, the authors suggested that less radiogenic Pb was volatilized. The resulting aerosols were then deposited in tree crowns and absorbed into the tree biomass.

Starting from the assumption that the B1 and B2 soils shared the same pre-fire $^{206}Pb/^{207}Pb$ ratio, much more anthropogenic Pb was released from the B1 topsoil during the wildfire. This was indicated by the relatively high content of Pb in the B2 topsoil (15.26 mg kg^{-1}) and B2 ash (average: 21.78 mg kg^{-1}). However, the presence of more litter in B2 must be taken into account, making it difficult to determine which effect was more critical: the amount of litter or Pb accumulation post-fire. The difference between the isotopic signatures of the ashes collected in the two profiles is more revealing than the elemental concentration. On average, the ash ratio from the B1 profile ($^{206}Pb/^{207}Pb =$ 1.180) was high and fell between the ratios for unburned topsoil and mineral layers. There is an increase in the ratio with the release of the more volatile, and less radiogenic Pb. However, because the B2 profile was affected by a lower-temperature fire, the ratio in the ash was much lower ($^{206}Pb/^{207}Pb = 1.166$), as the anthropogenic particles were not volatilized. Consequently, there was little or no release of anthropogenic Pb in the B2 profile.

4. Conclusions

The burning temperature plays a major role in Pb volatilization or accumulation, which affects the isotopic ratios in the topsoil and ash. Anthropogenic, less radiogenic Pb present in the topsoil was preferentially mobilized. Low-temperature fires did not volatilize any Pb and instead accumulated it in the topsoil and resulting ash. Our data indicated that the mobilized Pb originated from the deposition of contaminated aerosols, probably the legacy of leaded gasoline usage in the last

century. Since the preferentially mobilized Pb had a lower isotopic signature, Pb in ash resulting from low-temperature fires had a lower signature than in the original soil. The contrary was observed in soils affected by higher intensity fires where Pb can be mobilized. Here we observed an increase in Pb isotopic ratios as the lighter Pb is dispersed into the atmosphere.

Lead isotopic ratios may be used to document fire intensity. However, sampling must be carried out immediately after a forest fire because of the transportable nature of ash and the destruction of the soil structure. The studied soil profiles were all uncontaminated according to the regulations, but the organic layers held more metals than the mineral layers.

Declaration of competing interest

The authors declare that they have no known competing financial interests or personal relationships that could have appeared to influence the work reported in this paper.

Acknowledgments

This work was supported by the Czech Science Foundation (GAČR 19-18513S), the Center for Geosphere Dynamics (UNCE/SCI/006), and a student grant awarded to Rafael Baieta by the Charles University Grant Agency (GAUK 946120). In addition, the authors would like to thank the contributions from Marie Fayadová, Věra Vonásková, and Lenka Jílková in sample treatment. Finally, prof. Josef Ježek is thanked for his assistance in interpreting the data. The written English was checked by the native English speakers Madeleine Stulikova, and Chris Ash. The authors wish to thank prof. Jorg Matschulat and an anonymous reviewer for the constructive comments on the manuscript.

Appendix A. Supplementary data

Supplementary data to this article can be found online at https://doi.org/10.1016/j.geoderma.2022.115760.

References

Abraham, J., Dowling, K., Florentine, S., 2017. Risk of post-fire metal mobilization into surface water resources: a review. Sci. Total Environ. 599–600, 1740–1755. https://doi.org/10.1016/j.scitotenv.2017.05.096.

Arocena, J.M., Opio, C., 2003. Prescribed fire-induced changes in properties of sub-boreal forest soils. Geoderma 113. https://doi.org/10.1016/S0016-7061(02)00312-9.

Badía, D., Martí, C., 2003. Plant ash and heat intensity effects on chemical and physical properties of two contrasting soils. Arid L. Res. Manag. 17, 23–41. https://doi.org/10.1080/15324980301595.

Baieta, R., Mihaljevič, M., Ettler, V., Vaněk, A., Penížek, V., Trubač, J., Kříbek, B., Ježek, J., Svoboda, M., Sracek, O., Nyambe, I., 2021. Depicting the historical pollution in a Pb-Zn mining/smelting site in Kabwe (Zambia) using tree rings. J. African Earth Sci. 181, 104246.

Bartkowiak, A., Lemanowicz, J., 2017. Effect of forest fire on changes in the content of total and available forms of selected heavy metals and catalase activity in soil. Soil Sci. Annu. 68, 140–148. https://doi.org/10.1515/SSA-2017-0017.

Benito, E., Varela, M.E., Rodríguez-Alleres, M., 2014. Wildfire effects on soil erodibility in Galicia. Cuad. Investig. Geográfica 40, 353–370. https://doi.org/10.18172/cig.2502.

Bigalke, M., Weyer, S., Wilcke, W., 2011. Stable Cu isotope fractionation in soils during oxic weathering and podzolization. Geochim. Cosmochim. Acta 75, 3119–3134. https://doi.org/10.1016/j.gca.2011.03.005.

Biswas, A., Blum, J.D., Klaue, B., Keeler, G.J., 2007. Release of mercury from rocky mountain forest fires. Global Biogeochem. Cycles 21. https://doi.org/10.1029/2006GB002696.

Bollhöfer, A., Rosman, K.J.R.R., 2001. Isotopic source signatures for atmospheric lead: The Northern Hemisphere. Geochim. Cosmochim. Acta 65, 1727–1740. https://doi.org/10.1016/S0016-7037(00)00630-X.

Bose-O'Reilly, S., Yabe, J., Makumba, J., Schutzmeier, P., Ericson, B., Caravanos, J., 2018. Lead intoxicated children in Kabwe. Zambia. Environ. Res. 165, 420–424. https://doi.org/10.1016/j.envres.2017.10.024.

Campos, I., Abrantes, N., Keizer, J.J., Vale, C., Pereira, P., 2016. Major and trace elements in soils and ashes of eucalypt and pine forest plantations in Portugal following a wildfire. Sci. Total Environ. 572, 1363–1376. https://doi.org/10.1016/j.scitotenv.2016.01.190.

Canadian Council of Ministers of the Environment, 2007. Canadian Soil Quality Guidelines for the Protection of Environmental and Human Health: Summary tables.

Certini, G., 2005. Effects of fire on properties of forest soils: a review. Oecologia 143, 1–10. https://doi.org/10.1007/S00442-004-1788-8.

Company, R., Serafim, A., Lopes, B., Cravo, A., Kalman, J., Riba, I., DelValls, T.A., Blasco, J., Delgado, J., Sarmiento, A.M., Nieto, J.M., Shepherd, T.J., Nowell, G., Bebianno, M.J., 2011. Source and impact of lead contamination on δ-aminolevulinic acid dehydratase activity in several marine bivalve species along the Gulf of Cadiz. Aquat. Toxicol. 101, 146–154. https://doi.org/10.1016/J.AQUATOX.2010.09.012.

Csavina, J., Taylor, M.P., Félix, O., Rine, K.P., Eduardo Sáez, A., Betterton, E.A., 2014. Size-resolved dust and aerosol contaminants associated with copper and lead smelting emissions: Implications for emission management and human health. Sci. Total Environ. 493, 750–756. https://doi.org/10.1016/j.scitotenv.2014.06.031.

Depountis, N., Michalopoulou, M., Kavoura, K., Nikolakopoulos, K., Sabatakakis, N., 2020. Estimating soil erosion rate changes in areas affected by wildfires. ISPRS Int. J. Geo-Information 9. https://doi.org/10.3390/ijgi9100562.

Dickson, E.M., Patterson, C.C., Weiss, H.V., Koide, M., Goldberg, E.D., 1972. Mercury and lead in the greenland ice sheet: a reexamination of the data. New Ser. 177, 536–538.

Dunlap, C.E., Alpers, C.N., Bouse, R., Taylor, H.E., Unruh, D.M., Flegal, A.R., 2008. The persistence of lead from past gasoline emissions and mining drainage in a large riparian system: Evidence from lead isotopes in the Sacramento River, California. Geochim. Cosmochim. Acta 72, 5935–5948. https://doi.org/10.1016/j.gca.2008.10.006.

Durgin, P.B., Vogelsand, P.J., 2011. Dispersion of Kaolinite by water extracts of Douglas-fir Ash. Can. J. Soil Sci. 64, 439–443. https://doi.org/10.4141/CJSS84-044.

Ettler, V., Mihaljevič, M., Komárek, M., 2004. ICP-MS measurements of lead isotopic ratios in soils heavily contaminated by lead smelting: Tracing the sources of pollution. Anal. Bioanal. Chem. 378, 311–317. https://doi.org/10.1007/s00216-003-2229-y.

Fisher, R.F., Binkley, D., 2000. Soils of the major forest biomes. In: Ecology and Management of Forest Soils. John Wiley & Sons, INC., pp. 37–60

Flegal, A.R., Smith, D.R., 1992. Lead levels in preindustrial humans, in: The New England Journal of Medicine. United States, pp. 1293–1294. 10.1056/nejm199205073261916.

Friedland, A., Craig, B., Miller, E., Herrick, G., Siccma, T., Johnson, A., 1992. Decreasing lead levels in the forest floor of the Northeastern USA. Ambio 21, 400–403. https://doi.org/10.2307/4313971.

Gee, G.W., Or, D., 2002. Particle-size analysis. In Methods of Soil Analysis: Part 4 – Physical Methods. Soil Science Society of America, Madison. doi:10.2136/sssabookser5.4.frontmatter.

Giovannini, G., Vallejo, R., Lucchesi, S., Bautista, S., Ciompi, S., Llovet, J., 2001. Effects of land use and eventual fire on soil erodibility in dry Mediterranean conditions. For. Ecol. Manage. 147, 15–23. https://doi.org/10.1016/S0378-1127(00)00437-0.

Goodwin, F.E., Ponikvar, A.L., 2013. Lead processing [WWW Document]. Encycl. Br. URL https://www.britannica.com/technology/lead-processing (accessed 10.14.21).

Harrison, R.M., Laxen, D.P.H., Wilson, S.J., 1981. Chemical associations of lead, cadmium, copper, and zinc in street dusts and roadside soils. Environ. Sci. Technol. 15, 1378–1383. https://doi.org/10.1021/es00093a013.

Hernandez, L., Probst, A., Probst, J.L., Ulrich, E., 2003. Heavy metal distribution in some French forest soils: evidence for atmospheric contamination. Sci. Total Environ. 312, 195–219. https://doi.org/10.1016/S0048-9697(03)00223-7.

ICNF, 2020. Florestas - Mapas [WWW Document]. URL http://www2.icnf.pt/portal/florestas (accessed 8.28.20).

Isley, C.F., Taylor, M.P., 2020. Atmospheric remobilization of natural and anthropogenic contaminants during wildfires. Environ. Pollut. 267 https://doi.org/10.1016/J.ENVPOL.2020.115400.

Jiang, W., Liu, D., 2010. Pb-induced cellular defense system in the root meristematic cells of Allium sativum L. BMC Plant Biol. 10 https://doi.org/10.1186/1471-2229-10-40.

Komárek, M., Ettler, V., Chrastný, V., Mihaljevič, M., 2008. Lead isotopes in environmental sciences: a review. Environ. Int. 34, 562–577. https://doi.org/10.1016/J.ENVINT.2007.10.005.

Kristensen, L.J., Taylor, M.P., Odigie, K.O., Hibdon, S.A., Russell Flegal, A., 2014. Lead isotopic compositions of ash sourced from Australian bushfires. Environ. Pollut. 190, 159–165. https://doi.org/10.1016/j.envpol.2014.03.025.

Kutiel, P., Shaviv, A., 1992. Effects of soil type, plant composition and leaching on soil nutrients following a simulated forest fire. For. Ecol. Manage. 53, 329–343. https://doi.org/10.1016/0378-1127(92)90051-A.

Lobet, I., 2021. Finally, the end of leaded gas [WWW Document]. Natl. Geogr. Mag. URL https://www.nationalgeographic.com/environment/article/finally-the-end-of-leaded-gas.

Martin, D.A., Moody, J.A., 2001. Comparison of soil infiltration rates in burned and unburned mountainous watersheds. Hydrol. Process. 15, 2893–2903. https://doi.org/10.1002/HYP.380.

Mermut, A.R., Luk, S.H., Römkens, M.J.M., Poesen, J.W.A., 1997. Soil loss by splash and wash during rainfall from two loess soils. Geoderma 75, 203–214. https://doi.org/10.1016/S0016-7061(96)00091-2.

Mihaljevič, M., Ettler, V., Šebek, O., Sracek, O., Kříbek, B., Kyncl, T., Majer, V., Veselovský, F., 2011. Lead isotopic and metallic pollution record in tree rings from the copperbelt mining-smelting area, Zambia. Water. Air. Soil Pollut. 216, 657–668. https://doi.org/10.1007/s11270-010-0560-4.

Miller, E.K., Friedland, A.J., 1994. Lead migration in forest soils: response to changing atmospheric inputs. Environ. Sci. Technol. 28, 662–669. https://doi.org/10.1021/es00053a020.

Mitic, V.D., Stankov Jovanovic, V.P., Ilic, M.D., Nikolic Mandic, S.D., 2015. Impact of wildfire on soil characteristics and some metal content in selected plants species of

Geraniaceae family. Environ. Earth Sci. 73, 4581–4594. https://doi.org/10.1007/s12665-014-3744-1.
Monna, F., Lancelot, J., Croudace, I.W., Cundy, A.B., Lewis, J.T., 1997. Pb Isotopic Composition of Airborne Particulate Material from France and the Southern United Kingdom: Implications for Pb Pollution Sources in Urban Areas 31, 2277–2286. 10.1021/ES960870+.
Narodoslawsky, M., Obernberger, I., 1996. From waste to raw material – the route from biomass to wood ash for cadmium and other heavy metals. J. Hazard. Mater. 50, 157–168. https://doi.org/10.1016/0304-3894(96)01785-2.
Nriagu, J.O., 1996. A history of global metal pollution. Science (80-.) 272, 223–224. https://doi.org/10.1126/SCIENCE.272.5259.223.
Nriagu, J.O., 1990. The rise and fall of leaded gasoline. Sci. Total Environ. 92, 13–28. https://doi.org/10.1016/0048-9697(90)90318-O.
Nriagu, J.O., Pacyna, J.M., 1988. Quantitative assessment of worldwide contamination of air, water and soils by trace metals. Nat. 1988 3336169 333, 134–139. 10.1038/333134a0.
Nzihou, A., Stanmore, B., 2013. The fate of heavy metals during combustion and gasification of contaminated biomass-A brief review. J. Hazard. Mater. 256–257, 56–66. https://doi.org/10.1016/j.jhazmat.2013.02.050.
Odigie, K.O., Flegal, A.R., 2014. Trace metal inventories and lead isotopic composition chronicle a forest fire's remobilization of industrial contaminants deposited in the Angeles National Forest. PLoS One 9, e107835. https://doi.org/10.1371/JOURNAL.PONE.0107835.
Odigie, K.O., Flegal, A.R., 2011. Pyrogenic remobilization of historic industrial lead depositions. Environ. Sci. Technol. 45, 6290–6295. https://doi.org/10.1021/es200944w.
Oswald, B.P., Davenport, D., Neuenschwander, L.F., 1999. Effects of slash pile burning on the physical and chemical soil properties of Vassar soils. J. Sustain. For. 8, 75–86. https://doi.org/10.1300/J091v08n01_06.
Piechalak, A., Tomaszewska, B., Baralkiewicz, D., Malecka, A., 2002. Accumulation and detoxification of lead ions in legumes. Phytochemistry 60, 153–162. https://doi.org/10.1016/S0031-9422(02)00067-5.
Ré, A., Campos, I., Keizer, J.J., Gonçalves, F.J.M., Pereira, J.L., Abrantes, N., 2021. Effects of post-fire contamination in sediment-dwelling species of riverine systems. Sci. Total Environ. 771 https://doi.org/10.1016/j.scitotenv.2020.144813.
Santana, N.A., Morales, C.A.S., da Silva, D.A.A., Antoniolli, Z.I., Jacques, R.J.S., 2018. Soil biological, chemical, and physical properties after a wildfire event in a eucalyptus forest in the pampa biome. Rev. Bras. Ciência do Solo 42. https://doi.org/10.1590/18069657rbcs20170199.
Santorufo, L., Memoli, V., Panico, S.C., Santini, G., Barile, R., Di Natale, G., Trifuoggi, M., De Marco, A., Maisto, G., 2021. Early post-fire changes in properties of Andosols within a Mediterranean area. Geoderma 394. https://doi.org/10.1016/j.geoderma.2021.115016.
Shahid, M., Pinelli, E., Pourrut, B., Silvestre, J., Dumat, C., 2011. Lead-induced genotoxicity to Vicia faba L. roots in relation with metal cell uptake and initial speciation. Ecotoxicol. Environ. Saf. 74, 78–84. https://doi.org/10.1016/J.ECOENV.2010.08.037.
Shakesby, R.A., 2011. Post-wildfire soil erosion in the Mediterranean: Review and future research directions. Earth-Science Rev. 105, 71–100. https://doi.org/10.1016/j.earscirev.2011.01.001.
Shcherbov, B.L., 2012. The role of forest floor in migration of metals and artificial nuclides during forest fires in Siberia. Contemp. Probl. Ecol. 5, 191–199. https://doi.org/10.1134/S1995425512020114.
Stankov Jovanovic, V.P., Ilic, M.D., Markovic, M.S., Mitic, V.D., Nikolic Mandic, S.D., Stojanovic, G.S., 2011. Wild fire impact on copper, zinc, lead and cadmium distribution in soil and relation with abundance in selected plants of Lamiaceae family from Vidlic Mountain (Serbia). Chemosphere 84, 1584–1591. https://doi.org/10.1016/J.CHEMOSPHERE.2011.05.048.
Strømgaard, P., 1992. Immediate and long-term effects of fire and ash-fertilization on a Zambian miombo woodland soil. Agric. Ecosyst. Environ. 41, 19–37. https://doi.org/10.1016/0167-8809(92)90177-D.
Trefry, J.H., Metz, S., Trocine, R.P., Nelsen, T.A., 1985. A decline in lead transport by the Mississippi River. Science (80-.) 230, 439–441. https://doi.org/10.1126/SCIENCE.230.4724.439.
Tuhý, M., Ettler, V., Rohovec, J., Matoušková, Š., Mihaljevič, M., Kříbek, B., Mapani, B., 2021. Metal(loid)s remobilization and mineralogical transformations in smelter-polluted savanna soils under simulated wildfire conditions. J. Environ. Manage. 293, 112899 https://doi.org/10.1016/J.JENVMAN.2021.112899.
Varela, M.E., Benito, E., Keizer, J.J., 2015. Influence of wildfire severity on soil physical degradation in two pine forest stands of NW Spain. Catena 133, 342–348. https://doi.org/10.1016/j.catena.2015.06.004.
Varela, M.E., Benito, E., KEIZER, J.J., 2010. Wildfire effects on soil erodibility of woodlands in NW Spain. L. Degrad. Dev. 21, 75–82. 10.1002/ldr.896.
Vega, J.A., Fontúrbel, T., Merino, A., Fernández, C., Ferreiro, A., Jiménez, E., 2013. Testing the ability of visual indicators of soil burn severity to reflect changes in soil chemical and microbial properties in pine forests and shrubland. Plant Soil 369, 73–91. https://doi.org/10.1007/s11104-012-1532-9.
Weiss, D., Boyle, A.B., Wu, J., Chavagnac, V., Michel, A., Reuer, M.K., 2003. Spatial and temporal evolution of lead isotope ratios in the North Atlantic Ocean between 1981 and 1989. J. Geophys. Res. Ocean. 108 https://doi.org/10.1029/2000JC000762.
Yusiharni, E., Gilkes, R., 2012. Minerals in the ash of Australian native plants. Geoderma 189–190, 369–380. https://doi.org/10.1016/J.GEODERMA.2012.06.035.
Zahran, S., Laidlaw, M., McElmurry, S., Filippelli, G., Taylor, M., 2013. Linking source and effect: resuspended soil lead, air lead, and children's blood lead levels in Detroit, Michigan. Environ. Sci. Technol. 47, 2839–2845. https://doi.org/10.1021/ES303854C.
Zhao, X., Li, Z., Wang, D., Tao, Y., Qiao, F., Lei, L., Huang, J., Ting, Z., 2021. Characteristics, source apportionment and health risk assessment of heavy metals exposure via household dust from six cities in China. Sci. Total Environ. 762 https://doi.org/10.1016/J.SCITOTENV.2020.143126.